Performance Evaluation of Cross-Layer Energy-Efficient Transmit Antenna Selection for Spatial Multiplexing Systems

Elizabeth Mukhwana Okumu

Thesis Presented for the Degree of

DOCTOR OF PHILOSOPHY

in the Department of Electrical Engineering

in the Faculty of Engineering and the Built Environment

UNIVERSITY OF CAPE TOWN

September 2017

As the candidate’s supervisor, I have approved this thesis for submission.

Name: Associate Professor: Mqhele E. Dlodlo

Signed: _____

Date: _____

Declaration

I hereby declare that: (1) the above thesis is my own unaided work, both in conception and execution, and that apart from the normal guidance of my supervisor, I have received no assistance apart from that stated below; (2) except as stated below, neither the substance or any part of the thesis has been submitted in the past, or is being, or is to be submitted for a degree in the University or any other University.

I am now presenting the thesis for examination for the Degree of PhD in Electrical Engineering. I also grant the University free license to reproduce the above thesis in whole or in part, for the purpose of research.

Signed by candidate

Elizabeth Mukwana Okumu — September 2017

Name — Date

Dedication

To God Almighty

Luke 1:45 “Blessed is she who has believed that what the Lord has said to her will be accomplished!”

Acknowledgements

First and foremost, I would like to express my profound gratitude to God Almighty, who has been my source of inspiration, my strength, my guide, my provider and my all throughout my PhD journey.

I would also like to acknowledge my supervisor, A/Prof Mqhele Dlodlo, for his support and advice which are highly appreciated.

To my wonderful family, my husband David Atsaba and my son Neil Kutswa, I thank you for your love and support; all the sacrifices you made, which have enabled me to get where I am today - thank you for always believing in me. To my parents, William Omukuba and Refa Okumu, and all my siblings; thank you for your encouragement. To my entire family; including my in-laws; thank you for all your prayers.

I am extremely grateful to the Schlumberger Foundation, for awarding me a Faculty for the Future (FFTF) PhD grant; which funded both my PhD studies and conference attendances. Thank you for making me part of the FFTF community of strong women; who are doing amazing things in STEM, all over the world.

To the members of the COMMED and CRG research groups at the University of Cape Town, I say thank you for all your contributions.

And to all my brothers and sisters in Christ - in Cape Town and Kenya – thank you for all your encouragement and prayers. Agnes Obati – my sister – know that all your prayers and faith have not been in vain!

May God bless you all!

Table of Contents

List of Tables

List of Figures

List of Abbreviations

3G	3rd Generation
4G	4th Generation
5G	5th Generation
BLAST	Bell Labs Layered Space Time
CSI	Channel State Information
CCI	Co-Channel Interference
CR	Cognitive Radio
CDF	Cumulative Distribution Function
DLC	Data Link Control
D2D	Device to Device
DE	Diagonal Encoding
EE	Energy Efficiency
FSA	Fixed Spectrum Access
GBN	Go Back to N
HE	Horizontal Encoding
LTE	Long Term Evolution
M-QAM	M-ary Quadrature Amplitude Modulation
MRC	Maximal Ratio Combining
ML	Maximum Likelihood
MRT	Maximum Ratio Transmission
MSI	Multi-Stream Interference
MU	Multi-User
N-SAW	N-process Stop and Wait
OSTBC	Orthogonal Space Time Block Code
PAR	Peak to Average Ratio
PU	Primary User
RF	Radio Frequency
RX	Receiver

SU	Secondary User
SR	Selective Repeat
SINR	Signal to Interference plus Noise Ratio
SNR	Signal to Noise Ratio
SIMO	Single-Input Multiple-Output
SISO	Single-Input Single-Output
SVD	Singular Value Decomposition
SDR	Software Defined Radio
STTC	Space Time Trellis Code
SE	Spectral Efficiency
SAW	Stop and Wait
SUC	Successive Cancelation
SER	Symbol Error Rate
TX	Transmitter
VE	Vertical Encoding
WiMAX	Worldwide Interoperability for Microwave Access
ZF	Zero Forcing
ZMCSCG	Zero mean Circularly Symmetric Complex Gaussian

Notations

$\boldsymbol{A}$	the matrix $\boldsymbol{A}$ (boldface uppercase)
$\boldsymbol{x}$	the vector $\boldsymbol{x}$ (boldface lowercase)
$\mathbb{C}^{\boldsymbol{x}\times\boldsymbol{y}}$	the space of $x \times y$ matrices/vectors with complex entries
$\in$	element of
$\mathcal{E}\{.\}$	expectation of a random variable
$Tr(\boldsymbol{A})$	trace of matrix the matrix $\boldsymbol{A}$
$\boldsymbol{A}^H$	conjugate transpose of the matrix $\boldsymbol{A}$
$\boldsymbol{A}^T$	transpose of the matrix $\boldsymbol{A}$
$det(\boldsymbol{A})$	determinant of matrix $\boldsymbol{A}$
$log_2(.)$	logarithm with base 2
$\boldsymbol{I}_m$	$m \times m$ identity matrix
$diag\{a_1, a_2, \dots, a_n\}$	$n \times n$ matrix with $[diag\{a_1, a_2, \dots, a_n\}]_{i.i} = a_i$
$(a)^*$	complex conjugate of the complex number a
$\|\boldsymbol{A}\|_F^2$	squared Frobenius norm of $\boldsymbol{A}$
$\boldsymbol{A}^\dagger$	Moore-Penrose inverse (pseudo-inverse) of $\boldsymbol{A}$
$\binom{M}{m}$	the binomial coefficient $\frac{M!}{(M-m)!m!}$
$[\boldsymbol{A}]_{i,j}$	element in the ith row and jth column of matrix $\boldsymbol{A}$
$Q(x)$	Q-function, defined as $Q(x) = \left(1/\sqrt{2\pi}\right)\int_x^\infty e^{t^2}dt$
$\|a\|$	absolute value of the complex number a

Abstract

Multiple-input multiple-output (MIMO) and cognitive radio (CR) are key techniques for present and future high-speed wireless technologies. On the other hand, there are rising energy costs and greenhouse emissions associated with the provision of high-speed wireless communications. Consequently, the design of high-speed energy efficient systems is paramount for next-generation wireless systems.

This thesis studies energy-efficient antenna selection for spatial multiplexing multiple-antenna systems from a cross-layer perspective, contrary to the norm, where physical-layer energy efficiency metrics are optimized. The enhanced system performance achieved by cross-layer designs in wireless networks motivates this research. The aim of the thesis is to propose and analyze novel cross-layer energy-efficient transmit antenna selection schemes that enhance energy efficiency and system performance - with regard to throughput, transmission latency, packet error rate and receiver buffer requirements.

Firstly, this thesis derives the analytical expression for data link throughput for point-to-point spatial multiplexing multiple-antenna systems - which include MIMO and underlay CR MIMO systems - equipped with linear receivers with N-process stop-and-wait (N-SAW) as the automatic repeat request (ARQ) protocol. The performance of cross-layer transmit antenna selection, which maximizes the derived throughput metric, is then analyzed. The impact of packet size, number of SAW processes and the stalling of packets inside the receiver reordering buffer is considered in the investigation. The results show that the cross-layer approach, which takes into account system characteristics at both the data link and physical layers, has superior performance in comparison with the conventional physical-layer approach, which optimizes capacity.

Secondly, this thesis proposes a cross-layer energy efficiency metric, based on the derived system throughput. Energy-efficient transmit antenna selection for spatial multiplexing MIMO systems, which maximizes the proposed cross-layer energy efficiency metric, by jointly optimizing the transmit antenna subset and transmit power, subject to spectral efficiency and transmit power constraints, is then introduced and analyzed. Additionally, adaptive modulation is incorporated

into the proposed cross-layer scheme to enhance system performance. Cross-layer energy-efficient transmit antenna selection for underlay CR MIMO systems, where interference constraints now come into play, is then considered.

Lastly, this thesis develops novel reduced complexity versions of the proposed cross-layer energy-efficient transmit antenna selection schemes - along with detailed complexity analysis - which shows that the proposed cross-layer approach attains significant energy efficiency and performance gains at affordable computational complexity.

Chapter 1 Introduction

In the past decades, the technological trend of ubiquitous access and connectivity has been gaining momentum. To meet these requirements, the traditional communication concept based on wired networks, has evolved into a heterogeneous approach. This approach aims to achieve global coverage by incorporating different access technologies, and thereby providing the desired convenience and mobility to subscribers. Examples of wireless access technologies include Bluetooth, Wireless Fidelity (Wi-Fi), Worldwide Interoperability for Microwave Access (WiMAX) and Long Term Evolution (LTE) / LTE-advanced (LTE-A). Transport Control Protocol/Internet Protocol (TCP/IP) has been adopted in heterogeneous networks to facilitate interoperability between the different access technologies.

In addition to providing ubiquitous access, current and future wireless networks are expected to provide communication services at high speeds and reliability. MIMO is an innovative technique that significantly increases the spectral efficiency and reliability of wireless links [1] [2]. More specifically, the capacity of spatial multiplexing MIMO systems over fading channels increases linearly with the number of transmit-receive antenna pairs [1]. MIMO has become an essential part of wireless communication standards including Wi-Fi IEEE 802.11n [3], WiMAX IEEE 802.16m and LTE / LTE-A [4].

The proliferation of wireless devices, coupled with the rapid deployment of high-data rate communication services and applications, has seen an increasing demand for spectrum. However, the application of the fixed spectrum allocation policy has resulted in the inefficient use of the limited radio spectrum. The low utilization of most of the licensed spectrum, calls for innovative techniques that can exploit the available spectrum more dynamically and efficiently. Cognitive radio (CR) is an emerging technology promising increased spectrum utilization by enabling unlicensed users to access licensed spectrum opportunistically [5]. Therefore, the combination of cognitive radio and MIMO promises improved transmission performance for future wireless systems.

The need for ubiquitous high-speed wireless communications has seen a transition to wireless technologies that offer enhanced data rates and expanded coverage areas. For example, in cellular networks, there has been an evolution from third-generation (3G) standards, e.g., Universal Mobile Telecommunications System (UMTS), to fourth-generation (4G) standards, e.g., LTE-A. Evolving business and consumer demands, which include new innovative ways of using the wireless network, have triggered interest in developing a comprehensive standard for the upcoming fifth-generation (5G) wireless system [6].

The deployment of more powerful and faster wireless technologies, coupled with the increased number of subscribers, has resulted in rising energy costs and increased carbon footprint associated with operating wireless networks [7]. On the other hand, there has been an increased deployment of wireless networks that rely on power-constrained devices, e.g., wireless sensor networks [8]. Additionally, innovative ways of using wireless communications and power-constrained devices have emerged, e.g., device-to-device (D2D) communications [9]. Consequently, there is interest among academics and industrial researchers in developing techniques that reduce energy consumption in wireless networks.

1.1 Motivation

Antenna selection is a signal-processing technique that provides a cost-effective solution to the problem of increased hardware complexity and cost, attributed to the multiple radio frequency (RF) chains, associated with multiple antennas [10]. Antenna selection selects the subset of transmit/receive antennas, that optimize a given criterion, for transmission purposes. In the context of multiple antennas, channel capacity can be enhanced by performing some form of pre-processing at the transmitter [11]. Transmit antenna selection is a promising pre-processing technique; this is because it offers a solution that has low implementation cost and feedback requirements compared with other performance-enhancing techniques, such us, beamforming and precoding [12] [13]. Because of its practical simplicity and effectiveness, transmit antenna selection has been considered for the uplink of LTE-A [14].

The major performance metrics and optimization criteria in the design of antenna selection are capacity and error rate. Increasing global concern regarding energy consumption has seen the emergence of antenna selection approaches that are optimal with respect to energy efficiency. Recent works have investigated MIMO systems with energy-efficient antenna selection [15] [16], where the energy efficiency (EE) of the MIMO system is optimized. In these works, the EE is quantified in terms of "bits per Joule"; and it is defined as the ratio of the capacity to the total power consumed by the system. Consequently, the EE metric is a physical-layer metric; and such a physical-layer approach does not exploit the information available at the upper layers.

The implementation of the layered TCP/IP protocol stack in wireless networks comes with challenges brought about by the fragile nature of wireless links. In such a context, cross-layer designs, which combine functionalities and information from different protocol layers - in order to improve the performance of wireless systems - have been proposed in literature [17].

1.2 Problem Statement

Some research works have considered energy-efficient antenna selection for multiple-antenna systems in literature – however, these studies investigated energy-efficient antenna selection from a physical-layer perspective. Cross-layer designs enhance the overall performance of wireless systems; therefore, existing energy-efficient antenna selection approaches are not necessarily optimal in terms of energy efficiency and overall system performance. Consequently, the study of energy-efficient antenna selection, from a cross-layer perspective, is an open research problem.

1.3 Research Aim and Objectives

This thesis focuses on investigating the performance of energy-efficient transmit antenna selection for point-to-point spatial multiplexing multiple-antenna systems, from a cross-layer perspective - this is in contrast to other works, which restrict themselves to optimizing physical-layer energy

efficiency metrics. More specifically, the aim of this thesis is to propose a cross-layer energy efficiency metric – that utilizes parameters from the data link and physical layers; then use it to develop novel transmit antenna selection algorithms, for designing multiple-antenna systems - with high spectral efficiency and high energy efficiency - combined with an overall enhanced system performance, with reasonable computation complexity.

The framework chosen for the thesis is that of un-coded spatial multiplexing multiple-antenna systems, identified for this study as both MIMO and underlay CR MIMO systems; equipped with zero forcing (ZF) linear receivers with N-SAW as the ARQ protocol. Consequently, this thesis sets the following specific objectives:

- To derive an analytical expression for the data link throughput - for the proposed framework - and then analyze the performance of cross-layer transmit antenna selection, which maximizes the derived cross-layer selection criterion.
- To propose and derive an analytical expression for a cross-layer energy efficiency metric, based on the derived system throughput.
- To develop and analyze cross-layer transmit antenna selection schemes, which maximize the proposed throughput-based energy efficiency metric, by jointly optimizing the transmit antenna subset and the transmit power, subject to transmit power and spectral efficiency constraints.
- To develop algorithms that reduce the complexity of the proposed optimal exhaustive search cross-layer energy-efficient transmit antenna selection schemes.

1.4 Thesis Outline

The thesis consists of six chapters - the rest of the chapters in this thesis are structured as follows:

Chapter 2 first provides some fundamental background information on MIMO, CR, energy efficient wireless systems, cross-layer designs and conventional antenna selection techniques. The chapter then presents a literature review of the related works on energy-efficient antenna selection.

Chapter 3 investigates the performance of transmit antenna selection for spatial multiplexing MIMO systems, from a cross-layer perspective. An analytical expression for throughput, the cross-layer optimization criterion, for MIMO systems with N-SAW at the data link layer, is first derived. The performance of throughput-based transmit antenna selection is analyzed by comparing it with that of a physical-layer approach, which optimizes the capacity of the MIMO system. Finally, the proposed cross-layer design is extended to underlay CR MIMO systems, where the performance of throughput-based transmit antenna selection, subject to interference constraints at the primary user receiver(s), is analyzed.

The results in this chapter have been published in a journal paper [J-1] and in two conference papers [C-1] [C-2].

Chapter 4 investigates the performance of spatial multiplexing MIMO systems with cross-layer energy-efficient transmit antenna selection. A cross-layer energy efficiency metric, defined as the ratio of the throughput to the total power consumption of the system, is proposed. The throughput expression derived in Chapter 3, is used in the derivation of the analytical expression of the cross-layer energy efficiency metric. Energy-efficient transmit antenna selection, based on exhaustive search, which maximizes the proposed cross-layer energy efficiency metric by jointly optimizing the transmit antenna subset and transmit power, subject to transmit power and spectral efficiency constraints, is proposed and its performance is then evaluated. Moreover, low complexity algorithms that achieve near-optimal performance, as compared with the optimal exhaustive search method, are proposed.

The results in this chapter have been published in a conference paper [C-3], accepted for publication in a conference paper [C5], and submitted to a journal [J-2] for possible publication.

Chapter 5 extends the proposals in Chapter 4 to underlay CR MIMO systems, configured to exploit spatial multiplexing. Optimal exhaustive search and low complexity near and sub-optimal energy-

efficient transmit antenna selection algorithms, which maximize the cross-layer energy efficiency by jointly optimizing the transmit antenna subset and transmit power subject to spectral efficiency and interference (at the primary user receiver) constraints, are developed and analyzed.

Some of the results in this chapter are published in a conference paper [C-4].

Chapter 6 – This chapter concludes the study by summarizing the thesis and highlighting the main results and contributions. Suggestions for future work, based on this research, are also provided.

1.5 Publications

The main contributions of this thesis are contained in the following journals and conference papers.

[J-1] E. M. Okumu and M. E. Dlodlo, "Transmit antenna selection for multiple antenna systems with stall avoidance", *Computers and Electrical Engineering*, 58, pp. 144-153, 2017

[J-2] E. M. Okumu and M. E. Dlodlo, "Performance analysis of cross-layer energy efficient transmit antenna selection", *Computers and Electrical Engineering*, Submitted

[C-1] E. M. Okumu and M. E. Dlodlo, "Performance evaluation of N-process stop and wait in MIMO systems with transmit antenna selection", *Wireless Communications, Signal Processing and Networking (WiSPNET), International Conference on, IEEE*, pp.957-961, 2016

[C-2] E. M. Okumu and M. E. Dlodlo, "Throughput based transmit antenna selection for underlay CR MIMO systems", *Advanced Networks and Telecommunications Systems (ANTS), IEEE International Conference on*, pp.1-6, 2016

[C-3] E. M. Okumu and M. E. Dlodlo, "Energy efficient transmit antenna selection for MIMO systems: a cross layer approach", *Computing and Communication Workshop and Conference (CCWC), IEEE 7th Annual*, pp.1-6, 2017

[C-4] E. M. Okumu and M. E. Dlodlo, “Optimal and sub-optimal iterative cross-layer energy efficient schemes for CR MIMO systems with antenna selection”, *Smart Technologies, IEEE EUROCON, 17th International Conference on,* pp. 62-67, 2017.

[C-5] E. M. Okumu and M. E. Dlodlo, “Correlated MIMO systems with cross-layer energy efficient antenna selection”, *Global Wireless Summit,* pp. 57-61, 2017

Chapter 2 Background

This chapter provides some background information on the techniques and mechanisms encompassed in this thesis. An overview of the MIMO and CR techniques is presented in Sections 2.1 and 2.2 respectively. Section 2.3 presents the basic concepts of energy efficient wireless systems. The fundamentals of cross-layer design and conventional antenna selection are found in Sections 2.4 and 2.5 respectively. Section 2.6 provides a literature review on energy-efficient antenna selection. Finally, Section 2.7 concludes the chapter.

2.1 MIMO Wireless Systems

The provision of quality high-speed wireless communication services faces some challenges, including but not limited to, limited radio spectrum availability, multipath propagation and fading. The use of multiple antennas at the transmitter/receiver is an innovative technique that significantly overcomes these challenges by improving the spectral efficiency and the link reliability of wireless systems. Figure 2.1 illustrates the different antenna configurations for multiple-antenna wireless systems. In Figures 2.1 a) to d), single-input single-output (SISO), single-input multiple-output (SIMO), multiple-input single-output (MISO) and MIMO configurations are depicted for the single user scenario, i.e., point-to-point wireless systems. The MIMO multi-user (MIMO-MU) configuration, which consists of a base station equipped with multiple transmit/receive antennas that communicate with multiple users, each equipped with one transmit/receive antenna, is depicted in Figure 2.1 e). In the MIMO-MU configuration, the users can also be equipped with multiple transmit/receive antennas.

The focus of this thesis is on point-to-point MIMO systems, consequently, the fundamentals of MIMO wireless systems are presented in this section.

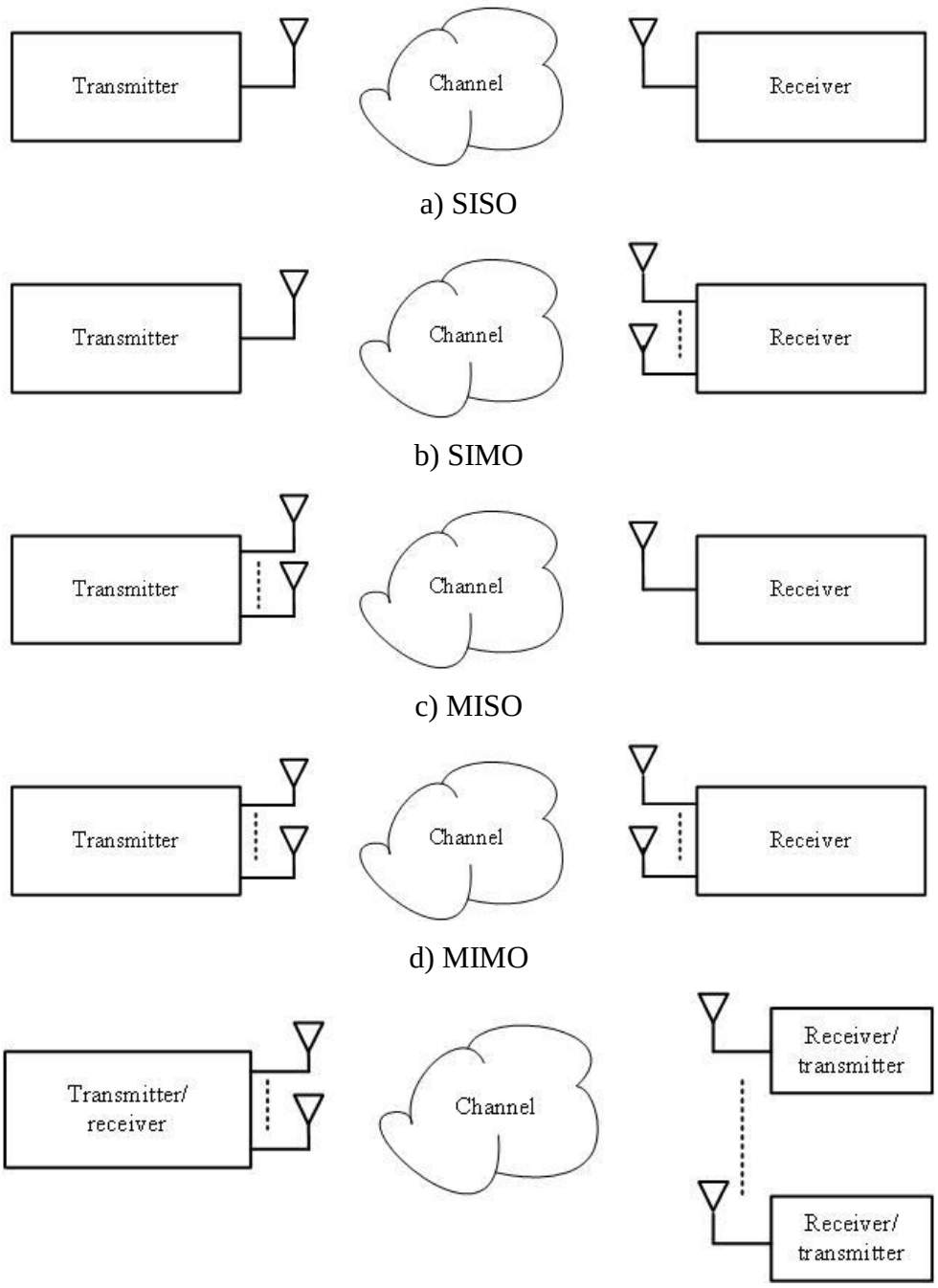

Figure 2.1. Antenna configurations for multiple-antenna wireless systems

2.1.1 MIMO System and Signal Model

Let us consider a point-to-point MIMO system with M_T transmit antennas and N_R receive antennas, as shown in Figure 2.2. The MIMO channel is assumed to have a bandwidth of 1 Hz and to experience frequency flat Rayleigh fading over the bandwidth in consideration. The transmit power, available over a symbol period of 1 second, is assumed to be P_T. The MIMO signal model, in matrix form, is represented by [11]:

$$\boldsymbol{y} = \sqrt{\frac{P_T}{M_T}}\boldsymbol{H}\boldsymbol{s} + \boldsymbol{n} \tag{2.1}$$

where $\boldsymbol{H} \in \mathbb{C}^{N_R \times M_T}$ is the MIMO channel, $\boldsymbol{y} \in \mathbb{C}^{N_R \times 1}$ the received signal vector, $\boldsymbol{s} \in \mathbb{C}^{M_T \times 1}$ the transmitted signal vector and $\boldsymbol{n} \in \mathbb{C}^{N_R \times 1}$ the noise vector. The elements of $\boldsymbol{H}$ are assumed to be zero mean circularly symmetric complex Gaussian (ZMCSCG) with unit variance; and $\boldsymbol{n}$ is assumed to have ZMCSCG elements with a variance of N_o. $\boldsymbol{s}$ is assumed to have zero mean symbols with a covariance matrix of $\boldsymbol{R}_{ss} = \mathcal{E}\{\boldsymbol{s}\boldsymbol{s}^H\}$, that must satisfy $Tr(\boldsymbol{R}_{ss}) = M_T$, in order to constrain the total average energy transmitted over a symbol period.

2.1.2 Capacity of MIMO Channels

In this section, the capacity of a frequency flat fading channel is described, with $\boldsymbol{H}$ assumed to be deterministic and perfectly known at the receiver. The channel can be estimated at the receiver by using training signals, blind estimation techniques or semi-blind techniques [18] [19] [20] [21]. The mutual information between $\boldsymbol{s}$ and $\boldsymbol{y}$ is given as [22] [23]:

$$I(\boldsymbol{s};\boldsymbol{y}) = log_2 det\left[\boldsymbol{I}_{N_R} + \frac{P_T}{M_T N_o}\boldsymbol{H}\boldsymbol{R}_{ss}\boldsymbol{H}^H\right] \; bits/Hz/s \tag{2.2}$$

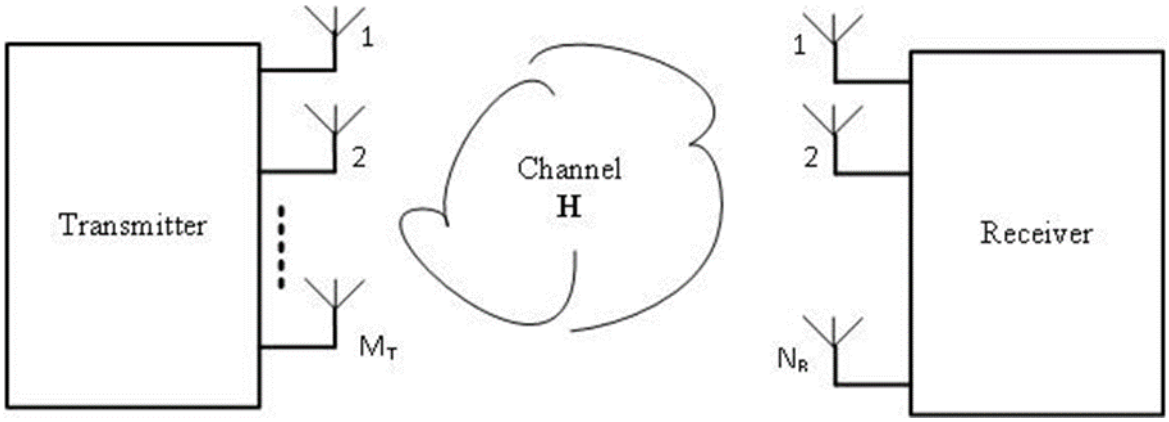

Figure 2.2. Block diagram of a MIMO wireless system

The capacity of the deterministic MIMO channel is obtained by maximizing $I(\boldsymbol{s};\boldsymbol{y})$ as given below [23]:

$$C = \max_{Tr(\boldsymbol{R}_{ss})=M_T} log_2 det\left[\boldsymbol{I}_{N_R} + \frac{P_T}{M_T N_o}\boldsymbol{H}\boldsymbol{R}_{ss}\boldsymbol{H}^H\right] \; bits/Hz/s \tag{2.3}$$

When the channel is unknown at the transmitter, the most logical strategy consists of selecting the transmit symbol vector, so that $\boldsymbol{R}_{ss} = \boldsymbol{I}_M$ [11]. This implies that the transmitted signals are independent (uncorrelated), with equal transmit powers. Therefore, the capacity of the MIMO channel, in the absence of channel knowledge at the transmitter is:

$$C = log_2 det\left[\boldsymbol{I}_{N_R} + \frac{P_T}{M_T N_o}\boldsymbol{H}\boldsymbol{H}^H\right] \; bits/Hz/s \tag{2.4}$$

which can be expressed as [11]:

$$C = \sum_{i=1}^{r} log_2\left(1 + \frac{P_T}{M_T N_o}\varrho_i\right) \; bits/Hz/s \tag{2.5}$$

where r is the rank of $\boldsymbol{H}$ and ϱ_i (for $i = 1,2,\ldots r$) are the positive *eigenvalues* of $\boldsymbol{H}\boldsymbol{H}^H$. Consequently, the capacity of the MIMO channel, when the channel is unknown at the transmitter,

can be expressed as the sum of the capacities of r parallel sub-channels (SISO) - each with a power gain of ϱ_i - with the transmit power allocated equally amongst the transmit antennas, i.e. P_T/M_T.

MIMO opens up multiple sub-channels between the transmitter and receiver - these can only be accessed (processed) when the channel is known at the transmitter. In general, the channel can be estimated at the transmitter using one of two techniques, i.e., channel estimation using feedback or reciprocity [11]. When the channel is known at the transmitter and receiver, $\boldsymbol{H}$ can be explicitly decomposed into r parallel spatial sub-channels through the linear processing of the signals at the transmitter and receiver [22] [23] [24]. To accomplish this, the singular value decomposition (SVD) of $\boldsymbol{H}$ is first determined as follows:

$$\boldsymbol{H} = \boldsymbol{U}\boldsymbol{\Sigma}\boldsymbol{V}^H \tag{2.6}$$

where $\boldsymbol{U} \in \mathbb{C}^{M_T \times r}$ and $\boldsymbol{V} \in \mathbb{C}^{N_R \times r}$ satisfy $\boldsymbol{U}^H\boldsymbol{U} = \boldsymbol{V}^H\boldsymbol{V} = \boldsymbol{I}_r$. $\boldsymbol{\Sigma}$ is a diagonal matrix given by $\boldsymbol{\Sigma} = \{diag[\sigma_1, \sigma_2, \ldots \sigma_r];\ \sigma_i \geq 0;\ \sigma_i \geq \sigma_{i+1}\}$ where σ_i is the ith singular value of $\boldsymbol{H}$ [25]. $\boldsymbol{V}$ is used to process the signal prior to transmission, while the received signal is processed using $\boldsymbol{U}^H$, this effectively decomposes $\boldsymbol{H}$ into r parallel sub-channels. The capacity of the MIMO channel, with the channel known at the transmitter, can now be expressed as:

$$C = \sum_{i=1}^{r} log_2\left(1 + \frac{P_T\gamma_i}{M_T N_o}\varrho_i\right)\ bits/Hz/s \tag{2.7}$$

where γ_i represents the transmit power for the ith sub-channel. Since the sub-channels are now accessible, the transmitter can now allocate transmit power to the sub-channels in order to maximize the mutual information. The optimal power allocation policy is determined iteratively by using the waterfilling algorithm [23] [26] [27]. For each iteration, ite, the constant μ, referred to as the water level, is first determined by using:

$$\mu = \frac{M_T}{r - ite + 1}\left[1 + \frac{N_o}{P_T}\sum_{i=1}^{r-ite+1}\frac{1}{\varrho_i}\right] \tag{2.8}$$

The power allocated to the ith sub-channel is then calculated using:

$$\gamma_i = \left(\mu - \frac{M_T N_o}{P_T \varrho_i}\right) \quad i = 1,2, \ldots r - p + 1 \tag{2.9}$$

The iteration process terminates when the optimal power allocation for each sub-channel, γ_i^o, has been determined; and this happens when $\sum_{i=1}^{r} \gamma_i^o = M_T$ and $\gamma_i^o \geq 0$ for all i are satisfied. The waterfilling algorithm allocates transmit power to sub-channels depending on the conditions they are currently experiencing. Sub-channels with good conditions are assigned more power and vice versa. This results in a capacity greater than or equal to when the MIMO channel is unknown at the transmitter.

The capacity, C, in (2.3), (2.4), (2.5) and (2.7) is referred to as the spectral efficiency. In actual fact, it is the normalized capacity with respect to the bandwidth. Therefore, given a bandwidth of $B\ Hz$, the capacity is simply $CB\ bits/s$. In this thesis, capacity will be used to refer to the normalized capacity as well; since this is common in literature.

The channel, $\boldsymbol{H}$, was assumed to have ZMCSCG elements with unit variance. The channel can only be modelled thus if a rich scattering environment is assumed, with the antenna spacing at both the transmitter and receiver being assumed to be sufficient. In practical scenarios, this might not be the case because of the existence of some factors, which includes spatial correlation, polarized antennas, the presence of line-of-sight components and the pin-hole effect [11]. These factors can have a negative influence on the capacity of the MIMO channel.

2.1.3 MIMO Techniques

In general, point-to-point MIMO systems are designed with the aim of exploiting spatial diversity, spatial multiplexing or beamforming. The focus of this thesis is on spatial multiplexing MIMO systems. This section presents an overview of these MIMO coding techniques.

2.1.3.1 Spatial Diversity

Diversity is a powerful technique used to combat fading in wireless channels; fading is the random fluctuation in signal power that occurs across space, time and frequency. Diversity provides the receiver with multiple replicas of the same signal transmitted over ideally independent fading links; and each replica constitutes a diversity branch. The proper combining of the replicas at the receiver results in improved link reliability, effectively stabilizing the wireless link [11]. Diversity can be implemented in either the frequency, time or space domains. Among the three, spatial diversity is preferred; because it provides diversity without additional transmission time or bandwidth expenditure; while additionally providing increased signal to noise (SNR) due to array gain, i.e. signal enhancement due to the coherent combining of signals at the receiver. The effectiveness of diversity is determined by the number of diversity branches and it is known as the diversity order. Spatial diversity can be divided into two categories, receive and transmit diversity.

Extracting receive diversity requires a wireless system equipped with multiple antennas at the receiver. Each antenna receives an independently faded version of the same transmitted signal; these are then combined in order to improve the signal quality. The optimal combining technique for receive diversity is maximal ratio combining (MRC); MRC requires perfect knowledge of the channel at the receiver. The MRC technique first weights the signals received by each antenna in a manner that maximizes the SNR [28]. MRC is optimal since it achieves full diversity. For example, a SIMO system with N_R receive antennas has a diversity order equal to N_R and an array gain of N_R [11].

Transmit diversity is extracted from systems with multiple transmit antennas; additionally, exploiting transmit diversity requires the transmission of pre-coded redundant signals over multiple transmit antennas. The transmit diversity technique used depends on whether there is channel knowledge at the transmitter or not. A classic transmit diversity technique, that does not require channel knowledge at the transmitter, is the Alamouti scheme [2]. The Alamouti technique assumes a MISO channel with two transmit antennas, therefore, the channel vector is given by $\boldsymbol{h} = [h_1 \quad h_2]$. The signal vectors $[s_1 \quad s_2]^T$ and $[-s_2^* \quad s_1^*]^T$ are transmitted consecutively over two symbol periods. At the receiver, a rearranged received signal vector is reformatted as, $\boldsymbol{y} =$

$[y_1 \quad y_2^*]^T$, where y_1 and y_2 are the signals received over the two consecutive symbol periods, assuming that the channel is frequency flat, and that it remains constant over the two symbol periods; $\boldsymbol{y}$ can be expressed as:

$$\boldsymbol{y} = \sqrt{\frac{P_T}{2}}\begin{bmatrix} h_1 & h_2 \\ h_2^* & -h_1^* \end{bmatrix}\begin{bmatrix} s_1 \\ s_2 \end{bmatrix} + \begin{bmatrix} n_1 \\ n_2^* \end{bmatrix} = \sqrt{\frac{P_T}{2}}\boldsymbol{H}_{eff}\boldsymbol{s} + \boldsymbol{n} \tag{2.10}$$

The effective channel matrix, $\boldsymbol{H}_{eff}$, is orthogonal, i.e. $\boldsymbol{H}_{eff}^H\boldsymbol{H}_{eff} = \|\boldsymbol{h}\|_F^2\boldsymbol{I}_2$. The Alamouti scheme extracts full diversity, i.e. a diversity order of 2, even in the absence of channel knowledge at the transmitter. Because of the absence of channel knowledge at the transmitter, the Alamouti scheme has no array gain. The Alamouti technique can be used to extract diversity in MIMO systems with two transmit antennas and any number of receive antennas. The Alamouti scheme shows that transmit diversity, in the absence of channel knowledge at the transmitter, can be realized using space-time coding.

There are several classes of space-time codes (STC) in literature, designed to exploit spatial diversity without channel knowledge at the transmitter, with the most popular being Orthogonal Space-Time Block Codes (OSTBC) [29] and Space time trellis codes (STTC) [30]. The Alamouti scheme is an example of an OSTBC, and from the discussions above, we can extract the main particularity of OSTBCs; i.e. the structure of the transmitted signal is such that the effective channel is rendered orthogonal regardless of the channel realization. The advantage of the effective channel matrix, $\boldsymbol{H}_{eff}$, being orthogonal is that it allows the transmitted symbols to be decoupled easily at the receiver by using simple linear processing. The orthogonality of $\boldsymbol{H}_{eff}$ also ensures that the elements of the noise vector, $\boldsymbol{n}$, are ZMCSCG; and therefore, independent optimal maximum likelihood (ML) detection can be carried out for each transmitted symbol. Orthogonal space-time codes words for OSTBC systems with any number of transmit antennas can be designed by using the solution to the Hurwitz-Radon problem [29] [31]. OSTBCs extracts the full diversity gain of $M_T N_R$, for the general MIMO channel with M_T transmit and N_R receive antennas [11].

As for STTC, the codes are an extension of the conventional trellis code to multiple-antenna systems [32]. In contrast to OSTBCs, STTCs can be designed to extract both diversity gain and coding gain, thereby resulting in a better bit error performance. However, decoding STTCs requires a multidimensional Viterbi decoder, whereby the computational complexity increases exponentially with the number of states.

When the channel is known at the transmitter, transmit diversity may be exploited by appropriately weighting the signal and then transmitting from each transmit antenna, with the weight vector chosen to maximize the SNR. The technique used to extract diversity for MISO systems is known as transmit maximal ratio combining (T-MRC) [29] [33], while that used for MIMO systems is known as the dominant *eigenmode* transmission [11]. The techniques extract full diversity order.

2.1.3.2 Spatial Multiplexing

Spatial multiplexing is used to improve the capacity of wireless channels. Consider an un-coded input data stream with a rate of δ; spatial multiplexing divides the data stream, at the physical layer, into M_T lower rate sub-streams of equal rate, i.e. δ/M_T. The sub-streams are then transmitted simultaneously from M_T transmit antennas over the same frequency band. Under favourable channel conditions, the signals induce unique signatures at the receiver; this, coupled with channel knowledge at the receiver, enables the separation of the received signal into parallel sub-streams. MIMO systems configured to exploit spatial multiplexing require that $M_T \leq N_R$ (where N_R is the number of receive antennas), in order to ensure the proper recovery of the transmitted signal at the receiver [10]. Spatial multiplexing linearly increases the data rate or capacity without any additional bandwidth or transmit power being required. The linear increase in capacity is limited by the lesser of the number of transmit and receive antennas, i.e.$\min(M_T, N_R)$ [11]. Consequently, spatial multiplexing is a very powerful technique for increasing the capacity of wireless systems, which allows support for high data rate applications.

In general, spatial multiplexing is used as a coding technique in wireless scenarios where there is no channel knowledge at the transmitter. The most popular encoder structures for spatial

multiplexing, with the channel unknown at the transmitter, are horizontal encoding (HE), vertical encoding (VE) and diagonal encoding (DE).

In HE, the input data stream is first divided into sub-streams, which are processed independently at the physical layer - before being transmitted. The processing includes, but is not limited to, channel coding, interleaving and modulation. HE, depicted in Figure 2.3, can achieve a diversity order of up to N_R, since each symbol is transmitted from only one transmit antenna, and is received by N_R receive antennas. Therefore, HE is considered sub-optimal in terms of diversity; but this is accompanied by a simplified receiver design; since each sub-stream is decoded independently. The Horizontal Diagonal Bell Labs Layered Space-Time (H-BLAST) architecture uses this encoding strategy [11] [34]. Un-coded spatial multiplexing is the same as HE, without channel coding; and it achieves the same diversity as HE. Because of its simplicity, un-coded spatial multiplexing will be considered in this thesis.

In VE, the data stream undergoes processing before being demultiplexed; therefore, the sub-streams require joint decoding at the receiver which can be quite complex. Unlike HE, VE can achieve optimal diversity, i.e. a diversity order greater than N_R, because the symbols are spread out over more than one antenna. VE is used in the Vertical-BLAST (V-BLAST) architecture [34] [35]. In DE, the data first undergoes horizontal encoding, before being formed into code words; each code word is then divided into frames/slots, which are then passed through a stream rotator that rotates the streams in a round-robin fashion so that the bit stream to antenna association is periodically cycled [11]. This allows information bits to be spread across all the antennas, enabling DE to achieve the full diversity order of $M_T N_R$. The D-BLAST transmission technique follows such an encoding strategy [23].

Regarding detection techniques, the optimal receiver for un-coded spatial multiplexing is the ML receiver. The ML receiver decodes by performing an exhaustive search over the entire transmitted signal vector constellation in order to determine the most probable transmitted signal. Consequently, ML decoding is complex and slow; and the complexity increases exponentially with

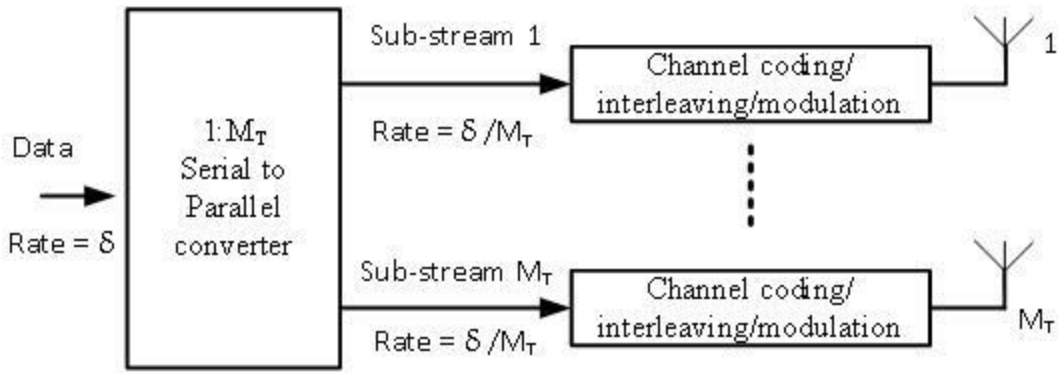

Figure 2.3. Horizontal encoding

the number of transmit antennas. Fast algorithms for sphere decoding that reduce the complexity significantly have been proposed [36] [37] [38] [39].

The decoding complexity can be further reduced by using sub-optimal linear receivers. Linear receivers use linear filters to separate the transmitted data streams before independently decoding them. Examples of linear filters include the zero forcing (ZF) and the minimum mean-squared error (MMSE) receivers. The ZF linear receiver uses a matrix filter, $\boldsymbol{G}_Z \in \mathbb{C}^{\boldsymbol{M_T \times N_R}}$, to separate the received signal into its component transmitted data streams. This is accomplished by inverting the channel, thus $\boldsymbol{G}_Z$ is given by:

$$\boldsymbol{G}_Z = \sqrt{\frac{M_T}{P_T}}\boldsymbol{H}^{\dagger} \tag{2.11}$$

Assuming that $N_R \geq M_T$ and that $\boldsymbol{H}$ has full column rank, the output of the ZF linear receiver is given by:

$$\boldsymbol{G}_Z\boldsymbol{y} = \boldsymbol{s} + \sqrt{\frac{M_T}{P_T}}\boldsymbol{H}^{\dagger}\boldsymbol{n} \tag{2.12}$$

From (2.12), it is observed that the ZF receiver decouples $\boldsymbol{H}$ into M_T parallel sub-channels ($\boldsymbol{s}$ is the $M_T \times 1$ transmit signal vector), with additive noise enhanced by $\boldsymbol{G}_Z$. The ZF linear receiver

decodes by completely eliminating multi-stream interference (MSI) at the expense of noise enhancement, resulting in significant performance degradation [11]. The SNR for the kth output data stream is given by [11] [40]:

$$\rho_k = \frac{P_T}{N_o M_T [(\boldsymbol{H}^H \boldsymbol{H})^{-1}]_{k,k}} \tag{2.13}$$

On the other hand, the MMSE receiver balances MSI mitigation with noise enhancement resulting in a minimized total error rate. The MMSE matrix filter, $\boldsymbol{G}_M$, is given by:

$$\boldsymbol{G}_M = \sqrt{\frac{M_T}{P_T}} \left(\boldsymbol{H}^H \boldsymbol{H} + \frac{M_T N_o}{P_T} \boldsymbol{I}_{M_T} \right)^{-1} \boldsymbol{H}^H \tag{2.14}$$

The output of the MMSE receiver consists of M_T decoded streams, with a SNR of [11]:

$$\rho_k = \frac{1}{\left[\left(\frac{P_T}{N_o M_T} \boldsymbol{H}^H \boldsymbol{H} + \boldsymbol{I}_{M_T} \right)^{-1} \right]_{k,k}} - 1 \tag{2.15}$$

Besides linear receivers, nonlinear detectors, e.g. successive cancellation (SUC) receivers, are also considered for spatial multiplexing systems. SUC receivers use layer peeling where the symbols are successively decoded and stripped away layer by layer. SUC receivers incorporate ZF or MMSE receivers and are more complex to implement than linear receivers. An example of a SUC receiver is the ordered successive cancellation receiver used for the V-BLAST [35] [41]. SUC receivers have sub-optimal performance; but they outperform ZF receivers; the performance is comparable or better than that of MMSE receivers, depending on the implementation.

In this thesis, linear receivers will be used, because of their reduced complexity; more specifically, the ZF linear receiver. Even though the MMSE receiver has a better performance than the ZF linear receiver, the ZF receiver is simpler to implement. Also, the SNR performance of MMSE at high SNR values is the same as that of the ZF linear receiver [11].

2.1.3.3 Beamforming

In beamforming, a directional beam pattern for the transmit/receive antenna array is created by controlling the phase and/or amplitude of the signals at the antenna elements. Additionally, the beam pattern can be steered in the desired direction. Beamforming can be used to improve the received SNR or to suppress co-channel interference (CCI) in a MU scenario, thereby improving the signal-to-interference plus noise ratio (SINR) at the receiver [42].

2.2 Cognitive Radio

The radio spectrum is a limited resource; spectrum regulatory authorities have traditionally shared it through the fixed spectrum access (FSA) policy. The application of FSA has established order by providing noninterfering wireless communication services. However, the high demand for spectrum has created two challenges for FSA, namely: Spectrum scarcity and spectrum underutilization. Spectrum scarcity has arisen from the licensing out of most of the available spectrum. Studies on actual spectrum utilization have revealed that large portions of the licensed spectrum are underutilized [43] [44], with most of the licensed users either using their assigned spectrum for short periods of time or not at all. The study in [45] highlighted that most bands allocated through FSA are used only in limited geographical regions, or over limited time periods, with the average utilization varying between $15\% - 85\%$. The FSA policy does not allow allocation of unutilized licensed spectrum to new applicants; even if it is only for those periods of time, when the licensed user is not using it. Studies show that the inflexibility and inefficiency of FSA contributes significantly to the spectrum underutilization problem.

The challenges mentioned above motivated the development of CR technology; the aim of which is to alleviate the problem of spectrum underutilization. The concept of cognitive radio was first proposed by J. Mitola [46]. CR technology enhances spectrum utilization by enabling unlicensed secondary users (SUs), i.e. CR users, to opportunistically access the radio spectrum allocated to the licensed primary users (PUs). Software-defined radio (SDR) has made implementing CR

networks possible. Unlike traditional wireless devices, which are designed to operate in a particular frequency band, SDRs are capable of operating in a wide range of frequencies. SDRs alter RF operating parameters using software; thereby giving CRs the ability to adapt their transmission parameters swiftly [47]. Motivated by this, some spectrum regulatory bodies (communication commissions) have been considering the more flexible and comprehensive use of the available spectrum by using the CR technology [48] [49]. Additionally, practical cognitive networks have been implemented, thereby proving that they are realizable and promising [50].

2.2.1 CR Spectrum-Access Models

A CR user can access licensed spectrum by using one of two distinct spectrum-access models; spectrum overlay and spectrum underlay access models [51], which are described below;

- In the overlay spectrum-access model, the CR user utilizes adaptive techniques to determine when, and on which spectrum band to transmit. The SU conducts spectrum sensing to determine which portions of the spectrum are available. The SU selects the best available channel; and then it reconfigures its transmission parameters to enable it to communicate in the identified band. While communicating, the SU has to monitor the spectrum continually; and when the licensed user is detected, the SU has to vacate the channel [47].
- In the underlay spectrum-access model, the CR user occupies the same bandwidth as a licensed user, i.e., the SU and PU access the spectrum concurrently. The SU has to transmit at power levels, such that the interference power produced at the PU receiver (PU RX) is below a predetermined threshold value. Therefore, the SU has to continually adapt its transmit power to ensure that its communications appear as white noise at the PU RX [47] [51].

Of the two spectrum-access models, the overlay model results in the highest spectrum efficiency. The disadvantage of the overlay access model is that it can be quite complex to implement; and

this is because detecting the available spectrum bands and the resumption of PU communications in a timely manner, is difficult. If the SU starts communicating prematurely or delays in vacating the licensed spectrum, then the performance of the PU can be severely affected. On the other hand, the underlay access model realizes lower spectrum efficiency; but its implementation is less complex. The CR user has to have the capability of predicting the interference power that its transmissions would produce at the PU RX. This thesis will focus on the underlay spectrum-access model.

2.2.2 Underlay CR MIMO Systems

SUs in underlay CR systems usually have limited access to transmission resources; since they have to transmit at low powers to ensure that their communications do not degrade the performance of the PUs. The MIMO technology brings about improved data rates by exploiting spatial multiplexing; and the increased spectral efficiency is achieved at no additional cost as regards bandwidth and transmit power [11]. Therefore, the spectrum efficiency of CRs can be improved significantly by equipping them with multiple antennas. Additionally, in underlay CR systems, multiple antennas can be used to control the interference caused at the PU RXs.

In scenarios where the SU channel is MISO, beamforming is the optimal strategy for secondary transmissions [52]; when the primary network only has a single PU RX, an optimal beamforming vector at the secondary transmitter, which results in the complete removal of interference at the PU RX, can be derived. For the more general MIMO scenario, sub-optimal and optimal techniques have been proposed in literature; their aim is to maximize the performance of the SU while keeping the interference power at the primary receivers below a predetermined threshold value [52] [53] [54]. These techniques can be quite complex to implement; therefore, in this thesis, the most intuitive and simplest method for controlling the interference at the PU RX, i.e., adapting the SU transmit power, will be used.

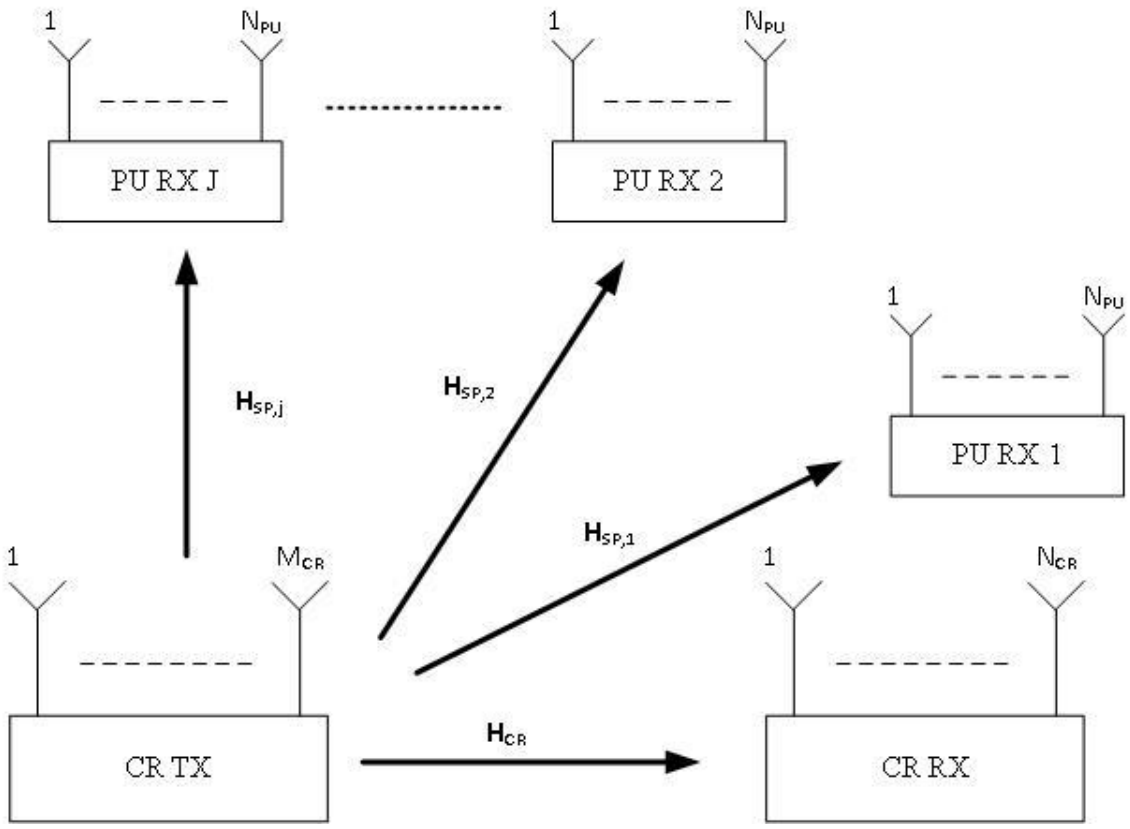

Figure 2.4. Block diagram of CR MIMO system model

2.2.2.1 Underlay CR MIMO System and Signal Model

Let us consider a wireless system where the secondary and primary networks coexist over the same spectrum band, whose bandwidth is assumed to be $1Hz$. The secondary network consists of a CR TX and CR RX equipped with M_{CR} and N_{CR} antennas respectively, as shown in Figure 2.4. The primary network consists of J primary receivers, each equipped with N_{PU} receive antennas. The cognitive (CR TX to CR RX) channel matrix, $\boldsymbol{H}_{CR} \in \mathbb{C}^{N_{CR} \times M_{CR}}$, is assumed to have ZMCSCG elements with unit variance. The interference channel for the jth PU RX, i.e. the channel from the CR TX to the jth PU RX, is represented by $\boldsymbol{H}_{SP,j}$ and is assumed to have ZMCSCG elements with a variance of α. All the channels are assumed to experience frequency flat Rayleigh fading. The signal model for the secondary network is given by:

$$\boldsymbol{y}_{CR} = \sqrt{\frac{P}{M_{CR}}}\boldsymbol{H}_{CR}\boldsymbol{s}_{CR} + \boldsymbol{n}_{CR} + \boldsymbol{I}_{PC} \tag{2.16}$$

where $\boldsymbol{y}_{CR} \in \mathbb{C}^{N_{CR}\times 1}$ is the signal received at the CR RX, $\boldsymbol{s}_{CR} \in \mathbb{C}^{M_{CR}\times 1}$ is the transmitted cognitive signal vector, $\boldsymbol{n}_{CR} \in \mathbb{C}^{N_{CR}\times 1}$ is the noise vector, P is the cognitive transmit power in one symbol period and $\boldsymbol{I}_{PC}$ represents the interference received form the PU TX(s), which is/are not shown in Figure 2.4. $\boldsymbol{n}_{CR}$ is assumed to have ZMCSCG elements with a variance of N_o. $\boldsymbol{s}_{CR}$ is assumed to have zero mean symbols with a covariance matrix $\boldsymbol{Q}_{CR} = \mathcal{E}\{\boldsymbol{s}_{CR}\boldsymbol{s}_{CR}^H\}$ that must satisfy $Tr(\boldsymbol{Q}_{CR}) = M_{CR}$ in order to constrain the total average energy transmitted over a symbol period.

The transmit power P, is limited by the cognitive user's transmit power constraint, together with the interference power constraints at the PU RX(s). If the maximum available cognitive transmit power in a symbol period (assumed to be 1 second) is P_T, then $P \leq P_T$. However, P must also satisfy the interference power constraints at the PU RX(s). The interference power at each PU RX will be calculated by using the total interference model [52]. Using this model, the interference power received by each PU RX is the sum of the interference powers received over all the receive antennas. Therefore, for each PU RX, the interference power due to cognitive transmissions is given by:

$$\frac{P}{M_{CR}} Tr\left(\boldsymbol{H}_{SP,j}\boldsymbol{Q}_{CR}\boldsymbol{H}_{SP,j}^H\right) \quad j = 1,2,\ldots J \tag{2.17}$$

If the secondary network is assumed to exploit spatial multiplexing, then $\boldsymbol{Q}_{CR} = \boldsymbol{I}_{M_{CR}}$; the cognitive transmit symbols are assumed to be uncorrelated and equally powered at the transmit antennas. The interference constraints at the PU RX(s) can now be expressed as follows:

$$\frac{P}{M_{CR}} \left\|\boldsymbol{H}_{SP,j}\right\|_F^2 \leq I_j \quad j = 1,2,\ldots J \tag{2.18}$$

where $\left\|\boldsymbol{H}_{SP,j}\right\|_F^2 = Tr\left(\boldsymbol{H}_{SP,j}\boldsymbol{H}_{SP,j}^H\right)$ and I_j is the total interference power threshold for the jth PU RX. From the transmit power and interference power constraints, P has to satisfy the following:

$$P \leq P_T$$

$$P \leq \frac{I_j M_{CR}}{\left\| \boldsymbol{H}_{SP,j} \right\|_F^2} \quad j = 1,2, \ldots J \tag{2.19}$$

From (2.4), the capacity of the secondary network is given by:

$$C = log_2 det \left[\boldsymbol{I}_{N_{CR}} + \frac{P}{M_{CR}[N_o + \boldsymbol{I}_{PC} \boldsymbol{I}_{PC}^H]} \boldsymbol{H_{CR}} \boldsymbol{H}_{CR}^H \right] bits/Hz/s \tag{2.20}$$

The multiple antenna CR TX adapts its transmit power, allowing it to meet the interference constraints at the PU RX and optimize its performance, while satisfying its own transmit power requirements.

2.3 Energy Efficient Wireless Systems

Energy efficient communications, or green radio, has recently drawn interest from both the academic and industrial communities. To this end, a research direction aimed at evolved energy efficient wireless architectures and techniques has emerged. As a result, international collaborations have led to research projects dedicated to energy efficient wireless communications. These research activities include Green Radio [55], Energy Aware Radio and Network Technologies (EARTH) project [56] [57] and Optimizing Power Efficiency in Mobile Radio Networks (OPERA-Net) project [58] [59]. Some of the energy efficient proposals and techniques that have emerged out of these projects include energy-efficient hardware, energy-efficient mobile radio access networks, energy-efficient architectures and energy-efficient resource management. The focus of this thesis is on energy-efficient transmit antenna selection from a cross-layer perspective; therefore, this chapter presents the fundamentals of energy efficient communications required for this study.

2.3.1 Why Energy Efficient Wireless Communications?

In recent years, information and communication technology (ICT) has evolved rapidly vis-a-vis the growth in the number of different types of applications and services offered. This has seen a corresponding growth in the resources required to meet the ever-increasing requirements of these services and applications. One such resource is energy; the energy consumption of ICT and the related greenhouse emissions are growing at a dramatic rate. The ubiquitous deployment of mobile wireless networks has seen the energy consumption of mobile networks growing at a much faster rate than that of ICT as a whole [60]. Additionally, as the worldwide coverage of the 4G system continues to increase rapidly, mobile networks will increasingly consume more energy - due to the growth in the number of mobile subscribers, increased mobile data traffic, as well as the increased deployment of the supporting network infrastructure.

Unless effective action is taken, wireless communications will continue to consume significantly more and more energy; this has seen an interest in the design of energy efficient wireless systems from both the industry and academic researchers. The main reasons that motivate research in green communication networks are as follows: From a network operator's perspective, the main reason for reducing energy consumption is economical; this is because of the huge electricity bill associated with increased energy consumption. In [61], it is pointed out that electricity bills account for about 18% and 32% of the operation expenditure (OpEx) for cellular network operators in the European and Indian markets respectively. Therefore, improving the energy efficiency of wireless networks has significant economic benefits.

During the past decades, much effort has been made to reduce climate change, which has seen the adoption of greenhouse gas emission targets by more than 100 countries - with the aim of limiting global warming to 2% or below that, in order to mitigate the adverse effects of climate change [62]. Most economists favour the cap, trade and carbon tax approaches for reducing the greenhouse emissions [63]. These approaches create incentives for businesses and households to conserve energy, to improve energy efficiency and to adopt clean energy technologies. Therefore, the pressure of social responsibility coupled with incentives (some of which are economic) motivates network operators to implement measures to reduce their energy consumption.

From a user's perspective, green communication is also essential. With most users now using 3G/4G services, while simultaneously running energy-hungry applications (e.g. video games, streaming multimedia services. mobile TV, video sharing, etc.) on their mobile devices, the battery life of the mobile devices negatively affects the user's mobile experience [61]. The solution to the problem of limited battery life is the development of improved battery technology. However, the development of improved battery technology occurs at a slower pace than the increase in energy consumption [64]. Consequently, in the meantime, the design of energy efficient wireless networks can be used to tackle this issue.

2.3.2 Power Consumption Model

Determining the power consumption of a wireless system requires a power consumption model. A power consumption model describes how much power is consumed by a wireless system. In this thesis, the power consumption model developed in [65], which is quite popular, will be used. In this model, the total power consumed by the wireless system is the sum of the power consumed by all the signal-processing blocks at the transmitter and receiver. This model is for a generic wireless system; and the constituent signal-processing blocks at both the transmitter and receiver are as shown in Figure 2.5. The transmit signal path is made up of a digital-to-analog converter (DAC), a low-pass filter, a mixer driven by a local oscillator (LO), a filter and a high-power amplifier (PA). The receive signal path is made up of a band-pass filter, a low noise amplifier (LNA), a filter, a mixer driven by the LO, a filter, an intermediate frequency amplifier (IFA) and the analog-to-digital converter (ADC). Therefore, a $N_R \times M_T$ MIMO system has M_T and N_R transmit and receive signal paths respectively, as shown in Figure 2.5.

In order to simplify the model, the baseband signal-processing blocks (e.g. source coding, digital modulation) and the error correction code (ECC) blocks are omitted, i.e. an un-coded system is assumed. However, the methodology used in describing the power consumption model makes including these blocks easy. The total average power consumption along the transmit and receive

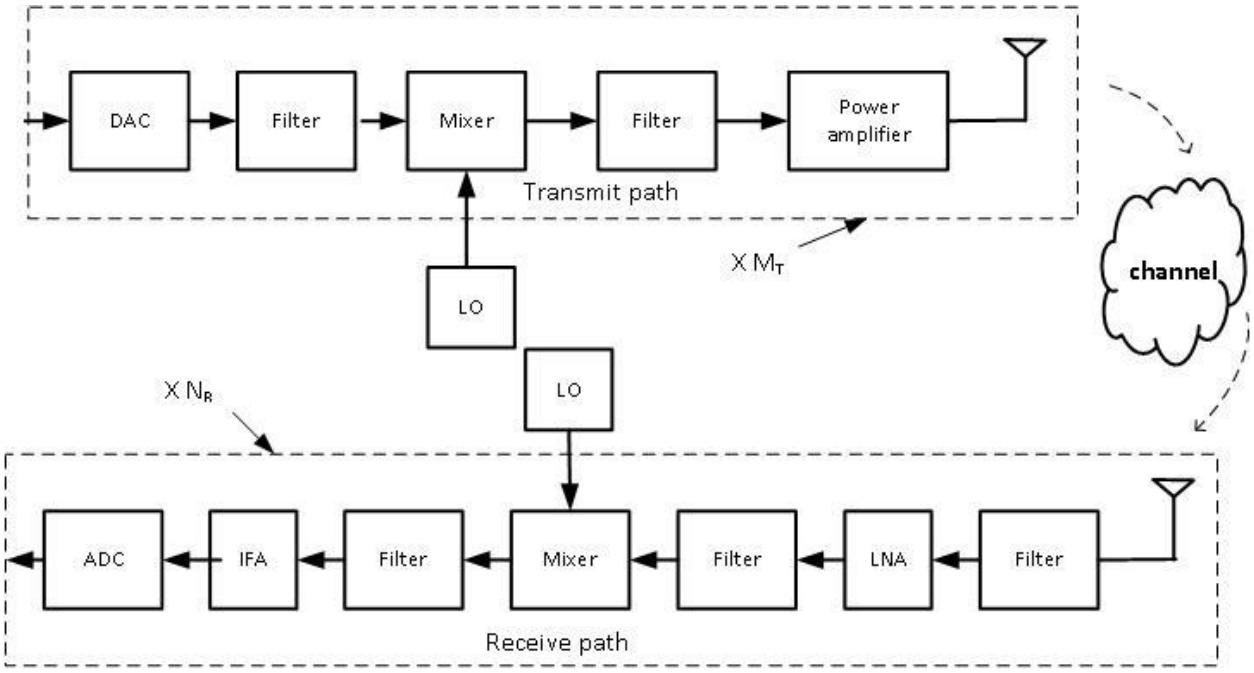

Figure 2.5. Transmitter/receiver circuit blocks in a MIMO wireless system

signal paths is given by [66]:

$$P_{total} = P_{PA} + P_c \tag{2.21}$$

where P_{PA} is the power consumed by all the power amplifiers and P_c is the power consumed by all the other circuit blocks [67]. The consumption of the power amplifiers, P_{PA}, can be modelled as [68]:

$$P_{PA} = \frac{P_{t1}}{\rho} + \frac{P_{t2}}{\rho} + \cdots + \frac{P_{tM_T}}{\rho} = \frac{P_t}{\rho} \tag{2.22}$$

where P_{ti} is the transmit power allocated to the ith transmit antenna and ρ is the power efficiency of each power amplifier, which is assumed to be the same for all the power amplifiers. P_t is the total transmit power; it is the sum of the powers allocated to the transmit antennas, i.e.:

$$P_t = P_{t1} + P_{t2} + \cdots P_{tM_T} \tag{2.23}$$

Therefore, P_{PA} consists of the actual transmit power and the wasteful power consumed by the power amplifiers. P_c is modelled as:

$$P_c \approx M_T\left(P_{DAC} + P_{mix} + P_{filt}\right) + 2P_{syn} + M_R\left(P_{LNA} + P_{mix} + P_{IFA} + P_{filr} + P_{ADC}\right) \qquad (2.24)$$

where P_{DAC}, P_{mix}, P_{LNA}, P_{IFA}, P_{filt}, P_{filr}, P_{ADC} and P_{syn} are the power consumption values for the active DACs, mixers (transmitter/receiver), LNAs and IFAs; the active filters at the transmit and receive side, the active ADCs and the frequency synthesizer (i.e. LO) respectively. The frequency synthesiser is assumed to be shared among all the antenna paths, i.e. the wireless system has two frequency synthesizers, one for the transmit paths, the other for the receive paths.

2.3.3 Energy Efficiency Metrics

An energy efficiency metric is of primary importance in the overall design of an energy efficient network, since it is directly related to the decisions made in optimizing the energy efficiency of the network. Several different EE metrics are proposed in literature, but the most popular is the 'bits-per-Joule' metric [61]. This metric is defined as the ratio between the capacity and the corresponding total power consumption of the system [69] i.e.:

$$EE = \frac{C}{P_{total}} \qquad (2.25)$$

where $C\ (bits/s)$ is the channel capacity and P_{total} is the total power consumption of the system.

The EE and spectral efficiency (SE) sometimes conflict with one another, i.e. optimizing one sacrifices the other. Therefore, it is common in literature to investigate a trade-off between EE and SE; an example can be found in [70]. In this thesis, a SE constraint is employed; and this will ensure that the designed energy-efficient antenna selection schemes achieve high EE while meeting a specific SE threshold.

2.4 Cross-Layer Design

The TCP/IP protocol suite provides end-to-end connections in communication networks through functionalities organized in five distinct layers, i.e., the application, transport, network, data link and physical layers. Exchange of data and services takes place between adjacent layers; a layer provides services to the layer directly above it, and it makes use of services provided by the layer directly below it. Within each layer, protocols are designed to realize the services that the layer provides. The modular architecture of TCP/IP enables research and design to occur independently at each layer; this has accelerated technological development and implementation. Additionally, the layered architecture allows different network architectures to be easily interconnected [71]. The massive proliferation of the Internet, together with the rapid growth of the services and the applications it offers, has been attributed to TCP/IP - making it the de-facto architecture for wireless networks. The layered IP architecture was first defined in the 3G standard; and it was then realized in beyond 3G (B3G) wireless networks; i.e., 4G networks; e.g., the LTE-A standard defines a wireless network that relies on packet-switching technologies entirely based on the IP protocol suite [72].

TCP/IP was initially designed for wired networks; when TCP/IP is implemented in the wireless environment, difficulties emerge. The limited spectrum availability and the unique nature of wireless channels creates several problems, which are not handled well in the framework of the layered architecture. In particular, wireless channels are affected by small-scale channel variations, caused by user mobility or changes in the physical environment; and large-scale variations (which are spatio-temporal), which are dependent on user location and the interference levels. These channel variations result in higher error rates, bursty errors, location dependent and time-varying wireless link capacity; which are not present in wireline networks. This motivated interest in adopting cross-layer designs (CLD), which combine functionalities and information between different layers, in order to improve the performance of wireless networks [17] [71] [73] [74] [75].

One of the earliest examples of the gains accrued from the information exchange between layers, are those achieved in a multi-user (MU) wireless system with channel scheduling; where the link

channel state information (CSI) for each user is fed back to the base station. The average throughput of the MU system is increased, if in each time slot, the user with the best channel conditions is scheduled; this is referred to as multi-user diversity gain [76]. Therefore, this represents a cross-layer design because CSI (physical layer) is used by the scheduler (data link layer) in order to improve the performance of the system.

2.4.1 Cross-Layer Design Coordination Model

The concept of a coordination plane was introduced in [74] [75] [77], to aid in the identification, description and management of cross-layer interactions. A coordination plane is a cross-sectional view of the protocol stack on which interlayer coordination algorithms can be applied; and it is focused on solving a set of problems of the same kind. In [75] cross-layer designs are modelled as a coordination model, consisting of three coordination planes, which describe the functionality that cross-layer designs can support. As shown in Figure 2.6, the three coordination planes are the security, quality of service (QoS) and mobility planes, which extend across the five TCP/IP protocol layers. The coordination planes represent the goals that cross-layer designs aim to achieve. A brief description of the coordination planes follows.

2.4.1.1 The Security Plane

The main purpose of the security coordination plane is to eliminate multiple layers of encryption. In [77], it is proposed that encryption methods such as secure shell (SSH) and Wi-Fi protected access, should be deployed in the security plane in a cross-layer design, which is aimed at secure communications. In [78], a cross-layer design for multi-hop wireless networks that share parameters in each layer, to avoid multi-layer attacks, is proposed. The design results in less routing overhead and fewer acknowledgment packets. Other examples of cross-layer designs in the security plane can be found in [79] [80].

Figure 2.6. Cross-layer coordination planes

2.4.1.2 The QoS Plane

The QoS plane aims to improve the quality of service of the wireless network by distributing the QoS requirements and restrictions along the whole protocol stack; and by coordinating their efforts in a cross-layer manner. More specifically, due to the unique nature of the wireless link, the upper layers may need to be aware of the information in the data link and physical layers in order to improve the QoS. As an example, the time-varying nature of wireless links makes them more susceptible to transmission errors, as compared to wireline links; and this affects the performance of TCP. TCP provides reliable connection-oriented end-to-end transmissions, as well as congestion control. The initial implementation of TCP regards all packets losses as being due to congestion. However, in wireless networks, high transmission errors also result in packet losses; therefore, the congestion and retransmission procedures of TCP can lead to the degradation of the system throughput. In [81], it was shown that if the packets are marked, based solely on congestion information, the time-varying nature of the wireless channel does not cause significant degradation

to the performance of TCP. In [82], the authors propose TCP based on Explicit Loss Notification (ELN) for wireless networks. The ELN mechanism is designed to notify the packet sender of the reason for the packet transmission error. ELN shares information between the TCP and MAC layers; and the evaluation results show that implementing ELN results in enhanced system performance. Other examples of cross-layer designs in the QoS plane can be found in [83] [84] [85] [86].

2.4.1.3 The Mobility Plane

The mobility plane deals with the problems created in mobile scenarios, in order to guarantee uninterrupted communications in wireless networks. Mobility results in events which need to be identified and handled. For example, horizontal and vertical handovers result in channel switch and route change events at the lower layers, which need to be communicated to the upper layers so that the communication maintained by the upper layers is not interrupted [77] [87] [88]. Channel fading, transmission delay, high bit error rate, and other failures that decrease QoS may affect the mobility as well; therefore, some cross-layer designs in the QoS plane also have the goal of mobility. Other examples of cross-layer designs in the mobility plane can be found in [73] [74].

2.4.2 Data link and Physical Layers Cross-layer Interactions

As mentioned in the previous chapter, the focus of this thesis is on the cross-layer interactions between the physical and data link layers. The data link layer has two sublayers, the data link control (DLC) and the media access control (MAC) sublayers. The primary functions of the DLC sublayer include, dealing with transmission errors and regulating the flow of data; while those of the MAC sublayer include managing access to the resources available on the shared medium. On a more specific note, this thesis focuses on the interaction between the DLC sublayer and the physical layer - with the aim of improving the performance of the system in terms of energy

efficiency, throughput, transmission latency, packet error rate and receiver buffer requirements. Therefore, the cross-layer algorithms developed in this thesis fall in the QoS coordination plane.

The DLC sublayer provides a well-defined interface to the network layer aimed at providing an error-free virtual link; this can be accomplished by implementing automatic repeat request (ARQ) schemes. ARQ protocols provide reliable communications over wireless links by combating channel fading [89] [90]. ARQ combines an error detecting code and a retransmission strategy. The error detecting code generates parity bits from blocks of data; the parity bits are then appended to each data block to form a code word (packet). At the receiver, the parity bits are used to determine whether the packets were correctly received, and if not, then the retransmission strategy determines how the erroneously received packets are to be retransmitted.

Because of their mode of operation, ARQ protocols achieve higher reliability, at reduced complexity and cost, compared to forward error correction (FEC) schemes [89]. Depending on the retransmission strategy, ARQ protocols can be divided into three basic categories; stop-and-wait (SAW), go-back-to-N (GBN) and selective repeat (SR). The simplest ARQ protocol to implement is SAW. In SAW, a packet is transmitted only after the preceding packet has been received correctly. Therefore, packets always arrive in sequence at the receiver, resulting in SAW having minimal signaling and buffer requirements. The idle time spent waiting for an acknowledgment (ACK) or a negative acknowledgment (NACK) for each transmitted packet, severely affects the throughput efficiency of SAW. To compensate for the idle time in SAW, the N-SAW retransmission protocol runs multiple SAW processes in parallel, resulting in improved throughput efficiency. N-SAW is part of the LTE/LTE-A communications standards [91].

Cross-layer designs that are ARQ aware have been proposed in literature. The cross-layer schemes use ARQ-related information, e.g. throughput, the number of packet retransmissions, transmission delay, etc., combined with physical-layer information in order to optimize the performance of the wireless link [92] [93]. In the context of spatial multiplexing MIMO systems with antenna selection, there is a recent trend aimed at optimizing cross-layer criteria, as opposed to physical layer metrics, like capacity, SNR or error rate. More specifically, the antenna selection schemes are designed to optimize the data link layer throughput, i.e. the number of successfully received

bits per second, which takes into consideration the receiver structure, packet size, modulation scheme ARQ scheme, etc. This trend will be discussed further in Section 2.5.1.1.

2.5 Antenna Selection

MIMO significantly improves the spectral efficiency and the reliability of wireless links, as discussed in Section 2.1; however, the deployment of multiple antennas incurs a problem of hardware complexity. Antenna selection is an innovative technique that provides a solution to the problem of increased hardware complexity, cost and power consumption attributed to the multiple RF chains associated with multiple antennas. In antenna selection, the optimal subset of antennas is selected from the available antennas for transmission purposes, thereby reducing the number of RF chains required. Antenna selection is cost-effective because the additional antenna elements required and the associated signal-processing is relatively cheaper than introducing complete RF chains. Moreover, the many benefits of MIMO are still provided by the optimally selected system [10] [94].

A typical MIMO wireless system, with antenna selection capabilities at both the transmitter and receiver, is depicted in Figure 2.7. The MIMO system is equipped with M_T and N_R transmit and receive antennas respectively; while the number of RF chains at the transmitter and receiver are m_T $(1 \leq m_T < M_T)$ and n_R $(1 \leq n_R < N_R)$ respectively. The channel matrix before antenna selection is represented by $\boldsymbol{H} \in \mathbb{C}^{N_R \times M_T}$. The best subset of m_T out of M_T transmit antennas and n_R out of N_R receive antennas are selected, based on a given selection criterion. The channel matrix after antenna selection, $\boldsymbol{H}_s \in \mathbb{C}^{n_R \times m_T}$, is formed by the m_T columns and n_R rows of $\boldsymbol{H}$, corresponding to the m_T and n_R selected transmit and receive antennas respectively.

The performance of the MIMO channel can be enhanced by performing some form of pre-processing at the transmitter [11]. Most pre-processing schemes require some degree of channel knowledge at the transmitter, i.e. full or partial channel knowledge; beamforming is an example of a pre-processing technique that exploits full channel knowledge at the transmitter [11] [42].

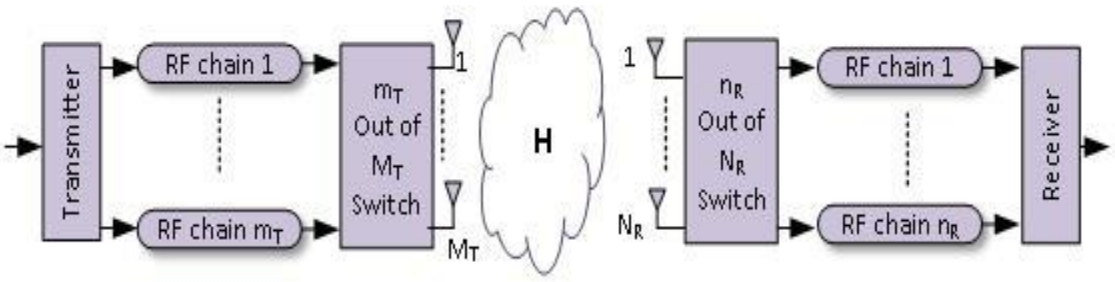

Figure 2.7. Block diagram of MIMO system with transmit and receive antenna selection

The pre-processing schemes are implemented to maximize the capacity, or to minimize the error rate. Unless channel knowledge at the transmitter is obtained through reciprocity, a feedback channel is required to convey the CSI from the receiver to the transmitter. However, the feedback channel usually has limited bandwidth; therefore, perfect and instantaneous CSI is seldom available at the transmitter. In such scenarios, antenna selection, more specifically transmit antenna selection, offers an effective pre-processing solution with low feedback requirements; channel knowledge is not required at the transmitter.

Transmit antenna selection exploits channel knowledge at the receiver; therefore, the CSI does not need to be conveyed to the transmitter. In transmit antenna selection, the subset of m_T out of M_T transmit antennas that optimize a given criterion are selected at the receiver. Then the antenna selection command is conveyed to the transmitter via a low bandwidth feedback channel; since as few as M_T bits are required to do so. Transmit antenna selection can also be used to enhance the performance of MIMO systems – without offering reduced hardware complexity and cost, i.e. the MIMO system is equipped with the same number of antennas as RF chains. When transmit antenna selection is implemented as a signal-processing technique for improving the performance of the MIMO system, the subset of M_t ($1 \leq M_t \leq M_T$) transmit antennas that optimizes a given criterion is selected. Therefore, the transmit antenna selection algorithm adapts the number of active transmit antennas to the varying channel conditions in order to improve the performance of the MIMO system.

Antenna selection was initially designed for capacity maximization or error rate minimization, aimed at reducing the hardware complexity and cost; and improved system performance – this will be referred to this as conventional antenna selection. The concern regarding the increasing energy consumption of wireless communications has seen antenna selection being proposed, in literature, as a technique for designing energy efficient MIMO systems. In the next section, a brief overview of conventional antenna selection is given; and then in Section 2.6, the current research work on energy-efficient antenna selection will be reviewed.

2.5.1 An Overview of Conventional Antenna Selection

The design of antenna selection algorithms depends on a variety of factors, including but not limited to, the coding technique (spatial diversity of multiplexing), selection criteria and receiver structure. Conventional antenna selection algorithms are designed with the aim of either improving the link reliability or the information rate, for spatial diversity or spatial multiplexing systems respectively. Several criteria are used for antenna selection, with SNR, error rate and capacity being the most popular.

Antenna selection was first proposed for spatial diversity schemes aimed at improving link reliability. In [95], receive antenna selection was proposed for SIMO systems; while transmit antenna selection for MISO systems was presented in [96]; in both schemes, a single antenna was selected, with channel gain and SNR as the selection criteria respectively. Transmit and receive antenna selection schemes, where multiple antennas are selected, with SNR as the selection criterion, are presented in [10] [94] [97] [98] [99].

Antenna selection schemes, in combination with MRC and MRT, are presented in [10] [94] [97] [98]; while antenna selection schemes combined with OSTBC are presented in [99]. In [100], transmit antenna selection for spatial multiplexing systems, based on minimizing the error rate, is presented. In these antenna selection schemes, it is shown that antenna selection maintains the

diversity order of the system; the diversity order of the optimally selected system is the same as that of the MIMO system with all the transmit/receive antenna in use.

Transmit and receive antenna selection algorithms for spatial multiplexing schemes - aimed at enhancing the data rate – are presented in [10] [94] [101]. The algorithms select the subset of transmit/receive antennas that maximize the system capacity. It is shown that, as long as the system with antenna selection has at least as many receive antennas as transmit antennas, then the optimally selected system has almost the same capacity as the full complexity system i.e. the MIMO system with all transmit/receive antennas in use.

In the context of CR MIMO systems, antenna selection schemes have been presented and studied in [102] [103] [104] [105] [106] [107]. Examples of the optimization criteria used include interference, capacity, SNR and SINR - which are all physical-layer metrics.

The optimal mechanism for selecting the subset of antennas, based on a given selection criterion, is based on performing an exhaustive search over all possible antenna subsets. Based on the MIMO system with antenna selection, as shown in Figure 2.7, the number of antenna subsets for transmit, receive and joint transmit/receive antenna selection is $\binom{M_T}{m_T}$, $\binom{N_R}{n_R}$ and $\binom{M_T}{m_T} \times \binom{N_R}{n_R}$ respectively. Therefore, the optimal exhaustive search algorithm is computationally complex, with a complexity that increases with the number of transmit/receive antennas. Consequently, sub-optimal algorithms, i.e. algorithms whose performance is not as good as that of the exhaustive search algorithms, but with reduced computational complexity, have been proposed in literature. For example, the norm-based selection algorithm is a simple sub-optimal algorithm that reduces the complexity of spatial diversity and spatial multiplexing systems, with antenna selection, by simply maximizing the norm of the selected channel matrix [94].

In [108], a fast incremental selection algorithm for capacity maximization is proposed. The algorithm begins with an empty set; then it adds the antenna with the highest capacity contribution in each step; the algorithm achieves near-optimal performance. The authors in [109] propose a joint transmit/receive antenna selection near-optimal greedy algorithm for capacity maximization.

Near-optimal reduced complexity algorithms, based on particle swarm and convex optimization, are proposed in [110] [111].

It is worth noting that the design of reduced complexity algorithms is highly dependent on the optimal exhaustive search algorithm whose complexity they are designed to reduce.

2.5.1.1 Throughput-Based Antenna Selection

As discussed in the previous section, the common criteria for conventional antenna selection include SNR, capacity and error rate, which are all physical-layer metrics. Antenna selection that optimizes these criteria does not exploit any information or functionalities from upper layers; therefore, these schemes are physical-layer approaches. In Section 2.4, it was pointed out that due to the fragile nature of wireless links, the constituent layers of the TCP/IP protocol stack may need to work together, in order to enhance the QoS or the performance of wireless systems.

With regard to antenna selection for spatial multiplexing systems, a new criterion, namely throughput, has been proposed in literature. Throughput is a cross-layer metric; this is because information from the physical and data link layers is used in its derivation. Therefore, antenna selection, which maximizes throughput, is a cross-layer approach. The pioneering example of cross-layer antenna selection is found in [112]. The authors propose transmit antenna selection that maximizes the data link throughput of a MIMO system with a BLAST architecture; with GBN as the ARQ protocol and QPSK as the modulation scheme. The results showed that the throughput-based approach outperforms the capacity-based approach in terms of data link and TCP throughput.

Throughput-based transmit antenna selection has also been studied in [113] [114] [115] [116]. From these works, it is evident that the design of cross-layer antenna selection algorithms depends on the receiver structure, modulation scheme, ARQ protocol, amongst other parameters. Throughput maximization is shown to have superior performance in terms of throughput and transmission delay, when compared with capacity maximization. The superior performance of the

throughput-based approach is attributed to its cross-layer design, which gives it the capability of exploiting the transmit power and the transmit antennas more efficiently, resulting in overall improved system performance.

The works in [117] [118] focus on designing low complexity throughput-based transmit antenna selection algorithms. The authors in [117] propose two recursive methods for reducing the complexity of throughput-based transmit antenna selection for MIMO systems employing the BLAST architecture and GBN as the ARQ protocol. In [118], the complexity of throughput-based transmit antenna selection, for MIMO systems; with GBN as the ARQ protocol and binary phase shift keying (BPSK) as the modulation scheme; is reduced by using particle swarm optimization. With regard to cognitive networks, [119] presents combined antenna selection and beamforming in cognitive networks, from a cross-layer perspective.

2.6 Antenna selection for Energy Efficient MIMO Systems

As mentioned in the previous section, antenna selection was initially considered for improved system capacity and link reliability. However, with the recent interest in energy efficient wireless communications, some research works have investigated energy-efficient antenna selection for point-to-point MIMO systems [15] [16] [120] [121] [122] [123] [124]. In these works, antennas are selected to optimize physical-layer energy efficiency metrics.

The authors in [15] propose energy efficiency (in bits-per-Joule-per-Hz) maximization, by jointly optimizing the transmit power, the number of active RF chains (antennas) and the antenna subset, subject to a SE constraint. The MIMO system considered employs normalized precoding and decoding vectors at the transmitter and receiver; the SNR is maximized by applying MRT and MRC respectively. Transmit, receive and joint transmit/receive antenna selection algorithms are considered. Additionally, sub-optimal reduced complexity algorithms are developed.

The works in [16] [120] focus on designing reduced complexity antenna selection algorithms for improving the energy efficiency of multi-stream MIMO systems. In [120], the authors propose a

low complexity near-optimal antenna selection algorithm that optimizes the EE by maximizing the capacity of a multi-stream MIMO system, under a total power consumption constraint. The algorithm determines the optimal number and subset of active transmit/receive antennas by iteratively selecting the receive or transmit antenna that leads to the highest increment in capacity. The iteration stops when there is a capacity decrease; and the optimal antenna subset is obtained. In [16], an iterative near-optimal algorithm that jointly selects the transmit antenna subset and determines the power, that maximize the EE (in bits-per-Joule-per-Hz), subject to a minimum transmission rate constraint, is proposed. The authors derive an iterative equation for energy efficiency for the multi-stream MIMO system with transmit antenna selection; this is then used to guide the selection of the transmit antenna that achieves the largest energy efficiency increment in each step. At each step, the optimal transmit power, which maximizes energy efficiency, is calculated.

The authors in [121] investigate the trade-off between energy efficiency and spectral efficiency in the context of transmit antenna selection for MIMO systems. The optimal value of SE that maximizes the EE, in bits-per-Joule, for the transmit antenna selection scheme, for a given number of antennas, is determined analytically and supported by numerical results. The results show that transmit antenna selection achieves a better EE-SE trade-off performance than spatial multiplexing and MRT MIMO schemes.

In [122], the EE of transmit antenna selection, with a large number of antennas available at the transmitter, is investigated. The authors first derive an approximation of the distribution of the mutual information of the antenna selection system; this is then used to analyze the energy efficiency performance, in bits-per-Joule-Hz, under different conditions, in relation to circuit power and transmit power. Two simple efficient antenna selection algorithms, are then proposed.

In [123], the authors compare transmit antenna selection for MIMO-MRC systems, with that of MIMO systems with transmit beamforming, in terms of energy efficiency. The EE is measured in terms of the cumulative distribution function (CDF) of the minimum energy-per-goodbit (EPG) required to attain a target outage probability. The EPG is defined in terms of the transmit power, capacity and the bit error rate (BER). The results show that, even though transmit antenna selection

is less efficient in terms of the outage probability as compared with transmit beamforming, it is more energy efficient; and this is attributed to it requiring less RF chains.

In [124], the authors propose an optimal energy efficient scheme for MIMO-based cognitive radio networks, with transmit antenna selection. The transmit antenna selection algorithm maximizes the EE, in bits-per-Joule, by jointly optimizing the transmit power and the number of active antennas, subject to the maximum interference (at the PU RX from the SU TX), the maximum SU transmit power and the minimum transmission rate (for the SU link) constraints. Power allocation algorithms, which use the bisection search technique, are derived; these are then used to determine the optimal transmit power.

In the literature review presented above, antenna selection is used as pre-processing technique for improving the energy efficiency of multiple-antenna systems. More specifically, in most of these works, transmit antenna selection is implemented as a signal-processing technique for improving the energy efficiency of MIMO systems, whereby, the transmitter and receiver are equipped with an equal number of antennas as RF chains. Consequently, transmit antenna selection is used to design energy efficient MIMO systems with high spectral efficiency. The optimization criteria, in these works, are all physical-layer quantities; with the most common being the EE metric defined as the ratio of the channel capacity to the total power consumption of the system. Therefore, all antenna selection schemes in these works are physical-layer approaches. Consequently, the study of energy-efficient antenna selection from a cross-layer perspective remains an open and ongoing research challenge.

2.7 Chapter Summary and Conclusions

In this chapter, overviews on MIMO, CR and cross-layer designs are presented. The fundamentals of conventional antenna selection, including a cross-layer perspective to transmit antenna selection, were discussed. Also, the power consumption model, which is used to determine the power consumed by wireless systems, was described.

From the literature review on the related works on energy-efficient antenna selection presented in this chapter, it is evident that the antenna selection techniques adopt a physical-layer approach. The discussions presented in Section 2.4, on cross-layer designs, show that employing information and functionalities across layers enhances the performance of wireless networks. With respect to spatial multiplexing MIMO systems, cross-layer transmit antenna selection, discussed in Section 2.5.1.1, maximizes throughput; subsequently resulting in overall improved system performance, as compared with the physical-layer approach which, maximizes capacity. The superior performance of the throughput-based approach is attributed to the utilization of parameters from the data link and physical layers. Therefore, with regard to antenna selection for energy efficient MIMO systems, maximizing an energy efficiency metric that exploits parameters from the physical and data link layers, which have a direct impact on the performance of the system, should also result in an overall improved system performance. Motivated by this, this thesis focuses on investigating cross-layer energy-efficient transmit antenna selection for multiple-antenna systems.

The framework chosen for the thesis is that of un-coded spatial multiplexing multiple-antenna systems - equipped with ZF linear receivers with N-SAW as the ARQ protocol. From the discussions in this chapter, it is observed that the chosen framework provides high spectral efficiency at reduced complexity.

Chapter 3 Transmit Antenna Selection for Spatial Multiplexing Systems – A Cross-Layer Approach

As discussed in the previous chapter, the design of cross-layer antenna selection schemes, which employ information from the data link and physical layers, depends on several factors, including receiver structure, modulation scheme and ARQ protocol. Therefore, cross-layer antenna selection algorithms are unique; they are dependent on the system model (framework) in use. In this chapter, we begin our study by deriving the analytical expression for system throughput, for spatial multiplexing multiple-antenna systems; equipped with ZF linear receivers, and N-SAW implemented at the data link layer. The throughput expression thereby derived, will be used in subsequent chapters to develop the cross-layer energy efficiency metric. Cross-layer transmit antenna selection algorithms that maximize the derived throughput, will then be developed and their performance analyzed, in comparison to the physical-layer approach, which maximizes capacity. This will make evident the remarkable benefits that the cross-layer design brings to antenna selection.

This chapter is organized as follows. In section 3.1, the performance of transmit antenna selection in MIMO systems, from a cross-layer perspective, is evaluated. This is then extended to underlay CR MIMO systems in Section 3.2. The conclusions of this chapter are presented in Section 3.3.

3.1 Performance Analysis of Transmit Antenna Selection for MIMO Systems

MIMO systems, configured to exploit spatial multiplexing, significantly improve the spectral efficiency of wireless channels. With regard to antenna selection, which can either be used to reduce the hardware complexity and cost or as a signal-processing technique for enhancing the system performance, capacity is the most common optimization criterion. However, capacity-based approaches do not exploit all the information available at the data link and physical layers,

which have a direct impact on the system performance; therefore, maximizing capacity does not necessarily improve the overall performance of the system. Consequently, a cross-layer approach to antenna selection, which exploits parameters from the data link and physical layers, with throughput as the selection criterion, has been proposed in literature. As mentioned in Section 2.5.1.1, throughput-based transmit antenna selection for spatial multiplexing systems was first proposed in [112] and subsequently studied in [113] [114] [115] [116].

In [113], the authors investigate the performance of a cross-layer approach to transmit antenna selection in which an adaptive number of transmit antennas is selected to optimize the throughput of a MIMO system, with a V-BLAST architecture, and hybrid ARQ (H-ARQ) implemented at the data link layer. The modulation schemes considered are QPSK and 16-QAM. Adaptive modulation is incorporated into the antenna selection scheme to enhance system performance. Throughput-based transmit antenna selection is shown to outperform the capacity-based approach in terms of throughput and transmission latency.

In [114], the performance of cross-layer transmit antenna selection with decision-feedback detection receivers, over spatially correlated Ricean fading MIMO channels, is investigated; GBN is used as the ARQ protocol and BPSK as the modulation scheme. The results show that the cross-layer approach delivers higher throughput gains when compared with the capacity-based approach. In [115] [116], the authors propose throughput-based transmit antenna selection when truncated SR ARQ or SR plus GBN are employed at the data link layer, with M-QAM as the modulation scheme. The cross-layer approach is shown to outperform capacity-based transmit antenna selection in terms of throughput.

In this section, the performance of transmit antenna selection for MIMO systems, from a cross-layer perspective, is investigated; N-SAW is implemented at the data link layer with QPSK as the modulation scheme. Further, the impact of packet size, number of ARQ (SAW) processes and the stalling of packets inside the receiver reordering buffer – caused by running multiple ARQ (SAW) processes in parallel - on system performance, is investigated. The previous works [112] [113] [114] [115] [116] do not consider these factors when analyzing the performance of throughput-based transmit antenna selection.

The rest of this section is organized as follows: The system model is described in Section 3.1.1; and the analytical throughput expression is derived in Section 3.1.2. In Section 3.1.3, the throughput-based transmit antenna selection scheme is developed; and its performance is evaluated by comparing it with that of capacity maximization. In Section 3.1.4, the performance analysis is extended to the system with antenna selection with a stall avoidance mechanism implemented.

3.1.1 System Description

Consider a point-to-point MIMO system with M_t transmit and N_r receive antennas, as shown in Figure 3.1. The MIMO system is configured to exploit spatial multiplexing, therefore $M_t \leq N_r$ [10]. The MIMO channel, represented by $\boldsymbol{H} \in \mathbb{C}^{N_r \times M_t}$, is assumed to have ZMCSCG elements with unit variance. The channel is assumed to experience frequency flat Rayleigh fading, and the channel is assumed known only at the receiver. Transmit antenna selection is implemented as a signal-processing technique for improving the performance of the MIMO system; therefore, the transmitter and receiver are equipped with an equal number of antennas as RF chains. The subset of transmit antennas that optimize a specific criterion is selected at the receiver. The selected subset consists of an adaptive number of transmit antennas, M_s, where $1 \leq M_s \leq M_t$. The information on the selected antenna subset is fed back to the transmitter, in the form a selection row vector, $\boldsymbol{sv}$, via a low bandwidth feedback channel, which is assumed to be error free with zero delay. The ith element of the $1 \times M_t$ selection vector is defined as follows:

$$\boldsymbol{sv}_i = \begin{cases} 1 & if\ the\ ith\ transmit\ antenna\ is\ seleted \\ 0 & otherwise \end{cases} \tag{3.1}$$

The received signal, after transmit antenna selection, is modeled as:

$$\boldsymbol{y} = \sqrt{\frac{P}{M_s}}\boldsymbol{H}_s\boldsymbol{x} + \boldsymbol{n} \tag{3.2}$$

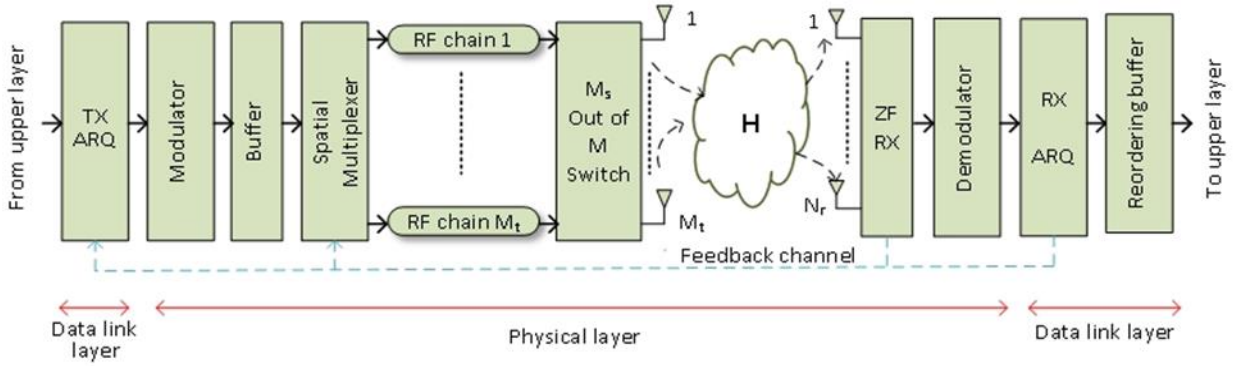

Figure 3.1. Block diagram of MIMO system model

where $\boldsymbol{H_s} \in \mathbb{C}^{N_r \times M_s}$ is the MIMO channel after transmit antenna selection, $\boldsymbol{x} \in \mathbb{C}^{M_s \times 1}$ is the transmit symbol vector, $\boldsymbol{n} \in \mathbb{C}^{N_r \times 1}$ the noise vector and P the transmit power available in one symbol period. $\boldsymbol{x}$ is assumed to have uncorrelated, zero mean symbols with unit energy drawn from the selected constellation; while $\boldsymbol{n}$ is assumed to have ZMCSCG elements with a variance of σ. P is assumed to have a value of $1W$, while a symbol period of 1 second is assumed. The available transmit power is divided uniformly among the selected transmit antennas. The receiver is equipped with a ZF linear receiver, which separates the received signal into its component M_s transmitted data streams.

N-SAW is implemented at the data link layer to control transmission errors. As mentioned in Section 2.4, N-SAW runs multiple instances of the protocol in parallel in order to compensate for the idle time associated with the round-trip delay of SAW. The operation of N-SAW is depicted in Figure 3.2. The parallel SAW processes experience unique channel conditions leading to SAW dependent packet error rates. Consequently, the packets transmitted in different SAW processes may require different number of retransmissions resulting in out-of-sequence packet arrival at the receiver. An example of this is seen in Figure 3.2, where packets are sent in sequence but are

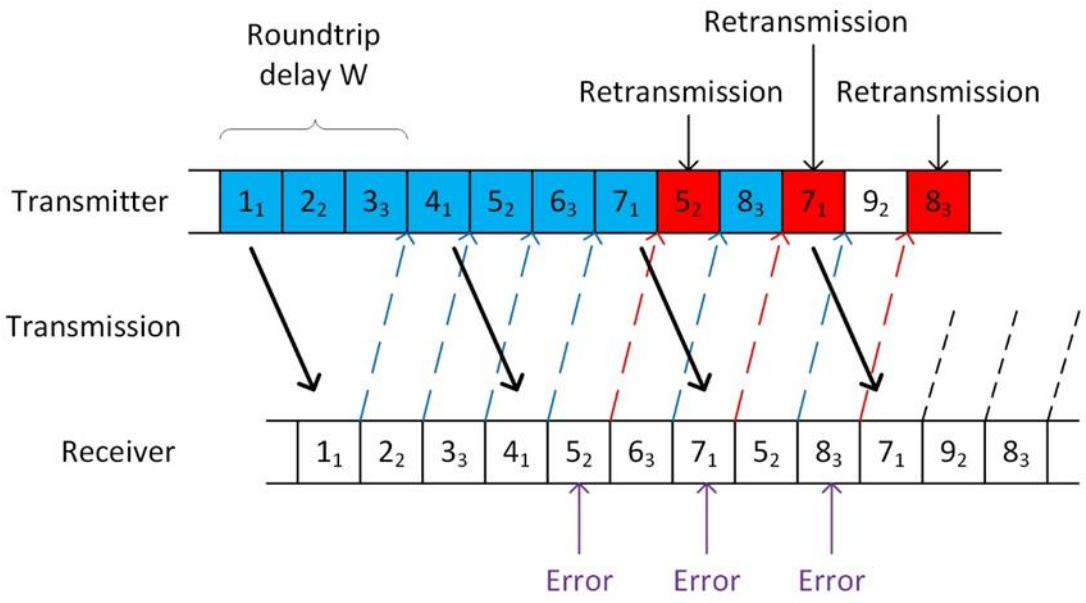

Figure 3.2. N-SAW with $N = 3$ SAW processes running in parallel

{In Figure 3.2, the packet numbering format, S_n, denotes a packet with sequence number S transmitted in the nth SAW process. The blue and red dashed arrows represent ACK and NACK respectively.}

received out-of-sequence, i.e. 1 2 3 4 6 5 7. A reordering buffer is now required at the receiver to temporarily store the received packets; they are reordered before being delivered in-sequence to the higher layer.

The bit stream received at the transmitter data link layer is divided into blocks of k −bits. Each k −bit block is encoded into an n −bit packet by an error detecting (n, k) linear block code. At the physical layer, each n −bit packet is modulated to produce an L −symbol packet, where $L = n/b$ with b being the number of bits per symbol. The packets are numbered in sequence and placed in the transmit buffer awaiting transmission. Before being transmitted, each packet is divided into M_s parallel data streams, as shown in Figure 3.3. The M_s modulated signals are then transmitted over the M_s selected transmit antennas. Each packet is transmitted in its own slot, of

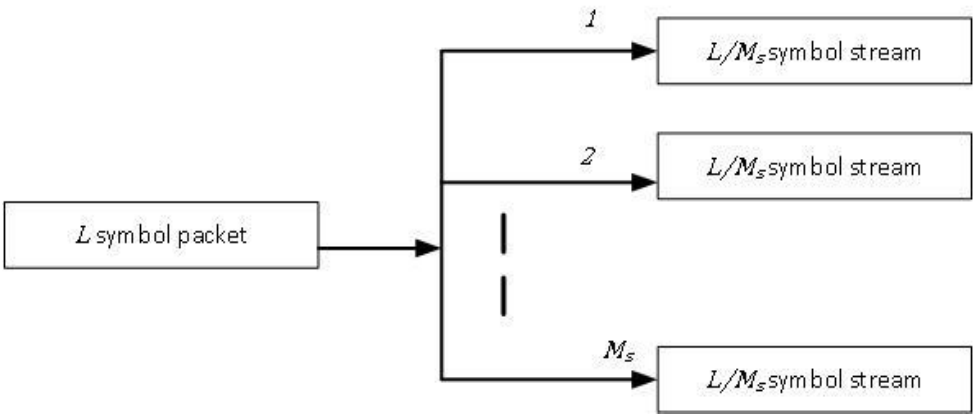

Figure 3.3. Transmitted packet structure

slot period L/M_s seconds. The channel response is assumed constant during the transmission of each packet.

At the receiver, the output of the ZF linear receiver – consisting of M_s data streams – are demodulated and the resultant bit streams are combined and passed on to the receiver data link layer. The bit stream is formed into packets, then the packets are examined to determine whether any transmission errors occurred. ACKs and NACKs are sent to the transmitter for correctly and erroneously received packets respectively; the error detecting code is used to determine whether a received packet is erroneous. Packets received with errors are retransmitted, according to the ARQ retransmission protocol. A limit is set on the number of times a packet can be retransmitted. The implication of this is that the receiver keeps a record of the number of times each packet is retransmitted; when a packet has been retransmitted the maximum number of times, it is accepted whether it has errors or not. Accepted packets are placed in the receiver reordering buffer from where they are passed on, in-sequence, to the higher layer, using the in-sequence algorithm given in Appendix A. Packets remain in the reordering buffer for as long as preceding packet(s) have not been correctly received or retransmitted the maximum number of times.

3.1.2 Throughput Expression for Spatial Multiplexing MIMO Systems

In this section, the analytical expression for throughput, for the system described in Section 3.1.1, is derived. As mentioned in the previous section, the ZF linear receiver separates the received signal into its component transmitted streams. The post processing SNR for the kth data stream is given by [40]:

$$SNR_k = \frac{P}{\sigma M_s} \frac{1}{[(\boldsymbol{H}_s^H \boldsymbol{H}_s)^{-1}]_{k,k}} \quad k = 1,2,3, \dots M_s \tag{3.3}$$

while the symbol error rate (SER) for the kth data stream, is given by:

$$SER_k = f(SNR_k, Mod) \qquad k = 1,2,3, \dots M_s \tag{3.4}$$

where Mod accounts for the modulation scheme in use (see Appendix B for SER expressions). Since each L −symbol packet is transmitted as L/M_s parallel data streams, and assuming an un-coded system, the packet error rate (PER) is given by:

$$\text{PER} = 1 - \prod_{k=1}^{M_s} (1 - SER_k)^{L/M_s} \tag{3.5}$$

Consider SAW implemented in a SISO system, where a symbol stream is transmitted at a symbol rate of δ_s, and a (n, k) linear block code is used for error detection. For k/b information symbols to be successfully accepted by the receiver, the average number of symbols that the transmitter needs to transmit is given by [89]:

$$\frac{L + \lambda\delta_s}{P_c} \tag{3.6}$$

where P_c is the probability of an L −symbol packet ($L = n/b$) being received without error and λ is the round-trip delay in seconds. To successfully transmit k/b symbols takes $((L + \lambda\delta_s)/P_c)/\delta_s$ seconds; therefore, the throughput for SAW in a SISO system, in symbols per second is given by:

$$\eta_{SAW} = \frac{\left({}^{k}/_{b}\right)}{((L + \lambda\delta_s)/P_c)/\delta_s} \ \ symbols/s \tag{3.7}$$

Moreover, the throughput in bits per second can now be expressed as:

$$\eta_{SAW} = b \times \frac{\left({}^{k}/_{b}\right)(1 - PER)}{(L + \lambda\delta_s)T_s} \ \ bits/s \tag{3.8}$$

where $P_c = 1 - PER$ and $T_s = 1/\delta_s$, with T_s the symbol period. In comparison to a SISO system which transmits only one symbol stream, M_s symbol streams are transmitted simultaneously in a MIMO system; therefore, the round-trip delay is given by $\lambda_m = \lambda/M_s$. Also, N-SAW runs N SAW processes in parallel. Taking these two points into consideration, the throughput for MIMO systems with N-SAW, can be expressed as:

$$\eta_{NSAW} = b \times N \times M_s \frac{\left({}^{k}/_{b}\right)(1 - PER)}{(L + \lambda_m\delta_s)T_s} \ \ bits/s \tag{3.9}$$

Rearranging (3.9), the throughput can be expressed as:

$$\eta_{NSAW} = b \times N \times M_s \frac{l \times (1 - PER)}{(1 + W)T_s} \ \ bits/s \tag{3.10}$$

where $l = (k/b)/L = k/n$ is the ratio of information symbols per packet and $W = \lambda_m\delta_s/L$ is the round-trip delay in slots (since a single L −symbol packet is transmitted per slot). Assuming that square pulses are used, then $T_s = 1/B$ can be assumed, where B is the bandwidth of the channel in hz. Therefore, the normalized throughput, with respect to bandwidth, for MIMO systems with N-SAW, is expressed as:

$$\eta = \frac{\eta_{NSAW}}{B} = b \times N \times M_s \frac{l \times (1 - PER)}{(1 + W)} \ \ bits/Hz/s \tag{3.11}$$

It is observed from (3.11) that the calculation of normalized throughput exploits information from both the physical and data link layers, making it a cross-layer quantity. As a note, in the system

description in section 3.1.1, a bandwidth of $B = 1Hz$, i.e. $T_s = 1$ second, was assumed, making the throughput and normalized throughput equal in this case. Therefore, in this chapter the terms throughput and normalized throughput will be used interchangeably. Validation of the throughput expression can be found in Appendix C.

3.1.3 Transmit Antenna Selection for MIMO Systems

As mentioned earlier, it is common practice to use capacity as the selection criterion in spatial multiplexing systems. The capacity of the MIMO system, given in Figure 3.1, after transmit antenna selection, is given by:

$$C = log_2 \det\left[\boldsymbol{I}_{N_r} + \frac{P}{\sigma M_s}\boldsymbol{H}_s\boldsymbol{H}_s^H\right] \; bits/Hz/s \tag{3.12}$$

In capacity-based transmit antenna selection, the subset of transmit antennas that maximizes the capacity, as given in (3.12), is selected. It is observed in (3.12) that calculating capacity only uses physical-layer parameters, e.g. transmit power, channel response, etc.; therefore, capacity maximization is a physical-layer approach.

In throughput-based transmit antenna selection, the subset of transmit antennas that maximize the data link throughput, as given in (3.11), is selected. It was pointed out in Section 3.1.2 that throughput is a cross-layer quantity; therefore, throughput maximization is a cross-layer approach. When compared to the capacity expression in (3.12), it is observed that the derivation of throughput exploits additional information from the physical layer, plus information from the data link layer, which have a direct impact on the overall performance of the system. These information includes the modulation scheme, packet size and the characteristics of the error detecting code and the ARQ retransmission protocol. This information enables throughput maximization to enhance the overall performance of the system, bringing remarkable benefits in comparison to capacity maximization.

Table 3.1. Simulation scenarios

	N	L (in symbols)	Error detecting code
Scenario A	3	528	CRC-32
Scenario B	3	1056	CRC-64
Scenario C	6	528	CRC-32

Given the throughput and capacity expressions in (3.11) and (3.12), the most straight forward way of determining the optimal transmit antenna subset in capacity and throughput-based transmit antenna selection, is by performing an exhaustive search over all transmit antenna combinations. In the exhaustive search algorithm, the capacity/throughput is calculated $\sum_{M_s=1}^{M_t} \binom{M_t}{M_s}$ times at the receiver. The transmit antenna subset that results in maximum capacity/throughput is then selected; and the information is then relayed to the transmitter.

3.1.3.1 Computer Simulations and Results

In this section, simulations are carried out to analyze and compare the performance of throughput and capacity-based transmit antenna selection. More specifically, the performance is evaluated at different values of L (packet size) and N (number of SAW processes). Three simulation scenarios, which are determined by different combinations of L and N, are used to evaluate the performance of the transmit antenna selection algorithms. The simulation scenarios are given in Table 3.1. The error detecting code used, is selected, so that the ratio of information symbols per packet, l, is the same in all the scenarios. The results are generated by transmitting 300 kilobytes of data per session, and then averaging over 1000 sessions. The metrics used to evaluate the performance are throughput and transmission latency, which are defined as follows:

$$throughput = \frac{information\ bits\ transmitted\ in\ a\ session}{time\ required\ to\ complete\ session}\ bits/Hz/s \qquad (3.13)$$

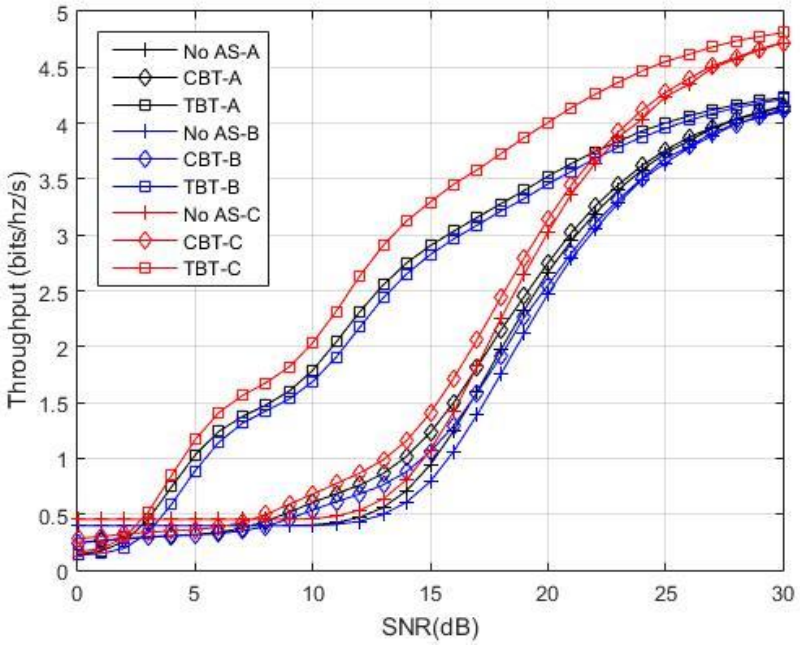

Figure 3.4. Plot of average normalized throughput against SNR

$$transmission\ latency = \frac{number\ of\ packets\ retransmitted\ in\ a\ session}{total\ number\ of\ packets\ transmitted\ in\ session} \qquad (3.14)$$

Additional simulations parameters are as follows; the number of transmit and receive antennas is $M_t = N_r = 3$, with a round-trip delay of $W = N$ slots. The value of the ratio of information symbols per packet is $l = 32/33$, while the maximum number of packet retransmissions is 10. The modulation scheme used is QPSK, therefore $b = 2$.

In Figure 3.4, the average throughput for throughput and capacity-based transmit antenna selection, TBT and CBT respectively, for scenarios A, B and C is plotted against SNR. The throughput with no antenna selection (No AS) is also included for comparison purposes. For all simulation scenarios, the performance of TBT and CBT is better than that of No AS, with TBT outperforming CBT over most of the SNR range. The limit imposed on the maximum number of times a packet can be retransmitted affects the performance of the system at low SNR values. It is observed that the throughput for No AS exceeds that of CBT and TBT for SNR values of $< 8\ dB$ and $< 3\ dB$ respectively, while that of CBT exceeds that of TBT for SNR$< 2\ dB$. This can be

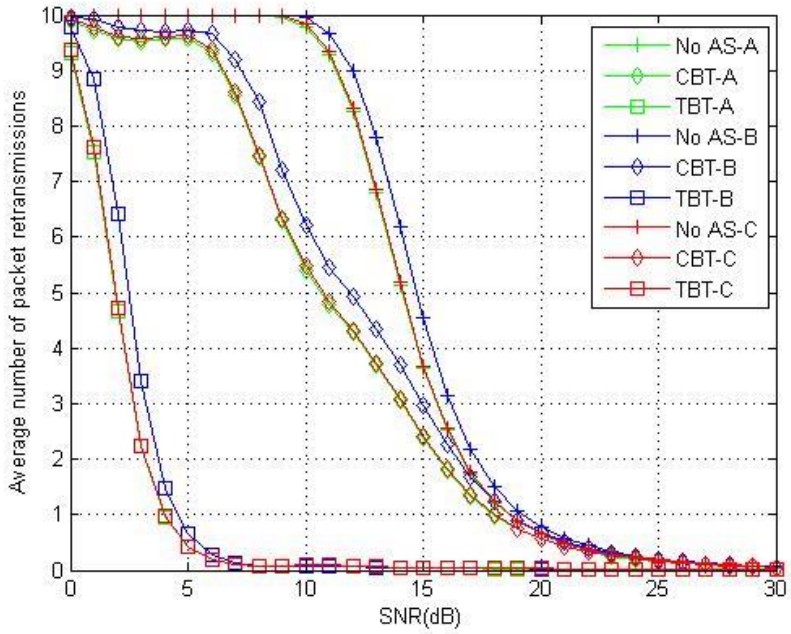

Figure 3.5. Plot of average number of packet retransmissions against SNR

explained by considering Figure 3.5, where the average number of packet retransmissions is plotted against SNR. For No AS, packets are retransmitted the maximum number of times for SNR $< 11\ dB$. The implication of this is that the packet retransmissions are less than they should be resulting in a higher throughput; similar observations can be made for CBT for SNR$< 6\ dB$. From Figure 3.5, it is observed that TBT is capable of keeping the packet retransmissions low over most of the SNR range, thus outperforming CBT in terms of transmission latency.

In Figure 3.4, it can be seen that the throughput for scenario B is less than that for scenario A, for TBT, CBT and No AS. The packet size for scenario B is twice that of scenario A. From (3.5) it is seen that the PER increases with the packet size; therefore a larger packet size increases packet retransmissions, as seen in Figure 3.5, resulting in reduced throughput. On the other hand, the throughput for scenario C is more than that for scenario A. N in scenario C is twice that in scenario A. From (3.11), it is observed that the throughput increases with $N/(N+1)$; since $W = N$, but from (3.5), N does not affect the PER, therefore, scenarios A and C have similar packet retransmissions as seen in Figure 3.5.

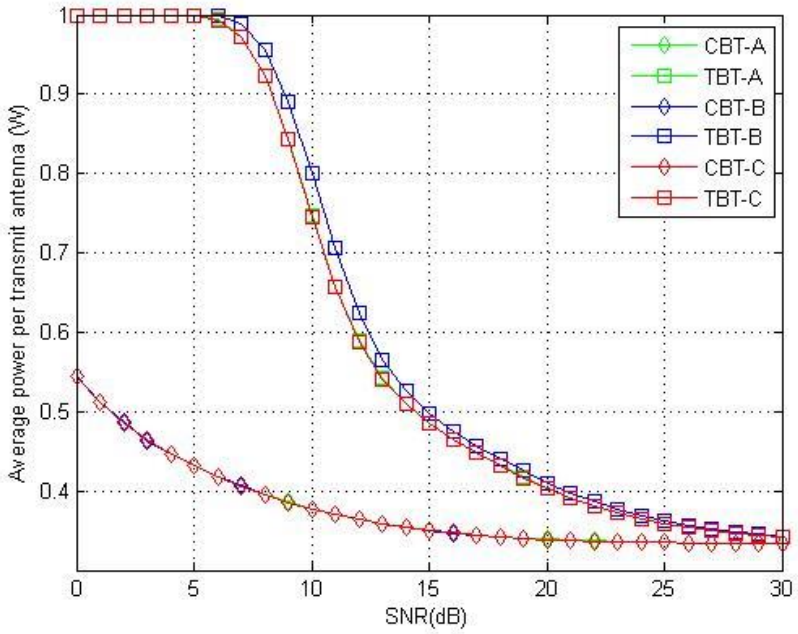

Figure 3.6. Plot of average transmit power per transmit antenna against SNR

The superior performance of TBT is because of its cross-layer design, compared to CBT which only uses information from the physical layer. This gives TBT the capability of concentrating power on the best transmit antennas, as shown in Figure 3.6, where the average power per transmit antenna (PPTA) is plotted against SNR. For all case scenarios, TBT has a higher PPTA than CBT at all SNR values. At high SNR values, both schemes tend to use more transmit antennas because the probability of the antennas having suitable conditions increases with SNR; but as the SNR decreases, less transmit antennas are used. This can be seen in Figure 3.7 where the bar charts for the transmit antenna usage percentage is shown at SNR values of $10\ dB$ and $25\ dB$, for all case scenarios. This explains why PPTA increases with decreasing SNR in Figure 3.6. From Figure 3.7, it is seen that TBT uses transmit antennas more efficiently (tends to use less antennas), which explains its higher PPTA value when compared with CBT.

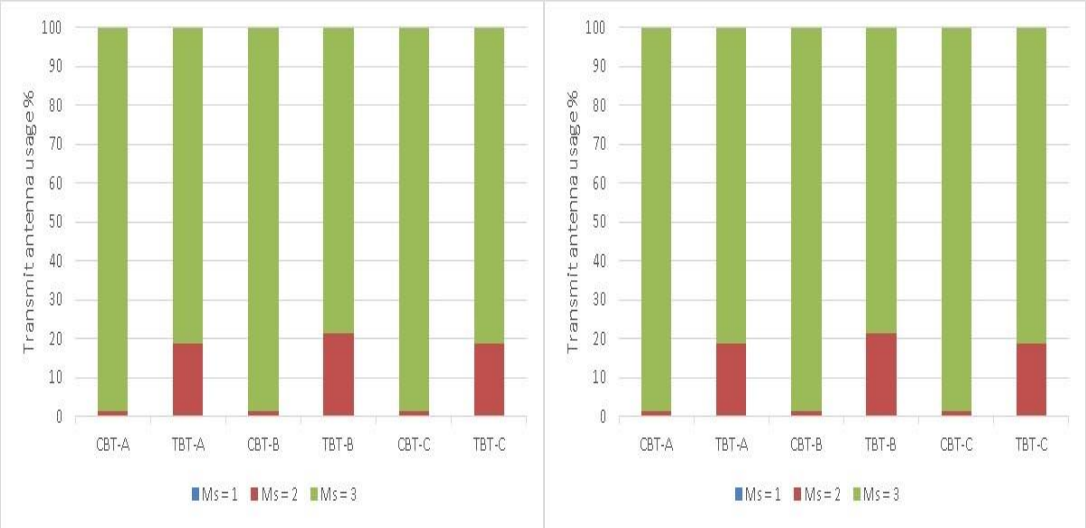

Figure 3.7. Bar charts of transmit antenna usage percentage at SNR of $10dB$ and $20dB$

Additionally, it is observed that because CBT does not explicitly consider packet size, PPTA and the percentage antenna usage is the same for all case scenarios. On the other hand, for TBT which considers packet size, scenarios A and C have similar power and antenna usage characteristics; since they use the same size of packet. Scenario B, which uses a larger packet size has a higher PPTA and it tends to use less antennas than scenarios A and C. As previously explained, the PER is higher for scenario B, hence the need for higher power per transmit antenna. TBTs knowledge of the packet size results in a lower percentage drop in throughput with increased packet size, e.g. doubling the packet size between scenario A and B results in a drop in throughput of 4.4% and 11.2% for TBT and CBT respectively at 10 dB. The similarity in the power and antenna usage characteristics between scenario A and C for both antenna selection schemes results in similar percentage increases in throughput from doubling N; 13.8% and 13.7% for CBT and TBT respectively at 15 dB.

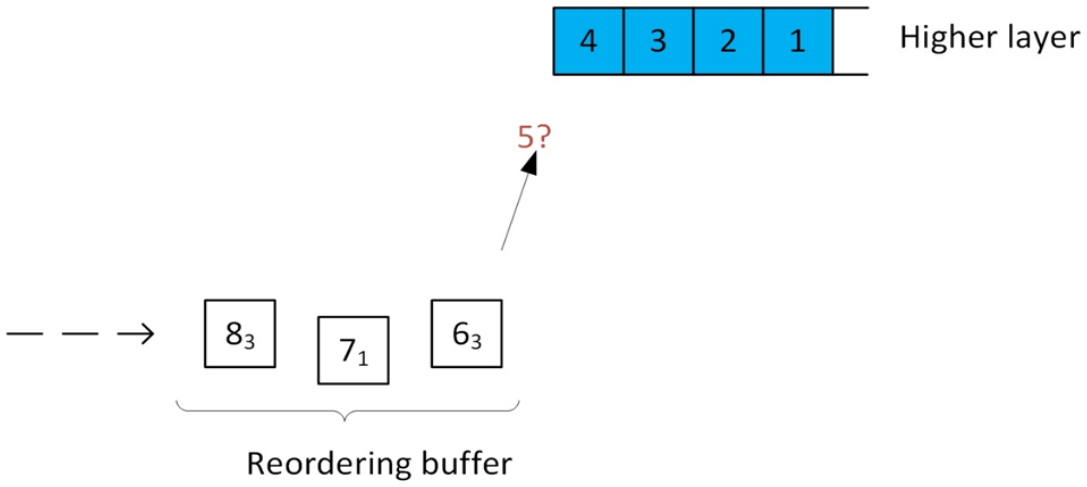

Figure 3.8. Stalling in the reordering buffer

{In Figure 3.8, the fifth packet in the sequence is missing from the reordering buffer preventing delivery to the higher layer of already correctly received successive packets}

3.1.4 Transmit Antenna Selection with Stall Avoidance

As described in Section 3.1.1, the implementation of N-SAW results in out-of-sequence packet arrival at the receiver. A reordering buffer is required at the receiver to ensure in-sequence packet delivery to the higher layer. With in-sequence packet delivery, a packet cannot be delivered to the higher layer if a preceding packet has not been correctly received; this results in packets stalling in the reordering buffer. An example of stalling is shown in Figure 3.8. The buffer storage requirements for MIMO systems with N-SAW, as a function of SNR, are investigated in Appendix D.

The latency in delivering packets, in-sequence, to the higher layer, and the increased buffer storage requirements due to stalling, can be reduced by implementing stall avoidance mechanisms. An example of a stall avoidance mechanism is the timer-based mechanism. The authors in [125]

Table 3.2. Timer-based stall avoidance algorithm

1	Initialize buffer and $SeqNum$
2	Receive packet
3	ACK or $Max\ ReTx$?
4	Place packet in buffer
5	Set packet timer to 1
6	$SeqNum$ in buffer?
7	Pass packet $SeqNum$ to higher layer
8	Last $SeqNum$?
9	Go to 22
10	Else
11	Increment $SeqNum$
12	Go to 20
13	Packets in buffer with timer $\geq$ threshold?
14	Send ACK for $SeqNum$
15	Last $SeqNum$?
16	Go to 22
17	Else
18	Increment $SeqNum$
19	Go to 20
20	Increment timers for all packets in buffer
21	Go to 2
22	Stop

investigated the performance of parallel SAW in High-Speed Downlink Packet Access (HSDPA) with timer-based stall avoidance; a timer is started when a packet cannot be delivered to the higher layer. When the timer expires, the missing packet is dropped. The timer-based stall avoidance algorithm implemented in this thesis is summarized in Table 3.2. The packets received correctly, or those which have been transmitted the maximum number of times ($Max\ ReTx$) are placed in the reordering buffer. The algorithm delivers packets to the higher layer in-sequence.

$SeqNum$ refers to the sequence number of the next packet to be passed to the higher layer. If $SeqNum$ is missing from the buffer and the timer for $SeqNum + 1$ expires ($\geq$ predetermined threshold timer value), then $SeqNum$ is dropped, i.e. an ACK is sent for $SeqNum$ to stop its retransmission.

3.1.4.1 Computer Simulations and Results

Monte Carlo simulations are used to evaluate the performance of throughput and capacity-based transmit antenna selection with stall avoidance. The simulation scenarios and parameters are as given in Section 3.1.3.1. Additionally, the threshold timer setting is set to $N + 1$ slots. The performance metric used to evaluate the performance is the number of dropped packets, which is measured in terms of the residual error rate (RER) [125], which is defined as follows:

$$RER = \frac{number\ of\ dropped\ packets\ in\ a\ session}{total\ packets\ transmitted\ in\ a\ session} \tag{3.15}$$

In Figure 3.9, the average RER is plotted against SNR. For all case scenarios, the RER increases exponentially, peaks and then decreases exponentially with decreasing SNR. At high SNR values, packet retransmissions are very low, as seen in Figure 3.5. This increases the probability of in-sequence packet arrival, which reduces stalling, therefore, very few packets are dropped. As the SNR decreases, packet retransmissions increase, resulting in decreased probability of in-sequence packet arrival; stalling of packets increases, leading to an increase in the number of dropped packets. As the SNR decreases further, a point is reached when the RER peaks, and then it begins to decrease. This is caused by the limit set on the maximum number of times a packet can be retransmitted. As the SNR decreases, the probability of packets being retransmitted the same number of times increases. Consequently, the probability of in-sequence packet arrival increases. The peaks correspond to the midpoints of the exponential parts of the plots in Figure 3.5, e.g. for scenario A the peaks for No AS, CBT and TBT occur at $14dB$, $8dB$ and $2dB$ respectively. For

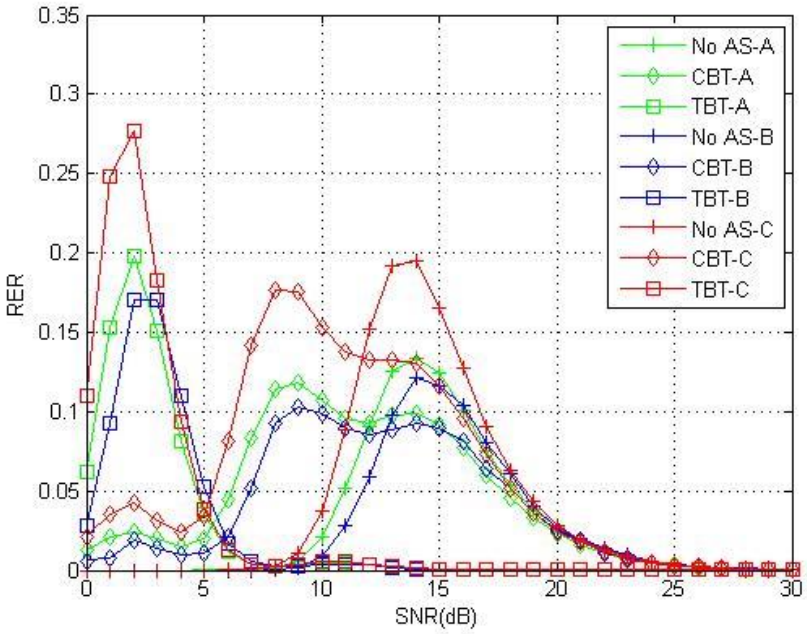

Figure 3.9. Plot of average RER against SNR

all case scenarios, the throughput-based approach is capable of keeping the number of dropped packets low over most of the SNR range, thereby outperforming the capacity-based approach over most of the SNR range.

From Figure 3.9, it is observed that the RER for scenario C is higher than for scenario A, for all SNR values. The higher number of SAW processes run in parallel in scenario C means that more packets stall, when a preceding packet is missing, resulting in increased packet timer expiration, leading to more dropped packets. The RER for scenario B is less than that for scenario A for all SNR values. Scenario B uses a larger packet size, and with the total amount of data transmitted in a session being the same for all scenarios, the number of packets transmitted per session is less for scenario B. Therefore, the trickle-down effect of a missing packet affects fewer packets, thereby resulting in less dropped packets.

It should be noted that there is a direct correlation between stalling and RER; as stalling increases, more packets are dropped. Increased buffer storage is required in order to prevent packets from being dropped. Therefore, the higher the RER, the higher the buffer storage requirements.

3.2 Performance Analysis of Transmit Antenna Selection in Underlay CR MIMO Systems

Cognitive radio is a promising technology for improving spectrum utilization. When combined with MIMO, which achieves high spectral efficiency, CR MIMO can serve as a solution to the ever-increasing demand for spectrum. Additionally, in coexisting environments, multiple antennas can be used to combat co-channel interference. In underlay CR MIMO systems, antenna selection can be used to reduce hardware complexity and cost, to improve system performance and to minimize the interference to the primary user receiver(s). Similar to MIMO systems, the main optimization criteria used in the design of antenna selection in CR MIMO systems, are physical-layer quantities.

In [102], ratio selection for coexisting systems is proposed. The proposed scheme selects a single cognitive transmit antenna in order to maximize the ratio between the cognitive and interference channel link gains. It is shown that ratio selection offers a good trade-off between the capacity of the secondary link and the interference to the PU RX, when fixed primary transmit power is used. The authors in [103] propose difference selection, where a single cognitive transmit antenna is selected according to the weighted difference between the channel gains of the cognitive and interference links. Difference selection is shown to be superior in performance compared with ratio selection - in cognitive networks with interference power constraints.

In [104], a low complexity transmit antenna selection algorithm for cognitive MISO systems, which use precoding techniques to control the interference to the primary system, is proposed. The proposed algorithm explores only a subset of all the available transmit antenna subsets, based on a ranking metric. This results in reduced computational complexity and near-optimal performance, compared with the optimal exhaustive search algorithm - which maximizes SINR. In [105], the authors formulate the antenna selection problem - with capacity as the criterion - as a combinatorial optimization problem. Low complexity algorithms, based on genetic algorithm and binary particle swarm optimization techniques, are then presented. Receive antenna selection for underlay CR networks, with SINR as the criterion, is analyzed in [106], while the authors in [107] propose

iterative and norm-based algorithms for underlay CR MIMO systems, which reduce the computational complexity of capacity-based transmit antenna selection.

With regard to the cross-layer design of antenna selection in cognitive networks, the authors in [119] propose throughput-based transmit antenna selection for underlay CR MIMO systems combined with beamforming - which is used to cancel out the interference at the PU RX; GBN is implemented at the data link layer. Consequently, the literature review in this section reveals the need for further work – in relation to cross-layer antenna selection in CR MIMO systems.

In this section, transmit antenna selection for underlay CR MIMO spatial multiplexing systems - from a cross-layer perspective - is addressed. The proposed throughput-based approach selects the subset of transmit antennas that maximize the throughput of the secondary system while satisfying the interference constraints at the PU RX(s). N-SAW is implemented as the ARQ protocol and the CR RX is equipped with a ZF linear receiver. The rest of this section is organized as follows: The system model is described in Section 3.2.1. In Section 3.2.2, the cross-layer transmit antenna selection algorithm is developed, and its performance is then evaluated.

3.2.1 System Description

Consider an underlay CR MIMO system, where the primary and secondary networks share the same spectrum band, whose bandwidth is assumed to be $1Hz$. The CR TX and CR RX are equipped with M and N_{cr} antennas respectively, as shown in Figure 3.10. The secondary system is configured to exploit spatial multiplexing, therefore, ($M \leq N_{cr}$) [10]. For the primary network, two different scenarios are considered separately, i.e. single-user (S-U) and multi-user (M-U). The two scenarios are represented in Figure 3.10 using the diagonal dashed line. The primary network consists of a single PU RX equipped with N_{PU} antennas in the S-U scenario, while the M-U scenario has N_{PU} single antennas PU RXs. For simplicity, the interference from the primary to the secondary system is not considered, since transmit antenna selection cannot be used to control the interference received from the primary network. The interference received from the primary

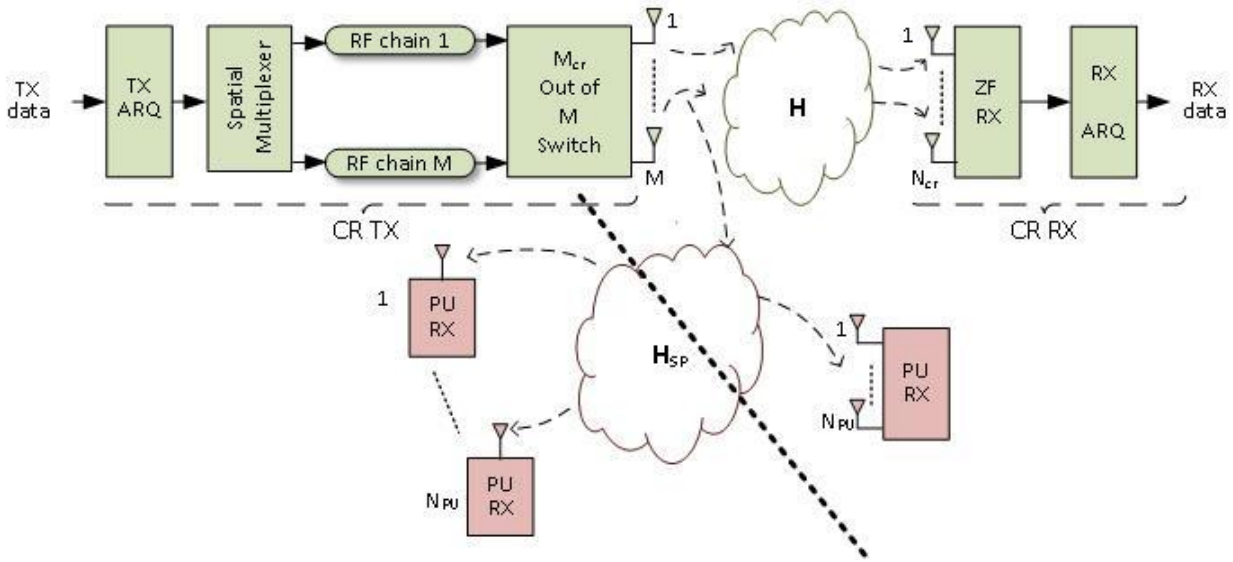

Figure 3.10. Underlay CR system model

network is dependent on the number of receive antennas the secondary system has, which remains constant. Therefore, the PU TX is not represented in the Figure 3.10.

The cognitive channel matrix, $\boldsymbol{H} \in \mathbb{C}^{N_{cr} \times M}$, is assumed to have ZMCSCG elements with unit variance. The channel from the CR TX to the PU RX(s), i.e. the interference channel, is represented by the channel matrix $\boldsymbol{H}_{SP} \in \mathbb{C}^{N_{PU} \times M}$, and it is assumed to have ZMCSCG elements with a variance of α. For the M-U scenario, the kth row in $\boldsymbol{H}_{SP}$ represents the interference channel vector to the kth PU RX, i.e.:

$$(\boldsymbol{h}_{SP})_k \in \mathbb{C}^{1 \times M} = \boldsymbol{H}_{SP}(k,:) \quad k = 1,2, \dots N_{PU} \tag{3.16}$$

All the channels are assumed to experience frequency flat Rayleigh fading and are assumed known at the CR TX. For antenna selection, the subset of M_{cr} ($1 \leq M_{cr} \leq M$) transmit antennas, which maximizes the performance of the secondary system, under interference constraints at the PU RX(s), is selected. Transmit antenna selection is implemented as a signal-processing technique for performance enhancement, therefore the secondary transmitter and receiver are equipped with an equal number of antennas as RF chains. The received signal at the CR RX, after transmit antenna selection (excluding the interference from the primary network), is given by:

$$\boldsymbol{y} = \sqrt{\frac{P_t}{M_{cr}}}\boldsymbol{H}_{cr}\boldsymbol{s} + \boldsymbol{n} \tag{3.17}$$

where $\boldsymbol{H}_{cr} \in \mathbb{C}^{N_{cr} \times M_{cr}}$ is the cognitive channel matrix after transmit antenna selection, $\boldsymbol{s}$ the cognitive transmit symbol vector, $\boldsymbol{n}$ the noise vector and P_t the average cognitive transmit power in one symbol period. $\boldsymbol{s}$ is assumed to have uncorrelated, zero mean symbols, with unit average energy, drawn from the selected constellation; while $\boldsymbol{n}$ is assumed to have ZMCSCG elements with a variance of N_o. The total power available to the CR TX in a symbol period - assumed to be 1 second - is $P = 1W$. The interference constraints at the PU RX(s) are met by the CR TX dynamically adjusting its transmit power P_t, where $P_t \leq P$; this is then allocated uniformly among the M_{cr} selected transmit antennas.

For the S-U scenario, the interference power at the PU RX is given by:

$$I = \frac{\|\boldsymbol{H}_{int}\|_F^2 P_t}{M_{cr}} \tag{3.18}$$

where $\boldsymbol{H}_{int} \in \mathbb{C}^{N_{PU} \times M_{cr}}$ is the interference channel matrix, after antenna selection. For the M-U scenario, the interference power at the PU RXs is given by:

$$I = \frac{\|\boldsymbol{h}_{int}\|_F^2 P_t}{M_{cr}} \quad k = 1,2, \ldots N_{PU} \tag{3.19}$$

where $\boldsymbol{h}_{int} \in \mathbb{C}^{1 \times M_{cr}}$ is the interference channel vector to the kth PU RX, after antenna selection. The interference constraints for the S-U and M-U scenarios are as stated below:

$$I \leq I_{SU} \tag{3.20}$$

$$I_k \leq (I_{MU})_k \quad k = 1,2, \ldots N_{PU} \tag{3.21}$$

Where I_{SU} and $(I_{MU})_k$ are the interference power thresholds values for the S-U and M-U scenarios respectively. The CR TX dynamically adjusts its transmit power to meet the interference

constraints given in (3.20) and (3.21); therefore, P_t needs to be calculated for each subset of selected transmit antennas. For the S-U scenario, P_t is determined from (3.18) and (3.20) as:

$$P_t = \begin{cases} P_n & when\ 0 \leq P_n \leq P \\ P & when\ P_n > P \end{cases} \tag{3.22}$$

where:

$$P_n = \frac{I_{SU} M_{cr}}{\|\boldsymbol{H}_{int}\|_F^2} \tag{3.23}$$

From (3.19) and (3.21), P_t in the M-U scenario, is calculated as follows:

$$P_t = \begin{cases} P_{min} = min_k P_k & when\ 0 \leq P_{min} \leq P \\ P & when\ P_{min} > P \end{cases} \tag{3.24}$$

where;

$$P_k = \frac{(I_{MU})_k M_{cr}}{\|\boldsymbol{h}_{int}\|_F^2} \quad k = 1,2, \ldots N_{PU} \tag{3.25}$$

3.2.2 Cross-Layer Transmit Antenna Selection in Underlay CR MIMO Systems

The selection criterion in cross-layer transmit antenna selection in underlay CR MIMO systems is data link throughput. Spatial multiplexing, N-SAW and modulation, are configured in the secondary network, as described in Section 3.1.1. Therefore, from (3.11), the normalized throughput for the secondary system, after antenna selection, can be expressed as:

$$\eta = b \times N \times M_{cr} \frac{l \times PCK_{no\_err}}{1 + W}\ bits/Hz/s \tag{3.26}$$

where b is the number of bits per symbol, N is the number of SAW processes run in parallel, W is the round-trip delay in slots and:

$$PCK_{no\_err} = \prod_{m=1}^{M_{cr}} (1 - SER_m)^{L/M_{cr}} \tag{3.27}$$

is the probability of an $L-$symbol packet being received without errors; given that each $L-$symbol packet is divided into M_{cr} streams before transmission, and assuming that the channel remains constant during the transmission of each packet. $SER_m = f(SNR_m, Mod)$ and $SNR_m = P_t/(M_{cr}N_o[(\boldsymbol{H}_{cr}^H \boldsymbol{H}_{cr})^{-1}]_{m,m})$ for $m = 1,2, \dots M_{cr}$, where SER_m and SNR_m are the post-processing SER and SNR for the mth data stream respectively.

In throughput-based transmit antenna selection for underlay CR MIMO systems, the transmit antenna subset that maximizes throughput, while satisfying the interference constraints at the PU RX(s), is selected. The optimization problem is formulated below:

$$\begin{aligned} P1 \max_{T(i)_j, P_t} \quad & \eta \\ subject\ to: \quad & P_t \leq P \\ & I \leq I_{SU} \text{ for S-U scenario} \\ & I_k \leq (I_{MU})_k \quad k = 1,2, \dots N_{PU} \text{ for M-U scenario} \end{aligned} \tag{3.28}$$

Given the throughput expression in (3.26) and the interference constraints in (3.20) and (3.21), the most straightforward and optimal way of solving $P1$ is through exhaustive search. The steps in the proposed scheme are summarized in Table 3.3. T_{ij} is used to represent the subset of selected transmit antennas, where $i = 1,2, \dots M$ and $j = 1,2, \dots \binom{M}{M_{cr}}$.

The performance of throughput-based transmit antenna selection is evaluated against that of capacity-based transmit antenna selection. Capacity-based transmit antenna selection in underlay CR MIMO systems selects the subset of transmit antennas that maximizes the capacity, as given

Table 3.3. Throughput-based transmit antenna selection algorithm

for $i = 1{:}\, M$

  for $j = 1{:} \binom{M}{M_{cr}}$

    Calculate P_t using (3.22) or (3.24)

    $\eta_{ij} = b \times N \times i \frac{l \times PCK_{no\_err}}{1+W}$

  end

end

Select the T_{ij} with the maximum throughput

i.e. $\{T_{ij}\}_{max} = \max_{i,j} \eta_{ij}$

in (3.29), while satisfying the CR transmit power constraint and the interference constraints at the PU RX(s).

$$C = log_2 \det\left[\boldsymbol{I}_{N_{cr}} + \frac{P_t}{N_o M_{cr}} \boldsymbol{H}_{cr} \boldsymbol{H}_{cr}^H\right] \; bits/Hz/s \tag{3.29}$$

3.2.2.1 Computer Simulation and Results

Simulations are carried out to evaluate the performance of throughput-based transmit antenna selection by comparing its performance with that of capacity-based transmit antenna selection. The simulation parameters are as follows; the number of CR transmit and receive antennas is $M = N_{cr} = 3$, $N = 3$ SAW processes are run in parallel with a round-trip delay of $W = 3$ slots. The error correcting code used is CRC-32, $l = 32/33$, $L = 128\ bytes$ and the limit on the maximum times a packet can be retransmitted is set to 10. The modulation schemes considered are QPSK and 16-QAM, with $b = 2$ and $b = 4$ respectively. Each point of the following results is generated by transmitting 300 kilobytes of data per session and then averaging over 10000 sessions. The metrics used to evaluate the performance are average throughput, average number of packet retransmissions (transmission latency) and PER.

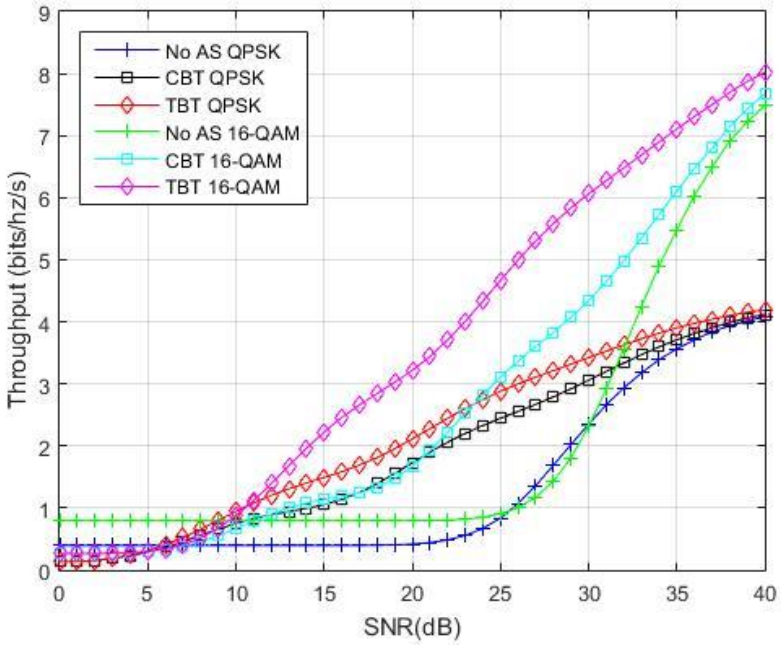

Figure 3.11. Plot of average throughput against SNR for M-U scenario

The throughput and transmission latency are calculated as described in Section 3.1.3.1. The PER is calculated as follows:

$$PER = \frac{number\ of\ erroneously\ accepted\ packets}{total\ number\ of\ packets\ transmitted\ in\ session} \tag{3.30}$$

The number of erroneously accepted packets is determined as follows. A received packet is accepted if the error detecting code detects no errors in the packet, or if the packet has been retransmitted the maximum number of times. The accepted packet is then compared with the packet that was actually transmitted, to determine whether it was accepted erroneously; therefore, the PER in (3.30) is a data link layer quantity.

In Figure 3.11, the average throughput for throughput-based (TBT) and capacity-based (CBT) transmit antenna selection for the M-U scenario is plotted against SNR, with $\alpha = 0.1$, $N_{PU} = 2$, $(I_{MU})_k = 10mW$. The throughput with no antenna selection (No AS) is also included for comparison purposes. The throughput performance of both TBT and CBT is superior to that of

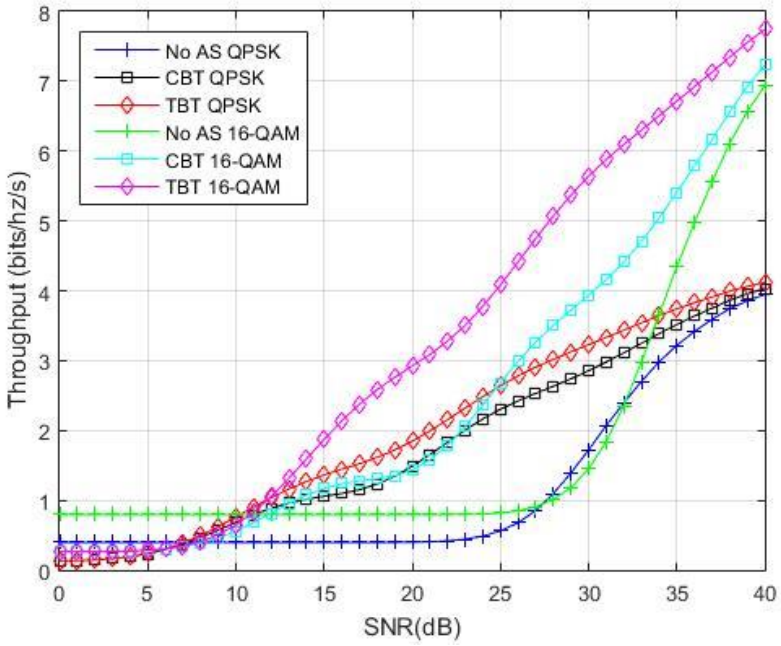

Figure 3.12. Plot of average throughput against SNR for S-U scenario

No AS; but TBT outperforms CBT over the entire range of SNR values for QPSK and 16-QAM. The magnitude by which the throughput of TBT exceeds that of CBT is higher for 16-QAM; e.g. at a SNR value of 30 dB the throughput of TBT exceeds that of CBT by 0.4 and 1.8 $bits/Hz/s$ for QPSK and 16-QAM respectively.

Similar results are obtained for the S-U scenario, as seen in Figure 3.12 - with $\alpha = 0.1$, $N_{PU} = 2$, $I_{SU} = 10mW$ - but with reduced throughput performance compared with the M-U scenario. The interference threshold per PU RX is the same for both scenarios, with two single antenna PU RXs and one PU RX with two antennas for M-U and S-U respectively. The interference power received by the PU RX in the S-U scenario is the sum of the interference powers received at each antenna; therefore, more interference power is received per PU RX compared with the MU scenario. This explains the better performance in the M-U scenario; e.g. at a SNR value of 30 dB, the throughput for TBT is 6.1 and 5.7 $bits/Hz/s$ for MU and SU respectively for 16-QAM.

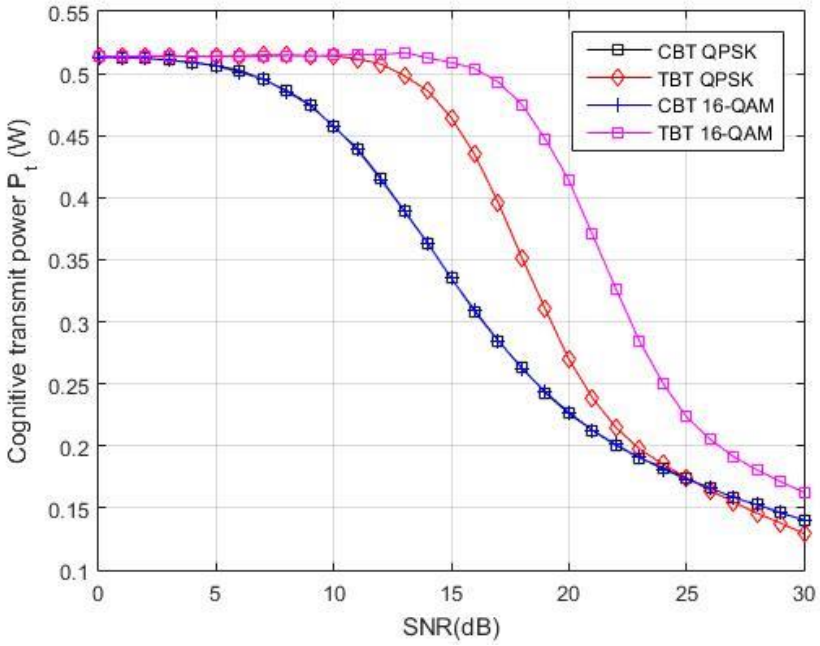

Figure 3.13. Plot of CR transmit power against SNR for MU scenario

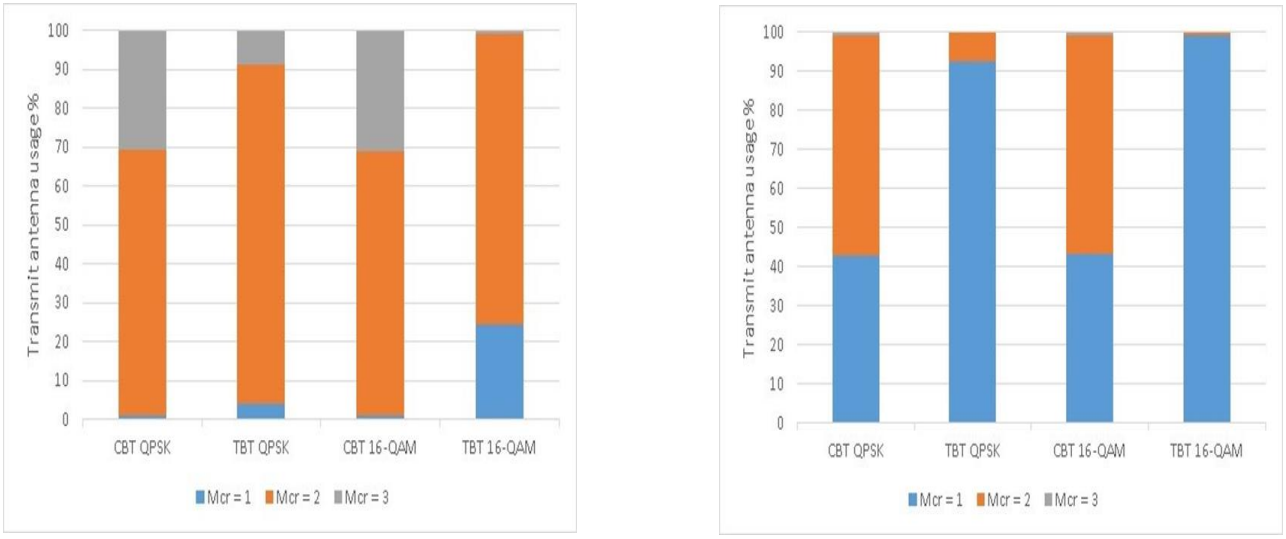

Figure 3.14. Bar charts of CR transmit antenna usage percentage at $15dB$ and $25dB$

TBT has superior performance because it considers additional parameters from the physical and data link layers, e.g. modulation scheme, packet size etc., which are not considered by CBT. This allows TBT to efficiently allocate cognitive transmit power as depicted in Figure 3.13, where the

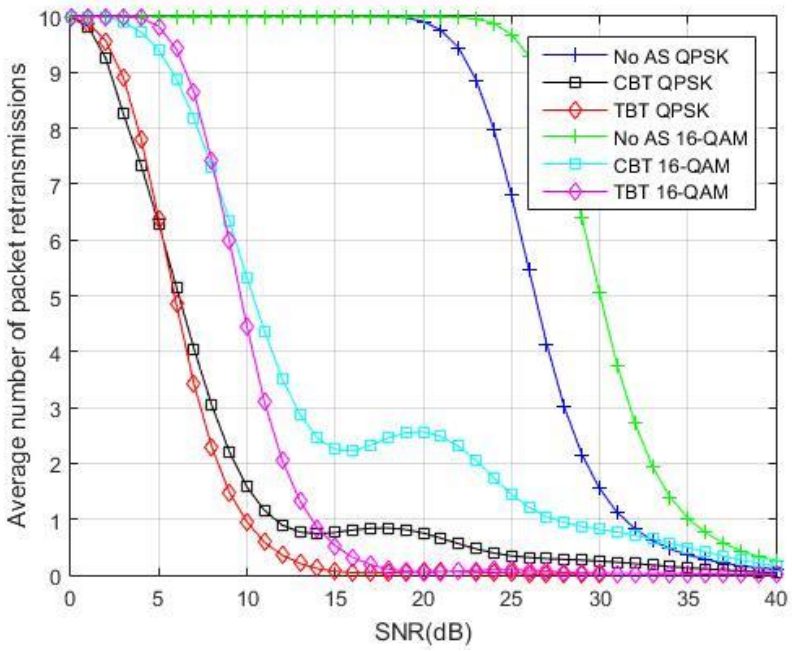

Figure 3.15. Plot of average number of packet retransmissions against SNR for S-U scenario

cognitive transmit power is plotted against SNR. Because TBT considers the modulation scheme, the cognitive transmit power for 16-QAM is higher than that of QPSK, while for CBT the transmit power is the same for both modulation schemes, at all SNR values.

The transmit power for TBT is higher than that of CBT for all SNR values. TBT's knowledge of the modulation scheme in use gives it the capability of exploiting the available transmit power more efficiently. In Figure 3.14, bar charts of the transmit antenna usage percentage are shown for TBT and CBT at SNR values of $15dB$ and $25dB$. It is observed that TBT uses transmit antennas more efficiently than CBT. At higher SNR values, both schemes tend to use more transmit antennas, because the probability of the antennas having suitable conditions increases with SNR.

In Figure 3.15, the average number of packet retransmissions is plotted against SNR for the S-U scenario. TBT outperforms CBT in terms of transmission latency for all SNR values for both QPSK and 16-QAM. TBT also outperforms CBT in terms of data link layer PER, as can be seen

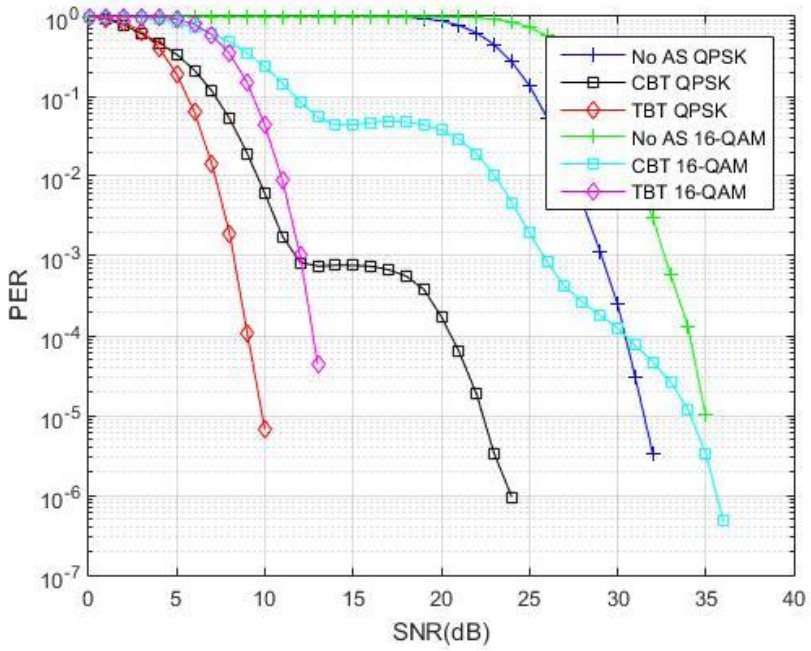

Figure 3.16. Plot of PER against SNR for M-U scenario

in Figure 3.16, where the PER is plotted against SNR for the M-U scenario. TBT has better PER for both QPSK and 16-QAM at all SNR values.

3.3 Chapter Summary and Conclusions

In this chapter, the analytical throughput expression for spatial multiplexing multiple-antenna systems (i.e. MIMO and underlay CR MIMO systems), equipped with ZF linear receivers and N-SAW implemented at the data link, was derived. A cross-layer approach to transmit antenna selection, based on throughput as the optimization criterion, was presented. For reference purposes, a physical-layer approach, based on capacity maximization, was also considered. The throughput-based approach outperforms the capacity-based approach in terms of throughput, transmission latency, data link layer packet error rate and storage buffer requirements. Moreover, in the presence of stalling in the receiver reordering buffer, throughput maximization drops fewer packets, when a timer-based stall avoidance mechanism is implemented.

Chapter 4 Cross-Layer Energy-Efficient Transmit Antenna Selection for MIMO Systems

In this chapter, energy-efficient transmit antenna selection for MIMO systems, is investigated from a cross-layer perspective. The proposed antenna selection scheme maximizes a cross-layer energy efficiency metric, by jointly optimizing the transmit antenna subset and the transmit power, subject to transmit power and spectral efficiency constraints. The chapter is organized as follows; Section 4.1 serves as an introduction and motivation. In Section 4.2, the description of the system model under consideration, is presented; while Section 4.3 proposes the cross-layer energy efficiency metric. In Section 4.4, cross-layer transmit antenna selection is presented and analysed. In Section 4.5, reduced complexity near-optimal algorithms are developed. In Section 4.6, the performance of the proposed cross-layer scheme is further enhanced by incorporating adaptive modulation. Sections 4.7 and 4.8 analyze the impact of correlation and packet size on energy efficiency respectively. Section 4.9 examines the effect that the number of transmit antennas has on energy efficiency. Finally, Section 4.10 concludes the chapter.

4.1 Introduction

From the literature review presented in Chapter 2, it is observed that energy-efficient transmit antenna selection can be used as a tool to design energy efficient wireless systems with high spectral efficiency. Additionally, the metrics used in literature were physical-layer metrics. The discussions on cross-layer designs in Chapter 2 showed that adopting a cross-layer approach, which combines functionalities and information between different layers in the TCP/IP architecture, greatly enhances the performance of wireless systems. Cross-layer transmit antenna selection for spatial multiplexing multiple-antenna systems, was presented and analysed in Chapter 3. The results showed that throughput-based transmit antenna selection achieves overall enhanced system performance; this is due to the utilization of characteristics from the data link and physical layers.

Capacity represents the transmitted bits in a second; therefore, the popular capacity-based bits-per-Joule EE metric is quantified as the number of transmitted bits per Joule. When ARQ is implemented at the data link layer, an error detecting code forms packets by appending parity bits to a block of information bits. Additionally, erroneously received packets are retransmitted, depending on the ARQ retransmission strategy. Therefore, the capacity consists of parity bits, retransmitted bits and successfully received information bits. Consequently, antenna selection that optimizes a capacity-based energy efficiency metric optimizes the energy required to transmit the parity bits, retransmitted bits and successfully received information bits. However, this does not necessarily result in an energy efficient system; optimizing the number of bits transmitted per unit energy does not necessarily optimize the number of transmitted bits required to receive a given number of information bits successfully. Therefore, packet retransmission is not optimal, and the energy used in packet retransmissions degrades the energy efficiency of the system.

Motivated by the above, this chapter proposes a cross-layer energy efficiency metric. The proposed energy efficiency metric is defined as the ratio of the system throughput to the total power consumption of the system, and is quantified in terms of the "bits per Joule" metric. The throughput derived in Chapter 3 is used in defining the proposed cross-layer EE metric, which is measured in terms of the number of successfully received information bits per unit energy.

4.2 System Description

Consider a point-to-point spatial multiplexing MIMO system equipped with M_T and N_r transmit and receive antennas respectively, where $M_T \leq N_r$ [10]. The MIMO channel, $\boldsymbol{H} \in \mathbb{C}^{N_r \times M_T}$, is assumed to have ZMCSCG elements with unit variance. The channel is assumed to experience frequency flat Rayleigh fading, and is assumed known only at the receiver. The subset, made-up of an adaptable number of transmit antennas M_t ($1 \leq M_t \leq M_T$), which maximizes the energy efficiency of the MIMO system, is selected at the receiver. Information relating to the selected transmit antenna subset is relayed to the transmitter via a low feedback channel, which is assumed to be error free with zero delay. N-SAW is implemented at the data link layer and the receiver is

equipped with a ZF linear receiver, which separates the received signal into its component M_t transmitted data streams.

The data bit stream received by the transmit data link layer is encoded using an error detecting (n, k) linear block code. At the physical layer, each n −bit packet is modulated into an L −symbol packet, where $L = n/b$, with b the number of bits per symbol. An un-coded spatial multiplexing system is assumed, where each packet is divided into M_t equal parallel streams, which are then switched to the best M_t antennas for transmission. Each packet is transmitted in its own slot, with a slot period of L/M_t symbol periods. The channel response is assumed to be constant during the transmission of each packet. The available transmit power, P_T, is divided uniformly among the selected transmit antennas. The received signal, after transmit antenna selection, is given by:

$$\boldsymbol{y} = \sqrt{\frac{P_T}{M_t}}\boldsymbol{H}_t\boldsymbol{s} + \boldsymbol{n} \tag{4.1}$$

where $\boldsymbol{H}_t \in \mathbb{C}^{N_r \times M_t}$ is the channel matrix after transmit antenna selection, $\boldsymbol{s} \in \mathbb{C}^{M_t \times 1}$ the transmit symbol vector and $\boldsymbol{n} \in \mathbb{C}^{N_r \times 1}$ the noise vector. $\boldsymbol{s}$ is assumed to have uncorrelated, zero mean symbols with unit average energy, drawn from the selected constellation, while $\boldsymbol{n}$ is assumed to have ZMCSCG elements with a variance of N_o.

4.3 Capacity vs. Throughput-based Energy Efficiency Metrics

As mentioned in Section 2.3, one of the most popular energy efficiency metrics is the 'bits per Joule' metric, which is defined in terms of the system capacity, i.e. capacity-based energy efficiency (CB-EE). In this section, we introduce an energy efficiency metric measured in terms of the number of successfully received information bits per Joule. The proposed EE metric is defined as the ratio of the throughput to the total power consumed by the system, i.e. throughput-based energy efficiency (TB-EE).

The power consumption of the system is required before the energy efficiency metrics can be derived. The power consumption model described in Section 2.3 will be used; according to this model, the total power consumption of the system is given by [65]:

$$P_{total} = P_{PA} + P_c \tag{4.2}$$

where P_{PA} is the power consumed by all the power amplifiers (PA) and P_c is the circuit power i.e. the power consumed by all the other circuit blocks excluding the power amplifiers. P_c is modelled as a function of the number of active RF chains [65] [66] as follows:

$$P_c = M_t P_{ct} + N_r P_{cr} + P_{co} \tag{4.3}$$

where P_{ct} and P_{cr} is the power consumed by each transmit and receive chain respectively and P_{co} is the power consumed in all the other parts of the circuitry. According to the consumption model in Section 2.3 and (2.24), P_{ct} and P_{cr} can be expressed as follows:

$$P_{ct} = P_{DAC} + P_{mix} + P_{filt} \tag{4.4}$$

$$P_{cr} = P_{LNA} + P_{mix} + P_{IFA} + P_{filr} + P_{ADC} \tag{4.5}$$

As mentioned in Section 2.3, the power model described is simplified and does not include all the signal-processing blocks of a wireless system. However, the methodology used in describing the power consumption makes it easy to incorporate any additional blocks. In this context, P_{co} represents the power consumed by any additional signal-processing blocks, e.g. source coding, digital modulation etc. For simplicity, we will also assume that the power consumed by the frequency synthesizers, $2P_{syn}$ (see (2.24)), is part of P_{co}; and that P_{co} is fixed.

The consumption of the power amplifiers, P_{PA}, is given by:

$$P_{PA} = P_{PA1} + P_{PA2} + \cdots + P_{PAM_t} \tag{4.6}$$

where P_{PAi} is the power consumed by the ith power amplifier. P_{PAi} is modelled as:

$$P_{PAi} = (1 + \alpha)P_{Ti} \tag{4.7}$$

where $\alpha = \xi/\varrho - 1$, with ϱ the drain efficiency of the power amplifier and ζ the peak to average ratio (PAR) - which is dependent on the modulation scheme and the associated constellation size [126]. P_{Ti} is the transmit power allocated to the ith transmit antenna. Assuming that all the power amplifiers are identical, P_{PA} can be expressed as follows:

$$P_{PA} = (1 + \alpha)\sum_{i=1}^{M_t} P_{Ti} = (1 + \alpha)P_T \tag{4.8}$$

where $P_T = \sum_{i=1}^{M_t} P_{Ti}$. The power consumption for the power amplifiers, used in this thesis, takes into account the modulation scheme in use, unlike the model described in Section 2.3, see (2.22). The power consumption model for the power amplifiers in (2.22) is also used in literature; when defining physical-layer energy efficiency metrics.

With regard to the energy efficiency metrics for the proposed system, we will first derive the capacity-based energy efficiency metric, followed by the proposed throughput-based energy efficiency metric. The post-processing capacity of the proposed system, will be used to calculate CB-EE. The normalized capacity of the kth data stream, after antenna selection, is given by:

$$C_k = log_2(1 + SNR_k) \;\; bits/hz/s \quad k = 1,2, \dots M_t \tag{4.9}$$

where $SNR_k = P_T/(u_k M_t N_o)$ is the post-processing SNR for the kth data stream, with $u_k = [(\boldsymbol{H}_t^H \boldsymbol{H}_t)^{-1}]_{k,k}$. The normalized capacity of the system, after antenna selection, is then given by:

$$C = \sum_{k=1}^{M_t} C_k = \sum_{k=1}^{M_t} log_2(1 + SNR_k) \;\; bits/Hz/s \tag{4.10}$$

From its definition, the capacity-based energy efficiency of the system, after antenna selection, can now be expressed as:

$$CB - EE = \frac{B \times C}{P_{total}} = \frac{B \times C}{(1+\alpha)P_T + P_c} \ \ bits/Joule \tag{4.11}$$

where B is the bandwidth in Hz. The normalized CB-EE - after antenna selection - with respect to bandwidth, is given by:

$$EE_{CB} = \frac{CB - EE}{B} = \frac{\sum_{k=1}^{M_t} log_2(1+SNR_k)}{(1+\alpha)P_T + P_c} \ \ bits/Hz/Joule \tag{4.12}$$

From (4.12), it is observed that only physical-layer parameters are used in calculating EE_{CB}, making it a physical-layer quantity. Therefore, energy-efficient antenna selection that optimizes EE_{CB} is a physical-layer approach.

Next, the proposed throughput-based energy efficiency is derived. From Chapter 3, see (3.11), the normalized throughput of the proposed system, after antenna selection, is given by:

$$\eta = b \times N \times M_t \frac{l \times (1 - PER)}{1 + W} \ \ bits/Hz/s \tag{4.13}$$

where N is the number of SAW processes run in parallel, W the round-trip delay in slots, $l = k/n$ the ratio of information symbols per packet with:

$$PER = 1 - \prod_{k=1}^{M_t} (1 - SER_k)^{L/M_t} \tag{4.14}$$

where $SER_k = f(SNR_k, Mod)$ is the SER for the kth data stream, with Mod accounting for the modulation specific SER expression. From its definition, the TB-EE of the system, after antenna selection, is given by:

$$TB - EE = \frac{B \times \eta}{P_{total}} = \frac{B \times \eta}{(1+\alpha)P_T + P_c} \ \ bits/Joule \tag{4.15}$$

Consequently, the normalized TB-EE, after antenna selection, is given by:

$$EE_{TB} = \frac{TB - EE}{B} = \frac{b \times N \times M_t \times l \times (1 - PER)}{(1 + W)\big((1 + \alpha)P_T + P_c\big)} \ \ bits/Hz/Joule \tag{4.16}$$

From (4.16), it is observed that information from the data link and physical layers is used to calculate EE_{TB}, making it a cross-layer metric. Therefore, energy-efficient antenna selection that optimizes EE_{TB} is a cross-layer approach.

4.4 Cross-Layer Energy-Efficient Transmit Antenna Selection

In this section, cross-layer energy-efficient transmit antenna selection, based on the proposed throughput-based energy efficiency metric, is presented. The proposed algorithm maximizes EE_{TB}, by jointly optimizing the transmit antenna subset and the transmit power, subject to transmit power and spectral efficiency constraints. The SE constraint, in terms of the SNR, is determined as follows; the SNR for the kth data stream is rewritten as follows:

$$SNR_k = \frac{P_T}{N_0 M_t} v_k \quad k = 1,2, \ldots M_t \tag{4.17}$$

where $v_k = 1/u_k$. The SE of the system, i.e. the normalized capacity as given in (4.10), can now be expressed as:

$$C = \sum_{k=1}^{M_t} \left(1 + \frac{P_T}{N_0 M_t} v_k\right) \ \ bits/Hz/s \tag{4.18}$$

Let $\mathbf{\Lambda} = diag\big(v_1, v_2, \ldots v_{M_t}\big)$. Using $\mathbf{\Lambda}$, (4.18) can now be represented as follows:

$$C = log_2 det\left(\boldsymbol{I}_{M_t} + \frac{P_T}{N_o M_t}\mathbf{\Lambda}\right) \ \ bits/Hz/s \tag{4.19}$$

From (4.19), the SE of the system in terms of SNR is given by:

$$SNR_{sum} = \sum_{k=1}^{M_t} SNR_k = \frac{P_T}{N_o M_t} \sum_{k=1}^{M_t} v_k \tag{4.20}$$

Finally, the optimization problem is formulated as follows:

$$\begin{aligned} P1 \max_{T(i)_j, P_T} \quad & EE_{TB} \\ subject\ to: \quad & P_T \leq P_{TMax} \\ & SNR_{sum} = \beta \end{aligned} \tag{4.21}$$

where $T(i)_j$ denotes the jth transmit antenna subset consisting of i active transmit antennas, P_{TMax} is the maximum available transmit power in a symbol period and β is the required SNR_{sum} at the receiver.

Given $P1$, the most straight forward and optimal method of solving it is by performing an exhaustive search over all possible transmit antenna combinations, i.e. transmit antenna subsets. For each transmit antenna subset, the transmit power, P_T, has to be determined before EE_{TB} can be calculated. The transmit power that satisfies the SE constraint is determined as follows:

$$P_{SE} = \frac{M_t N_o \beta}{\sum_{k=1}^{M_t} v_k} \tag{4.22}$$

However, the available transmit power has a maximum value of P_{TMax}, therefore, if $P_{SE} > P_{TMax}$ then the required SE will have to be decreased in order to satisfy the transmit power constraint. The optimal exhaustive search cross-layer energy-efficient transmit antenna selection algorithm is given in Table 4.1.

With regard to the physical-layer approach, the algorithm maximizes EE_{CB}, by jointly optimizing the transmit antenna subset and the transmit power, subject to transmit power and SE constraints. The optimization problem is formulated in (4.23).

Table 4.1. Optimal exhaustive search cross-layer energy-efficient transmit antenna selection

---

for $i = 1: M_T$

for $j = 1: \binom{M_T}{i}$

Calculate P_{SE} using (4.22)

if $P_{SE} > P_{TMax}$

$P_T = P_{TMax}$

else

$P_T = P_{SE}$

end

$P_c = iP_{ct} + N_r P_{cr} + P_{co}$

$EE_{TB}(T(i)_j) = \frac{b \times N \times i \frac{l \times (1-PER)}{1+W}}{(1+\alpha)P_T + P_c}$

end

end

select the $T(i)_j$ with the maximum EE_{TB}

i.e. $\{T(i)_j\}_{max} = \max_{i,j} EE_{TB}(T(i)_j)$

$$P2 \max_{T(i)_j, P_T} \quad EE_{CB}$$

$$subject\ to: \quad P_T \leq P_{TMax}$$

$$SNR_{sum} = \beta \tag{4.23}$$

Similar to $P1$, $P2$ is solved optimally through an exhaustive search.

4.4.1 Computer Simulations and Results

In this section, the performance of the proposed cross-layer energy-efficient transmit antenna selection algorithm is evaluated via Monte Carlo simulations. The performance of the cross-layer approach is analyzed by comparing it with that of the physical-layer approach. The results are generated by averaging over 100000 channel realizations. The following parameters are used in the simulations; the values of P_{ct}, P_{cr}, P_{co}, and ϱ are $120mW$, $85mW$, $30mW$ and 0.35 [16] [120] [126]. The maximum available transmit power P_{TMax} is $27dBm$, a noise power spectral density (PSD) of $-174dBm/Hz$, and a bandwidth of $B = 10MHz$. The number of transmit and receive antennas is $M_T = N_r = 4$, $N = 4$ SAW processes are run in parallel with a round-trip delay of $W = 4$ slots. A packet length of $L = 528$ symbols is used with $l = 32/33$. The modulation schemes considered are 4-QAM and 16-QAM, thus $b = 2$ and $b = 4$ respectively. The value for PAR for M-QAM is $\xi = 3\left(\sqrt{M} - 1/\sqrt{M} + 1\right)$, with $M = 2^b$, when a square constellation is assumed [126]. Log-distance path loss with an exponent of 4 is adopted; including this in (4.1), the received signal at a distance of d meters away from the transmitter is given by:

$$\boldsymbol{y} = \sqrt{\frac{P_T d^{-4}}{M_t}}\boldsymbol{H}_t\boldsymbol{s} + \boldsymbol{n} \tag{4.24}$$

In Figure 4.1, the normalized TB-EE, at $d = 200m$, for EE_{TB} and EE_{CB} maximization is plotted against SNR, for 4-QAM and 16 QAM. For comparison purposes, the TB-EE of the system with no antenna selection (No AS) is also included. It is observed that energy-efficient transmit antenna selection improves the energy efficiency of the MIMO system, i.e. both EE_{TB} and EE_{CB} maximization outperform the No AS system; additionally, the cross-layer approach outperforms the physical-layer approach for 4-QAM and 16-QAM over the entire SNR range.

The probability of transmit antennas having suitable conditions, in terms of post-processing SNR, increases with SNR. Consequently, the throughput of the No AS system (all transmit antennas active) increases with SNR. This can be seen in Figure 4.2, where the normalized throughput is plotted against the SNR, at $d = 200m$. However, from (4.22), it is observed that P_{SE}, and as a

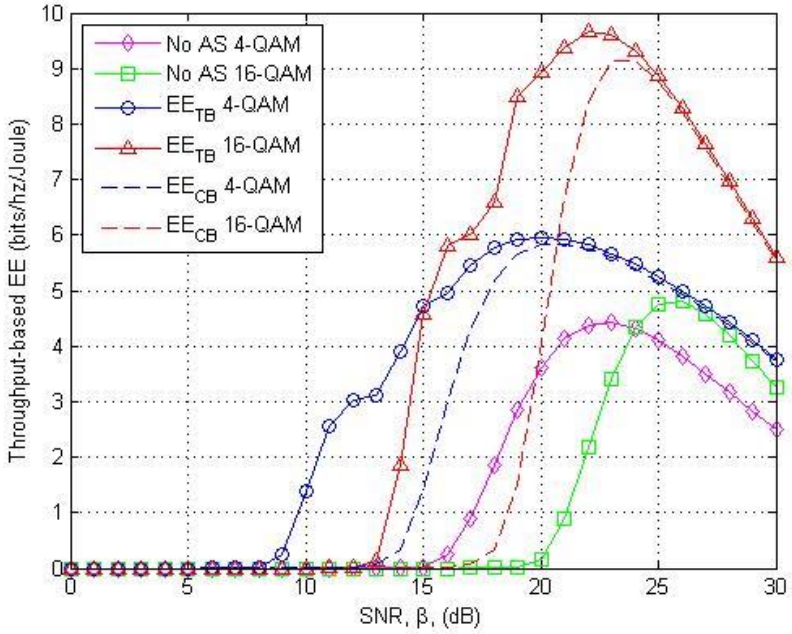

Figure 4.1. Plot of normalized throughput-based energy efficiency against SNR, $d = 200m$

result P_T, increases with SNR. Therefore, TB-EE, for the No AS system, increases with SNR until a maximum value is reached; the optimal SNR values (when the energy efficiency is maximum), for 4-QAM and 16-QAM are $23dB$ and $26dB$, with maximum energy efficiency values of 4.42 and 4.82 $bits/Hz/Joule$ respectively. After that, the increasing transmit power degrades the energy efficiency of the system, i.e. the increased power consumption of the system begins to outweigh the increasing system throughput.

With regards to EE_{TB} and EE_{CB} maximization, the algorithms adapt the number of active transmit antennas and transmit power, depending on the SNR and the varying channel conditions, in order to optimize TB-EE and CB-EE respectively. In Figure 4.3, the average number of active transmit antennas ($ANATA$) is plotted against the SNR. $ANATA$ is determined as follows:

$$ANATA = \sum_{t=1}^{M_T} t \times TAUR_t \tag{4.25}$$

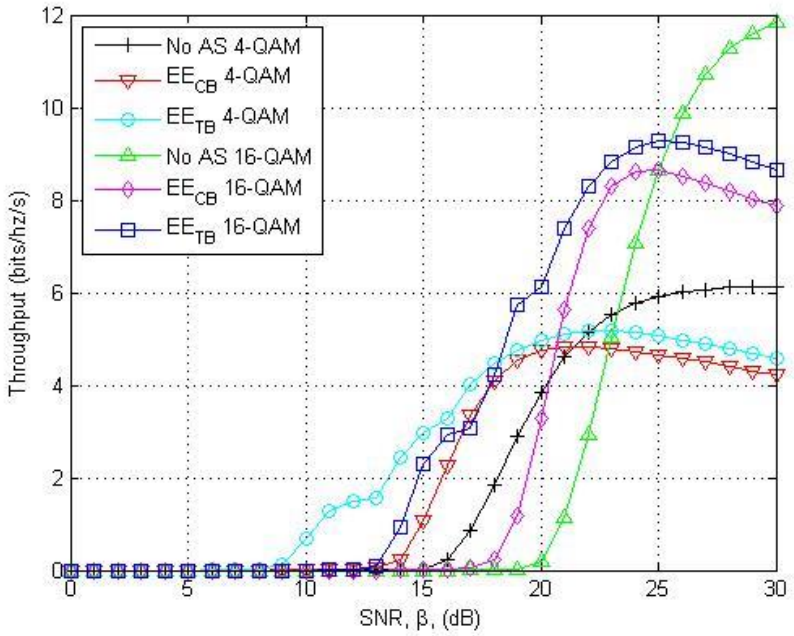

Figure 4.2. Plot of normalized throughput against SNR, $d = 200m$

$TAUR$ is the transmit antenna usage ratio for t transmit antennas; this is determined from simulations. $ANATA$ increases with SNR, and the combined increase in SNR and $ANATA$ results in increased throughput for both EE_{TB} and EE_{CB} maximization, see Figure 4.2. Consequently, TB-EE increases with SNR, until a maximum value is reached, see Figure 4.1. Thereafter, the increasing transmit power degrades the energy efficiency of the system; in an effort to optimize the energy efficiency, the algorithms use less antennas, resulting in $ANATA$ decreasing with SNR. The optimal SNR values for EE_{TB} maximization are $20dB$ and $22dB$ for 4-QAM and 16-QAM respectively, with maximum energy efficiency values of 5.96 and 9.65 $bits/Hz/Joule$. For EE_{CB} maximization the optimal SNR values are $21dB$ and $23dB$ with maximum EE values of 5.84 and 9.14 $bits/Hz/Joule$. Beyond the optimal SNR values, the throughput of the system begins to decrease, as $ANATA$ decreases, for both EE_{TB} and EE_{CB} maximization, see Figure 4.2. The maximum throughput values for EE_{TB} maximization occur at $23dB$ and $25dB$ for 4-QAM and 16-QAM respectively, while those for EE_{CB} maximization occur at $21dB$ and $25dB$.

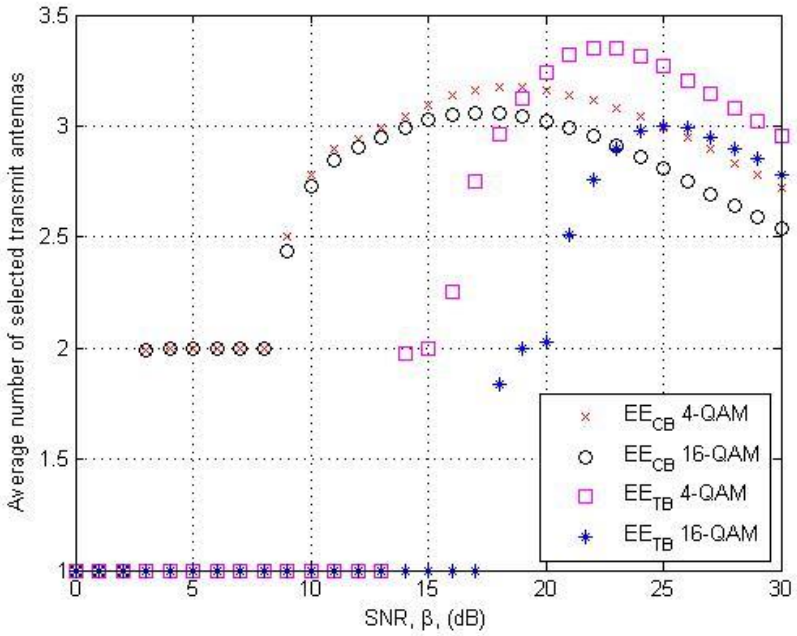

Figure 4.3. Plot of average number of transmit antennas against SNR, $d = 200m$

EE_{TB} maximization outperforms EE_{CB} maximization both in terms of energy efficiency and throughput over the entire SNR range, with lower optimal SNR and maximum EE values. The reason for this is that the cross-layer approach maximizes the number of successfully received bits per unit energy while the physical-layer approach maximizes the number of transmitted bits per unit energy. The cross-layer approach explicitly considers additional parameters from the physical and data link layers, e.g. modulation scheme, packet size, ARQ scheme etc., which are not considered by the physical-layer approach; allowing it to jointly exploit the transmit power and the transmit antennas more efficiently.

The gap between the normalized TB-EE curves for the physical and cross-layer approaches is wider for 16-QAM compared to 4-QAM, e.g. at $15dB$ the difference is 3.6 and 4.6 $bits/Hz/Joule$ respectively. However, as the SNR increases, the difference in performance decreases, this is attributed to the reduction in packet retransmissions as the PER decreases with SNR. Therefore, the contribution of the retransmitted bits to the capacity of the system reduces with increasing SNR, resulting in EE_{CB} maximization approaching EE_{TB} maximization.

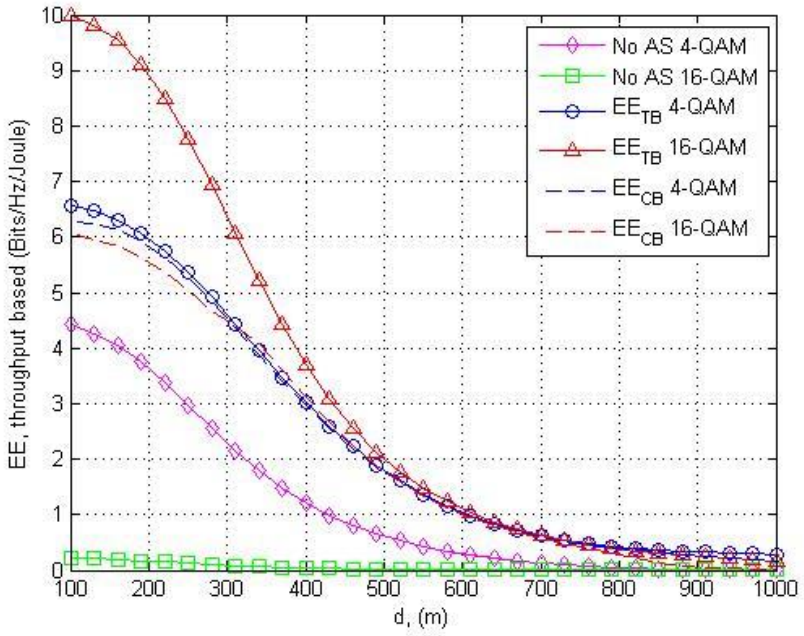

Figure 4.4. Plot of normalized throughput-based energy efficiency against d, SNR= $20dB$

More specifically, the difference in performance is less than $0.08\ bits/Hz/Joule$ for SNR values of more than $22dB$ and $26dB$ for 4-QAM and 16 QAM respectively.

In Figure 4.4, the normalized TB-EE is plotted against the transmission distance, d, at a SNR value of $20dB$. EE_{TB} maximization outperforms EE_{CB} maximization for both 4-QAM and 16-QAM for all d. As d increases, TB-EE degrades due to the increased transmit power, as can be deduced from (4.22) and (4.24), where it can be observed that the transmit power needed to meet the spectral efficiency constraint increases with increasing d. Additionally, in a bid to optimize the energy efficiency, both algorithms use less transmit antennas as d increases, resulting in decreased throughput; e.g. for EE_{TB} maximization (4-QAM) at $d = 400m$ and $700m$ the transmit power is $0.0335W$ and $0.2744W$, the normalized throughput 4.22 and 4.85 $bits/Hz/s$, with an $ANATA$ of 2.73 and 2.49. The rate at which TB-EE decreases with d is higher for 16-QAM compared to 4-QAM; 16-QAM has a larger value of PAR, resulting in the increasing transmit power having a larger impact on the TB-EE, e.g. between $d = 190\ m$ and $d = 490\ m$, the percentage decrease in TB-EE is 68.6 % and 76.6% for 4-QAM and 16-QAM respectively.

4.5 Reduced Complexity Algorithms for Cross-layer Energy-Efficient Transmit Antenna Selection

As mentioned in Section 4.4, exhaustive search is required to obtain the optimal solution for the optimization problem P1 given in (4.21); more precisely, a total of $\sum_{M_t=1}^{M_T} \binom{M_T}{M_t}$ different transmit antenna subsets must be taken into account. Additionally, complex matrix inversion is required in order to calculate the transmit power and throughput-based energy efficiency for each transmit antenna subset. This results in a computational complexity that increases with the number of transmit antennas. In this section, two algorithms that reduce the complexity of the optimal exhaustive search algorithm are proposed.

To develop the algorithms that reduce the complexity associated with the exhaustive search algorithm, we begin by upper bounding the PER given in (4.14) as follows:

$$PER \leq 1 - (1 - SER_{min})^L \tag{4.26}$$

Where SER_{min} is the symbol error rate for the data stream with the least SNR value, that is:

$$SNR_{min} = min_k SNR_k \quad k = 1,2, \dots M_t \tag{4.27}$$

Therefore, $SER_{min} = f(SNR_{min}, Mod)$. The normalized throughout given in (4.13) can now be lower bound as follows:

$$\eta \geq b \times N \times M_t \frac{l \times (1 - SER_{min})^L}{1 + W} \tag{4.28}$$

Therefore, for fixed number of selected transmit antennas, M_t, a simplified, but sub-optimal, method of maximizing the throughput is to select the transmit antenna subset that maximizes SNR_{min}. This method will not result in an optimization of EE_{TB}, as seen from (4.16); this is because every transmit antenna subset has a different value of P_{SE}, as calculated from the SE constraint, and P_{SE} has a direct impact on the value of P_T. Maximizing EE_{TB} requires the

simultaneous maximization and minimization of η and P_T respectively, since P_c is constant for a fixed M_t. Now, for a fixed number of transmit antennas, P_{SE} as given in (4.22) can be upper bound as follows:

$$P_{SE} \leq \frac{\beta N_o M_t}{M_s v_{min}} = \frac{\beta N_o}{v_{min}} \tag{4.29}$$

where:

$$v_{min} = min_k v_k \quad k = 1,2, \ldots M_t \tag{4.30}$$

Therefore, a simplified (sub-optimal) method of minimizing P_{SE}, and as a result P_T, is to select the transmit antenna subset that maximizes v_{min}. SNR_{min} can be expressed in terms of v_{min} as:

$$SNR_{min} = \frac{P_T v_{min}}{N_o M_t} \tag{4.31}$$

From [40], SNR_{min} can be lower bound as:

$$SNR_{min} \geq \lambda_{min}^2(\boldsymbol{H}_t) \frac{P_t}{N_o M_t} \tag{4.32}$$

where $\lambda_{min}(\boldsymbol{H}_t)$ is the minimum singular value of $\boldsymbol{H}_t$. Combining (4.31) and (4.32) we get:

$$v_{min} \geq \lambda_{min}^2(\boldsymbol{H}_t) \tag{4.33}$$

From (4.28), (4.29), (4.32) and (4.33), it is observed that for a fixed number of transmit antennas, EE_{TB} can be optimized (i.e. simultaneously maximizing of η and minimizing P_T) by selecting the transmit antenna subset that maximizes $\lambda_{min}(\boldsymbol{H}_t)$.

The result arrived at above, is used to develop an algorithm, based on exhaustive search; but with a complexity that is less than that of the optimal exhaustive search algorithm. The algorithm, referred to as Algorithm I, divides antenna selection into two stages; intra-level selection, performed first, followed by inter-level selection. A level is made up of antenna subsets with a

Table 4.2. Algorithm I

for $i = 1: M_T$

for $j = 1: \binom{M_T}{i}$

Determine $\lambda_{min}(\boldsymbol{H}_{ij})$

end

Select $T(i)_j$ with the maximum $\lambda_{min}(\boldsymbol{H}_{ij})$

i.e. $T(i)_{j-max} = \max_j \lambda_{min}(\boldsymbol{H}_{ij})$

Calculate P_{SE} for $T(i)_{j-max}$ using (4.22)

if $P_{SE} > P_{TMax}$

$P_T = P_{TMax}$

else

$P_T = P_{SE}$

end

$P_c = iP_{ct} + N_r P_{cr} + P_{co}$

$EE_{TB}(T(i)_{j-max}) = \frac{b \times N \times i \times l \times (1-PER)}{(1+W)((1+\alpha)P_T + P_c)}$

end

end

select the $T(i)_{j-max}$ with the maximum EE_{TB}

i.e. $T(i_{max})_{j-max} = \max_i EE_{TB}(T(i)_{j-max})$

fixed number of transmit antennas, i, where $i = 1,2, \ldots M_T$. The steps involved in Algorithm I are as follows;

- Determine the minimum singular value, $\lambda_{min}(\boldsymbol{H}_t)$, for all $\boldsymbol{H}_t$, i.e. channel matrices corresponding to all possible transmit antenna combinations.
- At each level, perform intra-level selection, i.e. select the transmit antenna subset with the maximum $\lambda_{min}(\boldsymbol{H}_t)$.
- Calculate the EE_{TB}, corresponding to the selected transmit antenna subset at each level.

- Perform inter-level selection, i.e. select the level, along with the corresponding transmit antenna subset, with the maximum EE_{TB}.

Algorithm I is described in Table 4.2.

Intra-level selection -in Algorithm I - does not require the computation of EE_{TB}, see Table 4.2, which implies that complex matrix inversion, $[\boldsymbol{H}_t^H \boldsymbol{H}_t]^{-1}$, is also not required. The major contributor to computational complexity is matrix inversion; therefore, Algorithm I reduces the complexity by decreasing the number of times $[\boldsymbol{H}_t^H \boldsymbol{H}_t]^{-1}$ is computed.

The transmit antenna subset selected by intra-level selection is not necessarily optimal. Algorithm I's performance can be improved by modifying intra-level selection as follows. The transmit antenna subsets in a level are first ordered by $\lambda_{min}(\boldsymbol{H}_t)$, in descending order. The intra-level algorithm then iterates through the ordered antenna subsets, calculating EE_{TB}, and terminating when EE_{TB} decreases between two adjacent transmit antenna subsets, bringing an end to intra-level selection. Inter-level selection is carried out after intra-level selection is complete at all levels. The algorithm, referred to as Algorithm II, is described in Table 4.3.

4.5.1 Analysis of the Reduced Complexity Algorithms

In this section, the performance of the proposed reduced complexity algorithms is evaluated via Monte Carlo simulations. The simulation parameters are as given in Section 4.4.1. In Figure 4.5, the normalized throughput-based energy efficiency for EE_{TB} maximization, for the optimal exhaustive search (OES) algorithm, Algorithm I and Algorithm II, is plotted against SNR at $d = 200m$; for 4-QAM and 16-QAM. It is observed that for SNR values of $< 13dB$ and $\geq 20dB$), for 4-QAM ($< 17dB$ and $\geq 23dB$ for 16-QAM), Algorithm I and Algorithm II have near-optimal performances. For SNR values of $> 20dB$ for 4-QAM ($> 23dB$ for 16-QAM), Algorithm II performs slightly better than its counterpart; as an example, the difference in performance between the OES algorithm and the two reduced complexity algorithms, Algorithm I and Algorithm II,

Table 4.3. Agorithm II

for $i = 1: M_T$

for $j = 1: \binom{M_T}{i}$

Determine $\lambda_{min}(\boldsymbol{H}_{ij})$

End

Order the transmit antenna subsets by $\lambda_{min}(\boldsymbol{H}_{ij})$ in descending order

$EE_{TB}(i) = 0$

for $j = 1: \binom{M_T}{i}$

Calculate P_{SE} using (4.22)

if $P_{SE} > P_{TMax}$

$P_T = P_{TMax}$

else

$P_T = P_{SE}$

end

$P_c = iP_{ct} + N_r P_{cr} + P_{co}$

$EE_{TB}(T(i)_j) = \frac{b \times N \times i \times l \times (1-PER)}{(1+W)((1+\alpha)P_T + P_c)}$

if $EE_{TB}(T(i)_j) \geq EE_{TB}(i)$

$EE_{TB}(i) = EE_{TB}(T(i)_j)$

else

break

end

end

end

From the M_T levels select the level with the maximum EE_{TB}

i.e. $i_{max} = \max_i EE_{TB}(i)$

at $24dB$ is 0.38% and 0.02% for 4-QAM (0.26% and 0.00% for 16-QAM) respectively. Between $13dB$ and $20dB$ for 4-QAM ($17dB$ and $23dB$ for 16-QAM), the reduced complexity

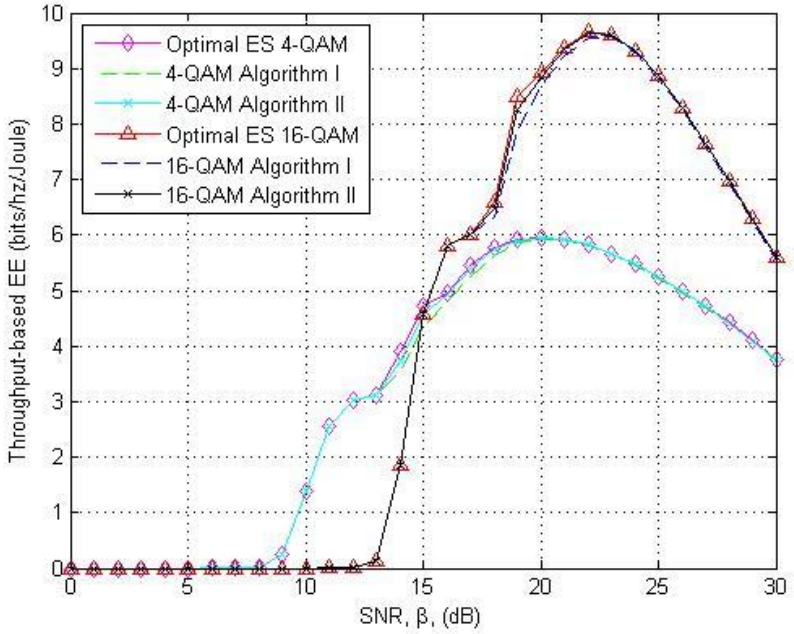

Figure 4.5. Plot of TB-EE against SNR at $d = 200m$, for OES, Algorithms I and II

algorithms exhibit reduced performances, with Algorithm II still outperforming Algorithm I.

In Figure 4.6, the normalized TB-EE for EE_{TB} maximization, for OES algorithm, Algorithm I and Algorithm II, is plotted against d at SNR$= 20dB$; for 4-QAM and 16-QAM. For 4-QAM, both reduced complexity algorithms have near-optimal performances for all d. For 16-QAM, Algorithm I and Algorithm II have near-optimal performances for distances of $\geq 290m$ and $\geq 230m$ respectively, with Algorithm II outperforming Algorithm I.

With regard to computational complexity, one can deduce from the number of times Algorithm I computes EE_{TB}, that it has a lower complexity than that of OES. This is because computing the singular values of $\boldsymbol{H}_t$ is less complex than computing the complex matrix inverse $[\boldsymbol{H}_t^H \boldsymbol{H}_t]^{-1}$, which is required to calculate EE_{TB} [25] [127]. $[\boldsymbol{H}_t^H \boldsymbol{H}_t]^{-1}$ is computed $\sum_{M_t=1}^{M_T} \binom{M_T}{M_t}$ and M_T times by OES and Algorithm I respectively. From simulations, for a 4×4 MIMO system, Algorithm II computes EE_{TB} on average 4.71 and 4.55 times for 4-QAM and 16-QAM respectively; in comparison, EE_{TB} is computed 15 and 4 times by OES and Algorithm I

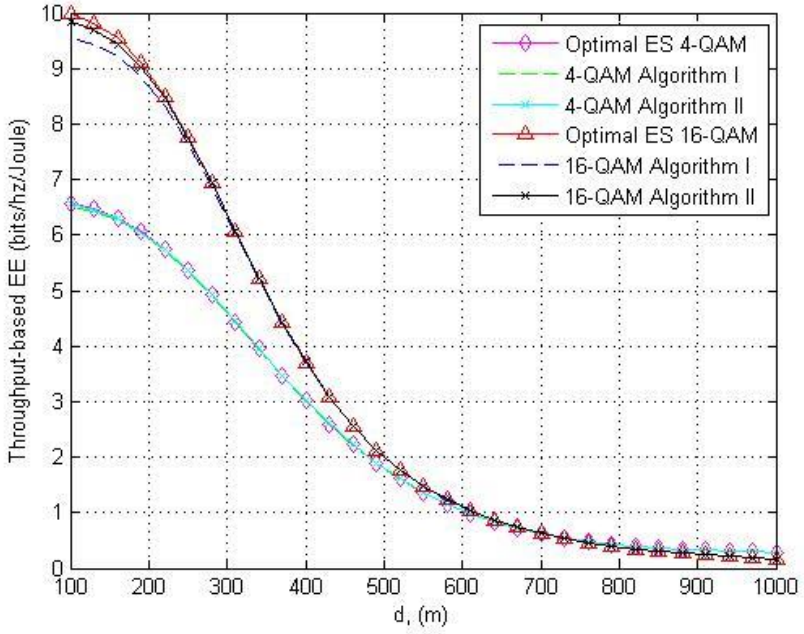

Figure 4.6. Plot of TB-EE against d at $20dB$ for OES, Algorithms I and II

respectively. Therefore, Algorithm II is less complex than OES, but slightly more complex than Algorithm I. This simplified complexity analysis (and the resulting deductions) is supported by the detailed computational complexity analysis found in Appendix E. The computational complexities, expressed in terms of floating point operations (flops), for OES, Algorithm I and Algorithm II, are given below:

$$\sum_{M_t=1}^{M_T} \binom{M_T}{M_t} \{72(M_t)^3 + 4(M_t)^2(8N_r + 1)\} \tag{4.34}$$

$$\sum_{M_t=1}^{M_T} \left\{72(M_t)^3 + 4(M_t)^2(8N_r + 1) + \binom{M_T}{M_t} \{32N_r(M_t)^2 - 32(M_t)^3\ /3\}\right\} \tag{4.35}$$

$$\frac{A_m}{M_T}\left\{\sum_{M_t=1}^{M_T}\{72(M_t)^3+4(M_t)^2(8N_r+1)\}\right\} + \sum_{M_t=1}^{M_T}\binom{M_T}{M_t}\{32N_r(M_t)^2-32(M_t)^3/3\} \tag{4.36}$$

A_m, in (4.36) represents the average number of times Algorithm II computes EE_{TB}. For the 4×4 MIMO system, the computational complexity for OES, Algorithm I and Algorithm II, determined using (4.34), (4.35) and (4.36) respectively is 26688, 19010 and 20991 flops (for 4-QAM). This represents a reduction in complexity of 28.8% and 21.3% for Algorithm I and Algorithm II, in comparison with OES.

4.6 Incorporation of Adaptive Modulation

In this section, the performance of the cross-layer energy efficient transmit antenna selection algorithm presented in Section 4.4, is further enhanced by incorporating adaptive modulation. Adaptive modulation and coding (AMC) techniques can be used to enhance the spectral efficiency of wireless links, particularly MIMO channels, by adjusting the transmission parameters to the time-varying channel conditions [128] [129]. Some pioneering work, in adaptive modulation and antenna selection, can be found in [130] [131].

Adopting a cross-layer energy efficiency criterion makes the integration of adaptive modulation into antenna selection easy and straightforward, this is because EE_{TB} explicitly considers the modulation scheme used. For simplicity, a common modulation scheme will be used for all active transmit antennas. Including adaptive modulation, in the selection scheme, consists of jointly selecting the transmit antenna subset, along with the corresponding modulation scheme, that maximizes EE_{TB}, subject to transmit power and SE constraints. This is accomplished as follows; for each transmit antenna subset, EE_{TB} is calculated for each modulation scheme; then, the modulation scheme with the maximum EE_{TB} is selected. Finally, the transmit antenna subset

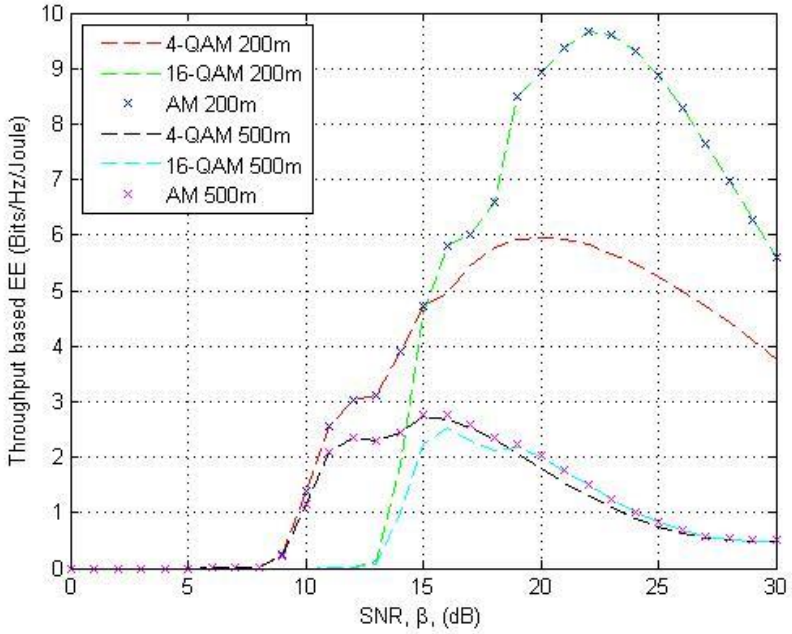

Figure 4.7. Plot of normalized TB-EE against SNR for EE_{TB} maximization with AM

(along with the optimal modulation scheme), which optimizes EE_{TB} is selected via exhaustive search.

4.6.1 Computer Simulation and Results

In this section, Monte Carlo simulations are used to evaluate the performance of cross-layer energy-efficient transmit antenna selection with adaptive modulation. The simulation parameters used are as given in Section 4.4.1. In Figure 4.7, the normalized throughput-based energy efficiency is plotted against SNR, for EE_{TB} maximization with adaptive modulation (AM), at $d = 200m$ and $d = 500m$. At $d = 200m$, for low ($< 15dB$) and high ($> 19dB$) SNR values the modulation scheme with the lowest and highest constellation size is selected, while between $15dB$ and $19dB$, both modulation schemes are used, this can be seen in Table 4.4, where the usage ratio for 4-QAM at fixed distances, for EE_{TB} maximization with adaptive modulation, is given. The additional degrees of freedom provided when adaptive modulation is incorporated into the antenna

Table 4.4. 4-QAM usage ratio at fixed distances

SNR (dB)	4	7	10	13	16	19	22	25	28
$d = 200m$	1	1	1	1	1	0.9	0	0	0
$d = 500m$	1	1	1	1	0.73	0.38	0.01	0.03	0.34

Table 4.5. 4-QAM usage ratio at fixed SNR values

$d\ (m)$	220	310	400	490	580	670	760	850	940
$15dB$	0.89	0.83	0.83	0.85	0.87	0.97	1	1	1
$20dB$	0	0	0.03	0.16	0.31	0.41	0.58	0.80	0.92

selection mechanism results in enhanced performance; i.e. a TB-EE that is higher than that of 4-QAM and 16-QAM for the SNR range $15dB - 19dB$. As an example, at $15dB$, the TB-EE with adaptive modulation is 4.7 compared to 4.72 and 4.56 $bits/Hz/Joule$ for 4-QAM and 16-QAM respectively. On the other hand, at $d = 500m$ 4-QAM is used for $< 15dB$, while both modulation schemes are used for $\geq 15dB$. The probability of the SE constraint being decreased, to ensure that the transmit power constraint is satisfied, increases with both d and SNR, this explains why both modulation schemes are used for $\geq 15dB$, resulting in enhanced performance.

Similar observations are found in Figure 4.8, where the normalized TB-EE is plotted against d, and in Table 4.5, where the usage for 4-QAM is given, at $15dB$ and $20dB$. As an example of the enhanced performance, for a SNR of $20dB$ at $d = 210m$, the TB-EE is 6.08 compared to 6.07 $bits/Hz/Joule$ for 16-QAM; while for $15dB$ at $d = 500m$, the TB-EE is 3.12 compared to 3.07 $bits/Hz/Joule$ for 4-QAM.

4.7 Impact of Correlation on Energy Efficiency

In this section, we examine the impact of spatial correlation on the energy efficiency and throughput of MIMO systems with cross-layer energy-efficient transmit antenna selection. The

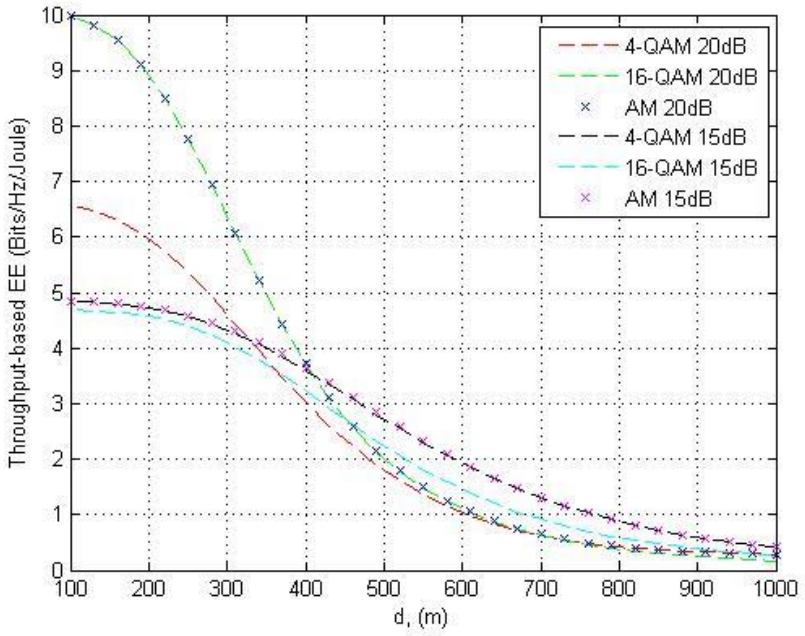

Figure 4.8. Plot of normalized TB-EE against d for EE_{TB} maximization with AM

MIMO channel, $\boldsymbol{H} \in \mathbb{C}^{N_r \times M_T}$, of the system described in Section 4.2 is now assumed to be a spatially correlated frequency flat Rayleigh fading channel. Transmit antenna correlation is assumed (i.e. no receive antenna correlation) therefore $\boldsymbol{H}$ is given by [11]:

$$\boldsymbol{H} = \boldsymbol{H}_w R_t^{1/2} \tag{4.37}$$

where $\boldsymbol{H}_w \in \mathbb{C}^{N_r \times M_T}$ is assumed to have ZMCSCG elements with unit variance, and $\boldsymbol{R}_t \in \mathbb{C}^{M_T \times M_T}$ is the transmit correlation matrix. The exponential correlation model in [132] is used, therefore, the entries of the transmit correlation matrix $\boldsymbol{R}_t$, are given by:

$$[\boldsymbol{R}_t]_{i,j} = \begin{cases} \rho^{j-i} & i \leq j \\ [\boldsymbol{R}_t]_{i.j}^* & i > j \end{cases} \tag{4.38}$$

where ρ is the complex correlation coefficient of neighbouring transmit branches ($|\rho| \leq 1$).

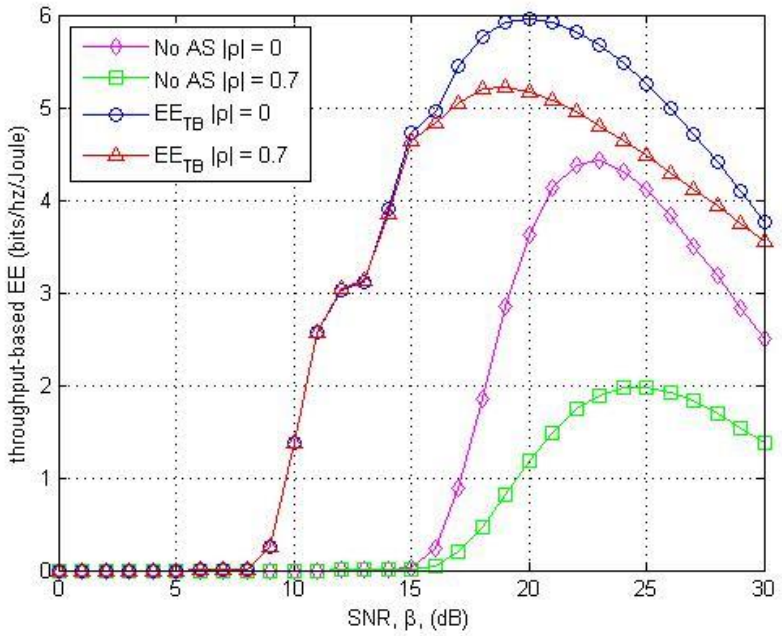

Figure 4.9. Plot of normalized TB-EE against SNR for a spatially correlated MIMO system

4.7.1 Computer Simulations and Results

In this section, the performance of cross-layer energy-efficient transmit antenna selection, in the presence of correlation, is evaluated via Monte Carlo simulations. The simulation parameters used are as given in Section 4.4.1. Two correlation settings are considered; the uncorrelated ($|\rho| = 0$) and the correlated ($[\rho] = 0.7$) cases.

In Figures 4.9 and 4.10, the normalized throughput-based energy efficiency and throughput respectively, for EE_{TB} maximization, at $d = 200m$, are plotted against the SNR for 4-QAM. The plots for the No AS are included for comparison purposes. It is observed that energy-efficient transmit antenna selection improves the TB-EE of the spatially correlated MIMO system. Furthermore, spatial correlation reduces the TB-EE and throughput of the No AS system for all SNR values; while for the system with cross-layer energy-efficient transmit antenna selection, the reduction occurs at high SNR values ($> 13dB$).

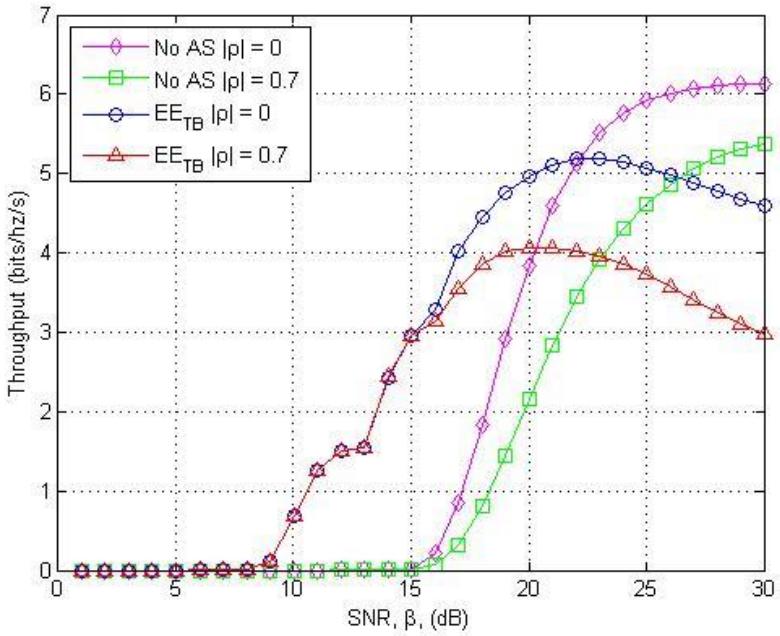

Figure 4.10. Plot of throughput against SNR for a spatially correlated MIMO system

As mentioned in Section 4.4.1, the probability of antennas having suitable conditions increases with SNR; therefore, for EE_{TB} maximization, the number of active transmit antennas used increases with SNR. This can be seen in Tables 4.6 and 4.7, where the transmit antenna usage ratio for $|\rho| = 0$ and $|\rho| = 0.7$ respectively, is given at different SNR values, at $d = 200m$. At low SNR values, the probability of antennas having suitable conditions is low, resulting in less antennas being used. More specifically, for SNR$\leq 13dB$, only one active transmit antenna is used for both $|\rho| = 0$ and $|\rho| = 0.7$, resulting in equal throughput and energy efficiency for both cases; since there is no correlation when only one transmit antenna is used, see Figures 4.9 and 4.10.

For SNR$> 13dB$, more than one transmit antenna is used. Spatial correlation results in SNR loss, which reduces the throughput, leading to reduced energy efficiency for $|\rho| = 0.7$. Because of the correlation induced SNR loss, more transmit power is required to meet the SE constraint. Therefore, for a fixed SNR value, $|\rho| = 0.7$ will tend to use less antennas, in order to reduce the transmit power - in a bid to optimize the energy efficiency, as compared to $|\rho| = 0$ (see Tables 4.6

Table 4.6. Transmit antenna usage ratio without correlation

SNR (dB)	1 Antenna	2 Antennas	3 Antennas	4 Antennas
5	1	0	0	0
10	1	0	0	0
15	0.00013	0.99987	0	0
20	0	0.01045	0.73597	0.25358
25	0	0.01731	0.69859	0.28410
30	0.00010	0.13409	0.77598	0.08983

Table 4.7. Transmit antenna usage ratio with correlation

SNR (dB)	1 Antenna	2 Antennas	3 Antennas	4 Antennas
5	1	0	0	0
10	1	0	0	0
15	0.00048	0.99952	0	0
20	0.01471	0.36096	0.59524	0.02909
25	0.16029	0.32467	0.46391	0.05113
30	0.32422	0.43318	0.23791	0.00469

and 4.7). The reduced number of active antennas at a fixed SNR results in a loss in throughput. For example, at a SNR value of $20dB$, the reduction in TB-EE is 67.4% and 14.1%; while that of throughput is 44.2% and 18.1% for No AS and EE_{TB} maximization respectively. The optimal SNR value for $|\rho| = 0$ and $|\rho| = 0.7$ is $20dB$ and $19dB$ with maximum energy efficiency values of 5.96 and 5.23 $bits/Hz/Joule$ respectively; for the No AS system, the optimal SNR values are $23dB$ and $25dB$ with maximum energy efficiency values of 4.42 and 1.97 $bits/Hz/Joule$ respectively. Therefore, other than improving the energy efficiency, cross-layer energy-efficient transmit antenna selection reduces the impact of spatial correlation.

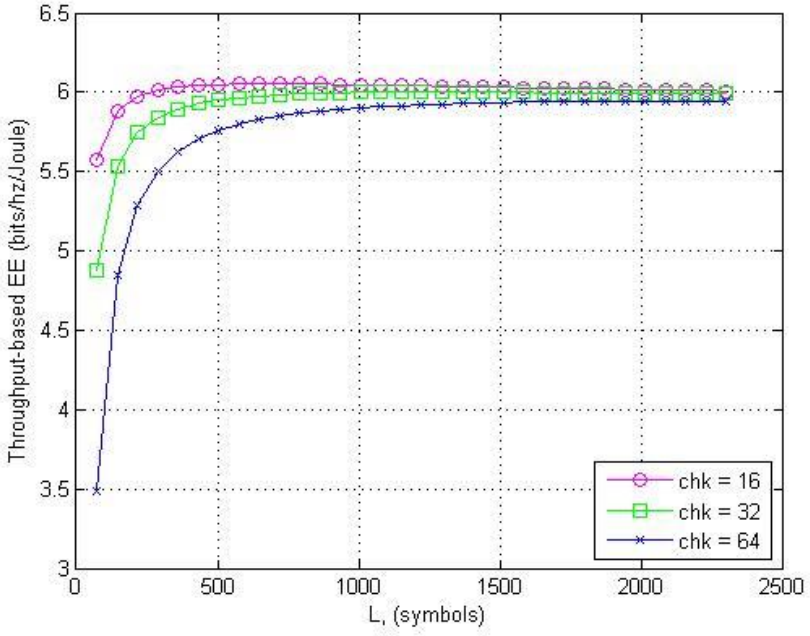

Figure 4.11. Plot of normalized TB-EE against L, at $d = 200m$ and SNR$= 20dB$

4.8 Impact of Packet Size on Energy Efficiency

In this section, the performance of cross-layer energy-efficient transmit antenna selection is evaluated with respect to the packet size, L, at fixed values of SNR and transmission distance d. The performance at different values of parity check bits, i.e. $chk = n - k$, is considered.

4.8.1 Computer Simulations and Results

In this section, the impact of packet size on energy efficiency is evaluated via Monte Carlo simulations. The simulation parameters used are as given in Section 4.4.1, except for L and l. In Figure 4.11, the normalized TB-EE for 4-QAM is plotted against L, at $d = 200m$ with a SNR value of 20dB; for $chk = 16$, 32, and 64. It is observed that for a fixed value of chk, TB-EE

Table 4.8. Performance metrics for 4-QAM at $l = 32/33$

	$10dB$		$20dB$		$30dB$	
L (symbols)	EE_{TB}	$ANATA$	EE_{TB}	$ANATA$	EE_{TB}	$ANATA$
264	2.08	1	6.00	3.30	3.76	2.96
528	1.38	1	5.95	3.24	3.76	2.96
1056	0.60	1	5.91	3.18	3.76	2.96

increases, peaks and then decreases with increasing L. Two factors contribute to EE_{TB} as L increases; firstly, from (4.16), it can be seen that for a fixed value of L, EE_{TB} increases with increasing l or decreasing chk since $l = (n - chk)/n$, where $n = bL$. Therefore, the TB-EE performance for $chk = 16$ is superior for all values of L, with that of $chk = 64$ being the least as can be seen in Figure 4.11. For a given value of chk, l increases with L; since $l = (bL - chk)/L$, thus contributing positively to EE_{TB}.

Secondly, as L increases, the PER increases, see (4.14); this results in decreased throughput, see (4.13). Considering the case when l is fixed; as L increases the algorithm reduces the number of active transmit antennas, in an effort to reduce the total power, so as to optimize EE_{TB}. The combination of increased PER and reduced $ANATA$ as L increases results in a reduction in energy efficiency. These can be seen in Table 4.8, where the normalized TB-EE and $ANATA$ for 4-QAM are given, for a fixed value of l, at various values of L at $d = 200m$. Therefore, for a given value of l the increase in PER as L increases contributes negatively to EE_{TB}.

From Table 4.8, it is observed that the percentage decrease in EE_{TB} as L increases reduces with increasing SNR; consequently, at $20dB$, the positive effects of l outweigh the negative effects of PER, at low values of L. Therefore, for a fixed value of chk, EE_{TB} increases with L, until a maximum value is reached. This is because the percentage increase in l decreases as L increases; correspondingly, the percentage increase in EE_{TB} reduces with increasing L. The optimal values of L for $chk = (16,32)$ are $(720,1224)$ with maximum EE_{TB} values of $(6.06,6.00)$. The percentage increase in l increases with chk; and that is why the optimal value of L for $chk = 32$ is higher than that of $chk = 16$, and why in the range of L considered, EE_{TB} for $chk = 64$ does

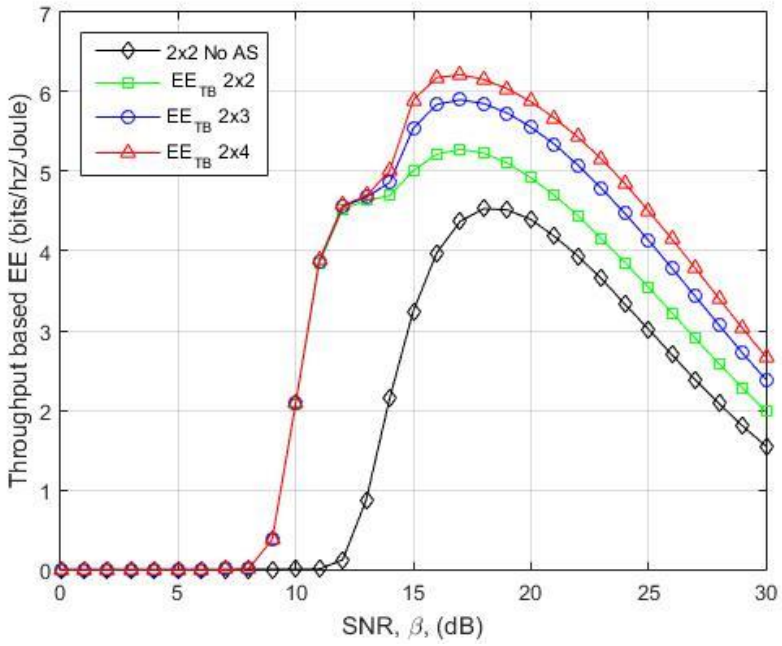

Figure 4.12. Plot of normalized TB-EE against SNR at $d = 200m$ and varying M_T

not peak. Beyond the optimal L value, the negative effects of PER outweigh the positive effects of l, thus degrading the EE of the system.

4.9 Energy Efficiency and the Number of Transmit Antennas

In this section, the impact of the number of transmit antennas on the energy efficiency and throughput, of MIMO systems with cross-layer energy-efficient transmit antenna selection, is examined. The system under consideration is a point-to-point MIMO system, with M_t and N_r transmit and receive RF chains respectively. The transmitter is equipped with M_T antennas, where $M_T \geq M_t$, while the receiver is equipped with N_r antennas. In cross-layer energy-efficient transmit antenna selection, M_r $(1 \leq M_r \leq M_t)$ antennas, where $M_r \leq N_r$ [10], are selected from the available M_T transmit antennas.

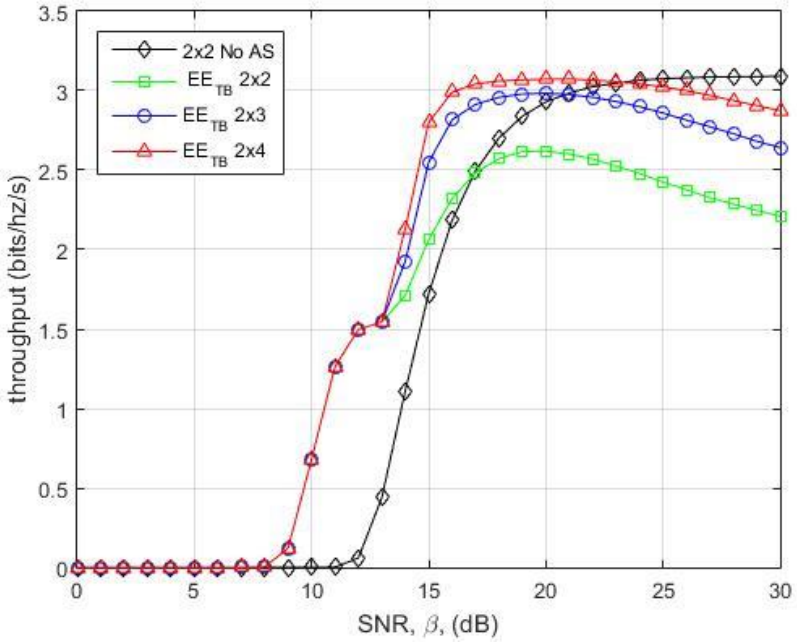

Figure 4.13. Plot of normalized throughput against SNR at $d = 200m$ and varying M_T

4.9.1 Computer Simulations and Results

In this section, the impact of the number of transmit antennas on the energy efficiency and throughput is evaluated via Monte Carlo simulations. A MIMO system with $N_r = M_t = 2$, is considered. Three different scenarios, determined by the number of available transmit antennas, i.e. $M_T = 2, 3, 4$, are considered. These correspond to 2×2, 2×3 and 2×4 MIMO systems. The rest of the simulation parameters are as given in Section 4.4.1.

In Figures 4.12 and 4.13, the normalized throughput-based energy efficiency and throughput, respectively, for EE_{TB} maximization for the 2×2, 2×3 and 2×4 MIMO systems are plotted against SNR at $d = 200m$, for 4-QAM. The plot of the 2×2 MIMO system with no antenna selection is included for comparison purposes. It is observed from Figure 4.12 that the energy efficiency improves with the addition of transmit antennas. The availability of additional transmit antennas to choose from provides increased diversity, which results in enhanced performance.

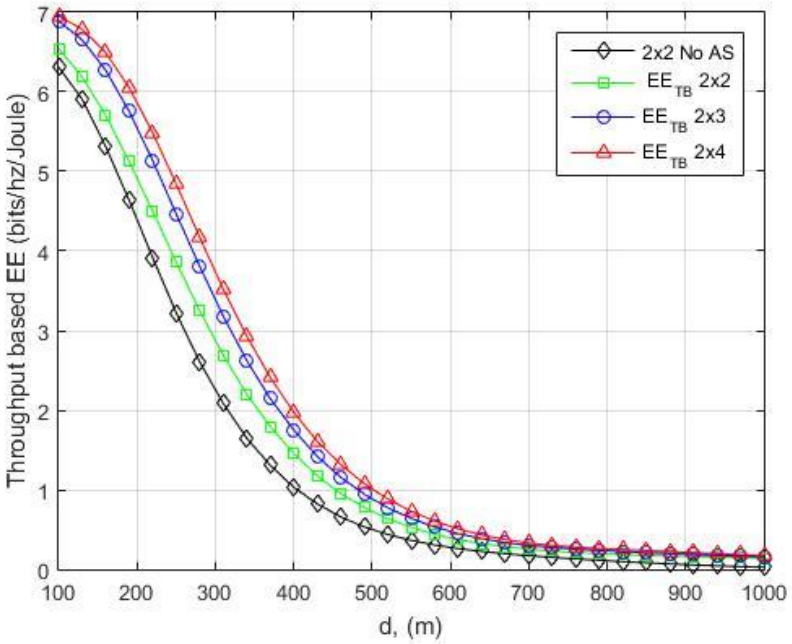

Figure 4.14. Plot of normalized TB-EE against d at SNR= $20dB$ and varying M_T

Increasing the number of transmit antennas increases the probability of more transmit antennas having favourable conditions. This makes it possible for the cross-layer algorithm to use more transmit antennas; e.g. at a SNR of $20dB$, the $ANATA$ values for the 2×2, 2×3 and 2×4 MIMO systems are 1.70, 1.93 and 1.98 respectively. From (4.13), the increased number of transmit antennas, coupled with their favourable conditions, result in increased throughput, as can be seen in Figure 4.13, leading to enhanced energy efficiency.

In Figure 4.14, the normalized TB-EE for EE_{TB} maximization for 2×2, 2×3 and 2×4 MIMO systems is plotted against the transmission distance d, at SNR= $20dB$. It is observed that the additional transmit antennas enhance the energy efficiency for all values of d. It should be noted that the enhanced performance is accompanied by increased algorithm computational complexity.

4.10 Chapter Summary and Conclusions

In this chapter, a cross-layer energy efficiency metric, based on system throughput, was proposed. The analytical expression for the throughput-based energy efficiency metric, for MIMO systems equipped with ZF linear receivers and N-SAW implemented at the data link layer, was derived. Cross-layer energy-efficient transmit antenna selection was proposed and its performance was investigated. Several key factors that affect energy efficiency, including modulation scheme, spatial correlation, the number of antennas and packet size, have been examined. An enhanced version of the cross-layer scheme, which incorporates adaptive modulation, was proposed. Reduced complexity algorithms that achieve near-optimal performance were also developed. Simulation results show that the proposed cross-layer approach outperforms traditional energy-efficient antenna selection, that maximizes a capacity-based energy efficiency metric, in terms of throughput for all SNR and at all distances.

Chapter 5 Optimal, Near and Sub-Optimal Iterative Cross-Layer Energy-Efficient Schemes for Underlay CR MIMO Systems

In this chapter, cross-layer energy-efficient transmit antenna selection, for underlay CR MIMO systems, is presented. The cross-layer approach selects the subset of transmit antennas that maximize the throughput-based energy efficiency metric proposed in Chapter 4, subject to interference constraints at the primary user receiver. Additionally, the proposed algorithm maximizes the cross-layer energy efficiency by jointly optimizing the transmit antenna subset and transmit power, subject to a spectral efficiency constraint. However, to find the optimal transmit antenna subset requires an exhaustive search, the computational complexity of which grows exponentially with the number of antennas. Consequently, iterative reduced complexity algorithms will be developed.

The chapter is organized as follows; the problem formulation is presented in Section 5.1. The optimal exhaustive search and the reduced complexity cross-layer energy-efficient transmit antenna selection algorithms are developed in Section 5.2. In Section 5.3, the performance and complexity of the proposed algorithms are analyzed. Finally, Section 5.4 concludes the chapter.

5.1 Problem Formulation

Consider a wireless system, which consists of a secondary user and a primary user that communicate concurrently over the same spectrum band, whose bandwidth is assumed to be $1Hz$. The CR TX and CR RX are equipped with M and N_{cr} antennas respectively, where $M \leq N_{cr}$; since the cognitive user is configured to exploit spatial multiplexing [10]. The cognitive (CR TX to CR RX) channel matrix, $\boldsymbol{H} \in \mathbb{C}^{N_{cr} \times M}$, is assumed to have ZMCSCG elements with unit variance. The PU RX is equipped with N_{PU} antennas, and the CR TX to PU RX (interference) channel matrix, $\boldsymbol{H}_{SP} \in \mathbb{C}^{N_{PU} \times M}$, is assumed to have ZMCSCG elements with a variance of α. All

the channels are assumed to experience frequency flat Rayleigh fading and the CSI for all channels is assumed known at the CR TX.

It is assumed that there is a sufficiently large number of sub-channels; let the channel matrix from the PU TX to the CR RX, for each sub-channel, be represented by $\boldsymbol{H}_{sc} \in \mathbb{C}^{N_{cr} \times M_{PU}}$, where M_{PU} is the number of PU transmit antennas. Each sub-channel matrix, $\boldsymbol{H}_{sc}$, is assumed to have ZMCSCG elements. According to the central limit theorem [133] [134], the interference produced at the CR RX by the PU TX can be modeled as additive white Gaussian noise (AWGN). The antenna selection scheme selects the M_{cr} ($1 \leq M_{cr} \leq M$) cognitive transmit antennas that optimize the energy efficiency of the secondary system.

N-SAW is implemented at the CR data link layer and the CR RX is equipped with a ZF linear receiver, which separates the received signal into its component M_{cr} transmitted data streams. At the CR TX data link layer, data is encoded by an (n, k) error detecting linear block code; then at the physical layer, each n −bit code word is modulated to form an L −symbol packet; $L = n/b$ where b is the number of bits per symbol. An un-coded spatial multiplexing CR MIMO system is assumed, therefore, an L −symbol packet is divided into M_{cr} equal parallel streams, which are then transmitted over the selected transmit antennas. Each packet is transmitted in its own slot, with a slot period of L/M_{cr} seconds, since a symbol period of 1 second is assumed. The channel response is assumed constant during the transmission of each packet. The cognitive transmit power, P_t, is divided uniformly among the selected transmit antennas. The received signal, at the CR RX, after transmit antenna selection, is given by:

$$\boldsymbol{y} = \sqrt{\frac{P_t}{M_{cr}}}\boldsymbol{H}_{cr}\boldsymbol{s} + \boldsymbol{n} \tag{5.1}$$

where $\boldsymbol{H}_{cr} \in \mathbb{C}^{N_{cr} \times M_{cr}}$ is the cognitive channel matrix after transmit antenna selection, $\boldsymbol{s} \in \mathbb{C}^{M_{cr} \times 1}$ is the cognitive transmit symbol vector - assumed to have uncorrelated zero mean symbols with unit average energy, and $\boldsymbol{n} \in \mathbb{C}^{N_{cr} \times 1}$ is the noise vector with ZMCSCG elements with a variance of N_o; the interference from the primary network, modelled as AWGN, is included in $\boldsymbol{n}$. The interference power at the PU RX is given by:

$$I = \frac{\|\boldsymbol{H}_{int}\|_F^2}{M_{cr}} \tag{5.2}$$

where $\boldsymbol{H}_{int} \in \mathbb{C}^{N_{PU} \times M_{cr}}$ is the interference channel matrix after antenna selection.

Using the throughput expression in (3.11), developed in Chapter 3, the normalized throughput for the SU, after antenna selection, can be expressed as:

$$\eta = b \times N \times M_{cr} \frac{l \times (1 - PER)}{1 + W} \; bits/Hz/s \tag{5.3}$$

where N is the number of SAW processes run in parallel, and W the round-trip delay in slots; $l = k/n$ is the ratio of information symbols per packet and $PER = 1 - \prod_{k=1}^{M_{cr}} (1 - SER_k)^{L/M_{cr}}$ is the packet error rate. $SER_k = f(SNR_k, Mod)$ is the SER for the kth data stream with Mod accounting for the modulation specific SER expression, with $SNR_k = P_t/(u_k N_o M_{cr})$ the post-processing SNR for the kth data stream, where $u_k = [(\boldsymbol{H}_{cr}^H \boldsymbol{H}_{cr})^{-1}]_{k,k}$ and N_o is the noise power. According to (4.16), the normalized throughput-based energy efficiency of the CR user can be expressed as:

$$EE_{TB} = \frac{b \times N \times M_{cr} \times l \times (1 - PER)}{(1 + W)\big((1 + \alpha)P_t + P_c\big)} \; bits/Hz/Joule \tag{5.4}$$

where $\alpha = \xi/\rho - 1$, with ρ the power amplifier efficiency and ζ is the PAR, which is dependent on the modulation scheme and constellation size [126]. P_c is the circuit power which is modelled as $P_c = M_{cr}P_{ct} + N_{cr}P_{cr} + P_{co}$, with P_{ct} and P_{cr} the power consumed by each transmit and receive secondary chains respectively, and P_{co} the power consumed by all the other parts of the circuitry [65] [66].

Cross-layer energy-efficient transmit antenna selection for underlay CR MIMO systems, maximizes EE_{TB} by jointly optimizing the transmit antenna subset and transmit power, subject to spectral efficiency (in terms of SNR as derived in Chapter 4) and interference (at the PU RX) constraints. Therefore, the optimization problem can be formulated as follows:

$$P1 \max_{T(i)_j, P_t} \quad EE_{TB}$$
$$subject\ to: \quad I \leq I_{int}$$
$$SNR_{sum} = \beta \tag{5.5}$$

where $T(i)_j$ denotes the jth transmit antenna subset consisting of $i = M_{cr}$ active transmit antennas, I_{int} is the tolerable threshold power at the PU RX and β is the required SNR_{sum} at the receiver.

5.2 Cross-Layer Energy-Efficient Transmit Antenna Selection

In this section, the cross-layer energy-efficient transmit antenna selection optimal exhaustive search (OES) and the reduced complexity iterative algorithms for underlay CR MIMO systems, are proposed. In Section 5.3, the performance of the proposed algorithms is evaluated, and a complexity analysis of the algorithms is presented.

5.2.1 Optimal Exhaustive Search Algorithm

Given the optimization problem, $P1$, the optimal method of solving it is through an exhaustive search (ES). For each transmit antenna subset, the transmit power has to be determined before EE_{TB} can be calculated. The transmit power that satisfies the interference constraint at the PU RX is given by:

$$P_{int} = \frac{I_{int} M_{cr}}{\|\boldsymbol{H}_{int}\|_F^2} \tag{5.6}$$

while the transmit power that satisfies the SE constraint is given by:

$$P_{SE} = \frac{N_o M_{cr} \beta}{\sum_{k=1}^{M_{cr}} (u_k)^{-1}} \tag{5.7}$$

The interference constraint at the PU RX must be satisfied; this means that it may not be possible to meet the SE constraint. Therefore, the required SE for the cognitive user may have to be decreased in order to maintain the interference power at the PU RX below the tolerable threshold value. The cognitive transmit power, for each transmit antenna combination, is determined as shown in Table 5.1. Once P_t is determined, the EE_{TB} corresponding to the selected transmit antennas is calculated using (5.4). The transmit antenna subset with the maximum EE_{TB} is then selected. The algorithm is described in Table 5.2.

5.2.2 Reduced Complexity Iterative Algorithms

The optimal exhaustive search algorithm requires $\sum_{M_{cr}=1}^{M} \binom{M}{M_{cr}}$ calculations of P_t and EE_{TB}, which includes complex matrix inversion. To develop an algorithm that reduces the complexity associated with OES, we begin by re-writing the constraints in (5.5) as:

$$P_t \leq P_{int} \quad and \quad P_t = P_{SE} \tag{5.8}$$

for the interference and SE constraints respectively. A single unified constraint can be obtained by dividing the constraints and then rearranging, as given below:

$$\frac{\sum_{k=1}^{M_{cr}} u_k}{\|\boldsymbol{H}_{int}\|_F^2} \geq \frac{N_o \beta}{I_{int}} \tag{5.9}$$

For a fixed number of transmit antennas, M_{cr}, the constraint in (5.9) is met when both the interference and SE constraints are satisfied; otherwise the required SE may have to be reduced in order to satisfy (5.9). It is observed that the probability of the constraint in (5.9) being met decreases as the interference channel gain, $\|\boldsymbol{H}_{int}\|_F^2$, increases.

Table 5.1. Transmit power algorithm

Calculate P_{int} using (5.6)

Calculate P_{SE} using (5.7)

if $P_{SE} > P_{int}$

$P_t = P_{int}$

else

$P_t = P_{SE}$

end

Table 5.2. OES energy efficient transmit algorithm for underlay CR MIMO system

for $i = 1: M$

for $j = 1: \binom{M}{M_{cr}}$

Determine P_t using the transmit power algorithm

$P_c = iP_{ct} + N_{cr}P_{cr} + P_{co}$

$P = (1 + \alpha)P_t + P_c$

$\eta(T(i)_j) = b \times N \times M_{cr} \frac{l \times (1 - PER)}{1 + W}$

$EE_{TB}(T(i)_j) = \frac{\eta(T(i)_j)}{P}$

end

end

Select the $T(i)_j$ with the maximum EE_{TB}

i.e. $\{T(i)_j\}_{max} = \max_{i,j} EE_{TB}(T(i)_j)$

The constraint in (5.9) will be used to develop an iterative algorithm that reduces the complexity of the optimal ES algorithm. The algorithm, referred to as Iterative I, divides antenna selection into two stages; intra-level selection, which is performed first, followed by inter-level selection.

A level is made up of antenna subsets with a fixed number of cognitive transmit antennas, i, where $i = 1,2, \ldots M$. The steps involved in Iterative I are as follows;

- Compute $\|\boldsymbol{H}_{int}\|_F^2$ for all possible secondary transmit antenna combinations.
- Order the transmit antenna subsets in a level by $\|\boldsymbol{H}_{int}\|_F^2$, in ascending order.
- At each level, perform intra-level selection by using the following iterative technique. Determine if the constraint in (5.9) is met, for the first subset; if it is, iterate through the ordered antenna subsets, determining (5.9) and calculating EE_{TB}, until either (5.9) is not met or EE_{TB} decreases. If (5.9) is not satisfied for the first subset, then iterate until EE_{TB} decreases or until (5.9) is satisfied.
- Perform inter-level selection, i.e. select the level, along with its corresponding transmit antenna subset, with the maximum EE_{TB}.

Iterative I, is described in Table 5.3.

Iterative I only considers the numerator of the left side of (5.9); the performance of the algorithm can be improved if both the numerator and denominator are considered. The left side of (5.9) can be expressed as follows:

$$\frac{\sum_{k=1}^{M_{cr}} u_k}{\|\boldsymbol{H}_{int}\|_F^2} = \frac{\sum_{k=1}^{M_{cr}} \frac{1}{v_k}}{\|\boldsymbol{H}_{int}\|_F^2} \tag{5.10}$$

where $v_k = 1/u_k$. For a fixed number of selected transmit antennas, M_{cr}, selecting the transmit antenna subset that maximizes $\sum_{k=1}^{M_{cr}} \frac{1}{v_k} / \|\boldsymbol{H}_{int}\|_F^2$ increases the probability of the constraint in (5.9) being met. (5.10) can be upper bound as follows:

$$\frac{\sum_{k=1}^{M_{cr}} \frac{1}{v_k}}{\|\boldsymbol{H}_{int}\|_F^2} \leq \frac{M_{cr}}{v_{min}\|\boldsymbol{H}_{int}\|_F^2} \tag{5.11}$$

Table 5.3. Iterative I

for $i = 1{:}\,M$

Order transmit antenna subsets by $\left\|\boldsymbol{H}_{int}(i)_j\right\|_F^2$ in ascending order

$EE_{TB}(i) = EE_{TB}(T(i)_1)$

if (5.9) is met for $T(i)_1$

for $j = 2{:}\binom{M}{i}$

If (5.9) is met and $EE_{TB}\left(T(i)_j\right) > EE_{TB}(T(i)_{j-1})$

$EE_{TB}(i) = EE_{TB}(T(i)_j)$

else

break

end

end

else

for $j = 2{:}\binom{M}{i}$

if (5.9) is not met and $EE_{TB}\left(T(i)_j\right) > EE_{TB}(T(i)_{j-1})$

$EE_{TB}(i) = EE_{TB}(T(i)_j)$

else if (5.9) is met

$EE_{TB}(i) = EE_{TB}(T(i)_j)$

break

else

break

end

end

end

end

Select level ($Lv(i)$) with the maximum EE_{TB}

i.e. $\{Lv(i)\}_{max} = \max_i EE_{TB}(i)$

where:

$$v_{min} = min_k v_k \quad k = 1,2, \ldots M_{cr} \tag{5.12}$$

SNR_{min}, is defined as:

$$SNR_{min} = min_k SNR_k \quad k = 1,2, \ldots M_{cr} \tag{5.13}$$

Therefore, SNR_{min} can be expressed in terms of v_{min} as follows:

$$SNR_{min} = \frac{P_t v_{min}}{N_o M_{cr}} \tag{5.14}$$

From [40], SNR_{min} can be lower bound as:

$$SNR_{min} \geq \lambda_{min}^2(\boldsymbol{H}_{cr}) \frac{P_t}{N_o M_{cr}} \tag{5.15}$$

where $\lambda_{min}(\boldsymbol{H}_{cr})$ is the minimum singular value of $\boldsymbol{H}_{cr}$. Combining (5.14) and (5.15), v_{min} can be expressed as:

$$v_{min} \geq \lambda_{min}^2(\boldsymbol{H}_{cr}) \tag{5.16}$$

Substituting v_{min}, as expressed in (5.16), into (5.11) gives:

$$\frac{\sum_{k=1}^{M_{cr}} \frac{1}{v_k}}{\|\boldsymbol{H}_{int}\|_F^2} \leq \frac{M_{cr}}{\lambda_{min}^2(\boldsymbol{H}_{cr})\|\boldsymbol{H}_{int}\|_F^2} \tag{5.17}$$

Multiplying both sides of the inequality in (5.17) by -1, gives:

$$-\left(\frac{\sum_{k=1}^{M_{cr}} \frac{1}{v_k}}{\|\boldsymbol{H}_{int}\|_F^2}\right) \geq -\left(\frac{M_{cr}}{\lambda_{min}^2(\boldsymbol{H}_{cr})\|\boldsymbol{H}_{int}\|_F^2}\right) \tag{5.18}$$

Dividing (5.18) by (5.9) and rearranging, gives:

$$\frac{M_{cr}}{\lambda_{min}^2(\boldsymbol{H}_{cr})\|\boldsymbol{H}_{int}\|_F^2} \leq \frac{N_o\beta}{I_{int}} \tag{5.19}$$

Therefore, from (5.19), for a fixed M_{cr}, selecting the transmit antenna subset that minimizes $1/\lambda_{min}^2(\boldsymbol{H}_{cr})\|\boldsymbol{H}_{int}\|_F^2$ increases the probability of the constraint in (5.9) being met, i.e. as $1/\lambda_{min}^2(\boldsymbol{H}_{cr})\|\boldsymbol{H}_{int}\|_F^2$ increases, the probability of the constraint being met decreases. Therefore, the probability of the constraint in (5.9) being met decreases as $\lambda_{min}^2(\boldsymbol{H}_{cr})\|\boldsymbol{H}_{int}\|_F^2$ decreases.

The above result can be used to modify Iterative I, thereby improving its performance. This is done in intra-level selection; instead of ordering the transmit antennas subsets in a level by $\|\boldsymbol{H}_{int}\|_F^2$ in ascending order, the subsets are instead ordered by $\lambda_{min}(\boldsymbol{H}_{cr})\|\boldsymbol{H}_{int}\|_F^2$ in descending order. The intra-level and inter-level selection then operate as described for Iterative I; the resulting algorithm is referred to as Iterative II.

5.3 Computer Simulations and Results

In this section, the performance of the proposed algorithms is evaluated using Monte Carlo simulations. All points of the following results are generated by averaging over 100000 channel realizations. The following parameters are used in the simulations; the values of P_{ct}, P_{cr}, P_{co}, and ρ are $120mW$, $85mW$, $30mW$ and 0.35 [16] [120] [126]. The values for α, N_o and I_{int} are 0.1, $5 \times 10^{-4}W$ and $10mW$. The number of cognitive transmit and receive antennas is $M = N_{cr} = 4$, the number of PU receive antennas is N_{PU}, $N = 4$ SAW processes are run in parallel with a round-trip delay of $W = 4$ slots. A packet length of $L = 528$ symbols is used with $l = 32/33$. The modulation schemes considered are 4-QAM and 16-QAM, thus $b = 2$ and $b = 4$ respectively. The value for PAR for M-QAM is $\xi = 3\left(\sqrt{M} - 1/\sqrt{M} + 1\right)$, with $M = 2^b$, when a square constellation is assumed [126].

The performance of the cross-layer approach is first evaluated by comparing it with the physical-layer approach, which optimizes a capacity-based energy efficiency metric EE_{CB}; i.e. the normalized capacity-based energy efficiency of the SU. From (4.12) in Chapter 4, the EE_{CB} for the CR user, after antenna selection, is given by:

$$EE_{CB} = \frac{\sum_{k=1}^{M_{cr}} log_2(1 + SNR_k)}{(1+\alpha)P_t + P_c} \quad bits/Hz/Joule \tag{5.20}$$

The transmit antenna subset that maximizes EE_{CB}, while maintaining the interference power at the PU RX below a tolerable threshold value, subject to a spectral efficiency constraint, is selected. The maximization involves determining the optimal transmit antenna subset and transmit power. Therefore, the optimization problem can be formulated as follows:

$$\begin{aligned} P2 \max_{T(i)_j, P_t} \quad & EE_{CB} \\ subject\ to: \quad & I \leq I_{int} \\ & SNR_{sum} = \beta \end{aligned} \tag{5.21}$$

The optimization problem $P2$ is solved through exhaustive search, similar to the optimal solution for $P1$.

In Figure 5.1, the normalized throughput-based energy efficiency for optimal EE_{TB} and EE_{CB} maximization, for 4-QAM and 16-QAM, for the SU, is plotted against SNR. The plot for the system with no antenna selection (No AS) is included for comparison purposes. It is observed that energy-efficient transmit antenna selection improves the energy efficiency of the secondary system; with EE_{TB} and EE_{CB} maximization outperforming the No AS system for all SNR values, for both 4-QAM and 16-QAM. The energy efficiency exhibits a similar behavior to that of MIMO systems, discussed in Chapter 4; i.e. the TB-EE increases, peaks and then decreases with increasing SNR. In underlay CR systems, the transmit power of the CR user is limited by the interference power that can be tolerated by the PU RX, this means that the cognitive transmit power is very low. Therefore, the interference constraint has a much higher impact on the transmit power than the SE constraint (see Table 5.1); this results in reduced degradation of the energy efficiency

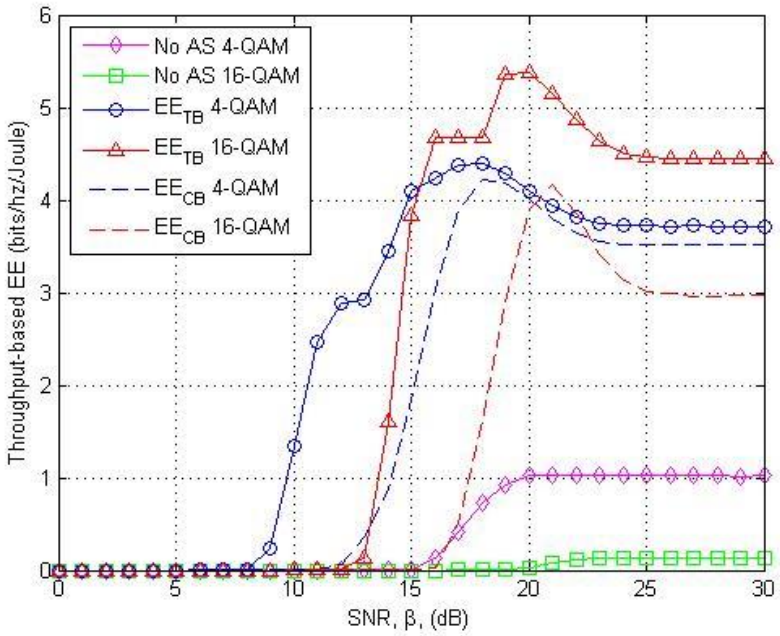

Figure 5.1. Plot of normalized TB-EE against SNR for the SU

beyond the optimal SNR values, as can be seen in Figure 5.1.

For the No AS system, the optimal SNR values for 4-QAM is $20dB$, with a maximum energy efficiency value of 1.03 $bits/Hz/Joule$; 16-QAM does not have an optimal SNR value in the SNR range considered. For EE_{TB} maximization, $18dB$ and $20dB$ are the optimal SNR values for 4-QAM and 16-QAM respectively, and the corresponding TB-EE values are 4.40 and 5.37 $bits/Hz/Joule$. Beyond the optimal SNR values, the energy efficiency decreases as the SNR increases, up to a SNR value of $24dB$ for 4-QAM ($27dB$ for 16-QAM), beyond which the energy efficiency remains constant. This is because increasing the SNR does not result in increased transmit power; the interference constraint has to be met, and this limits the transmit power, even as SNR increases. Optimal SNR values for 4-QAM and 16-QAM, for EE_{CB} maximization, are $18dB$ and $21dB$ respectively, with maximum TB-EE values of 4.21 and 4.17 $bits/Hz/Joule$; the energy efficiency values level of beyond SNR$= 24dB$ for 4-QAM ($26dB$ for 16-QAM).

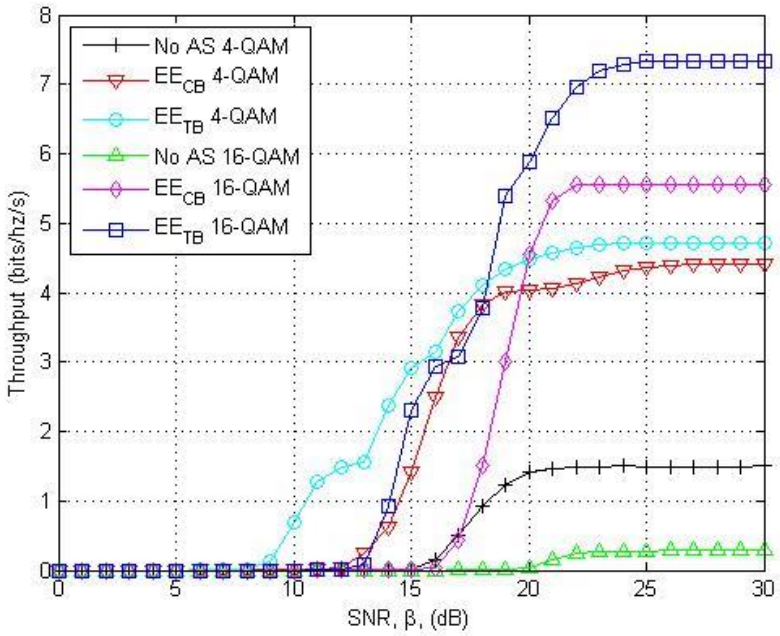

Figure 5.2. Plot of normalized throughput against SNR for the SU

In Figure 5.2, the normalized throughput for optimal EE_{TB} and EE_{CB} maximization, for 4-QAM and 16-QAM, for the SU is plotted against SNR. It is observed that energy-efficient transmit antenna selection improves the throughput for all SNR values, unlike for the MIMO case in Chapter 4. This is due to the limit that the interference constraint imposes on the transmit power, as already discussed; additionally, the throughput for EE_{TB} and EE_{CB} maximization does not peak. From Figure 5.1 and 5.2, it is observed that EE_{TB} maximization outperforms EE_{CB} maximization in terms of energy efficiency and throughput over the entire SNR range. This is attributed to the additional information from the physical and data link layers utilized by the cross-layer approach, which allows for the optimal exploitation of the transmit resources, i.e. transmit power and transmit antennas.

In Figures 5.3 and 5.4, the normalized TB-EE for OES, and the reduced complexity algorithms, i.e. Iterative I and Iterative II, is plotted against SNR, for 4-QAM and 16-QAM respectively. It is

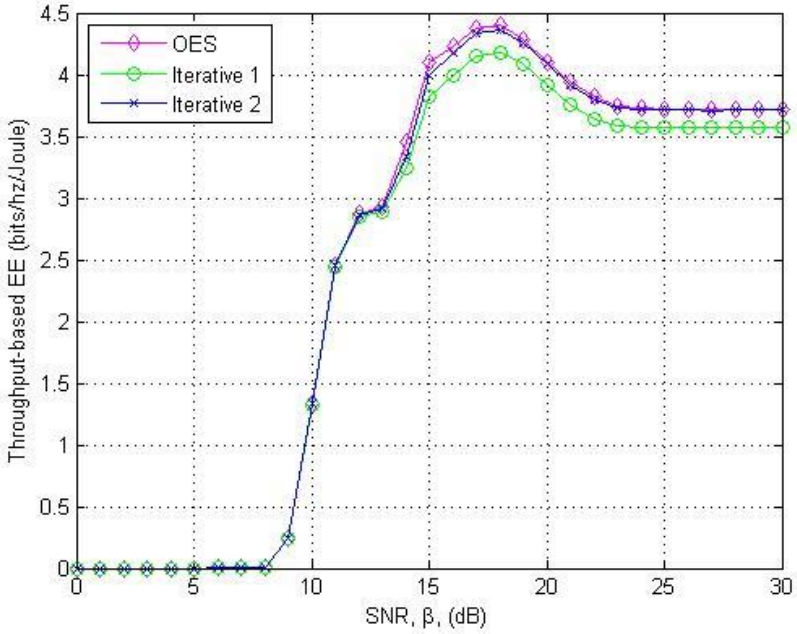

Figure 5.3. Plot of normalized TB-EE against SNR (4-QAM) for OES, Iterative I and II

observed that for low SNR values ($< 13dB$ and $< 17dB$ for 4-QAM and 16-QAM respectively), both Iterative I and Iterative II have near-optimal performances. At high SNR values, the performance of the iterative algorithms with respect to OES decreases; the performance of Iterative I becomes sub-optimal, but that of Iterative II remains near-optimal. Iterative II has a better performance because it takes into consideration both the interference channel and the cognitive channel when selecting transmit antennas; Iterative I only considers the interference channel. However, the improved performance of Iterative II is accompanied by increased computational complexity.

A simple measure of algorithm complexity is the number of times EE_{TB} is evaluated. For the OES algorithm, EE_{TB} is computed $\sum_{M_{cr}=1}^{M} \binom{M}{M_{cr}}$ times, i.e. 15 times for a 4×4 CR MIMO system. From simulations, the number of times Iterative I computes EE_{TB} is 6.6 and 5.7 for 4-QAM and 16-QAM respectively; therefore, Iterative I is less complex than OES. On the other hand, Iterative II computes EE_{TB}, 4.5 and 4.3 times for 4-QAM and 16-QAM respectively. Iterative II computes

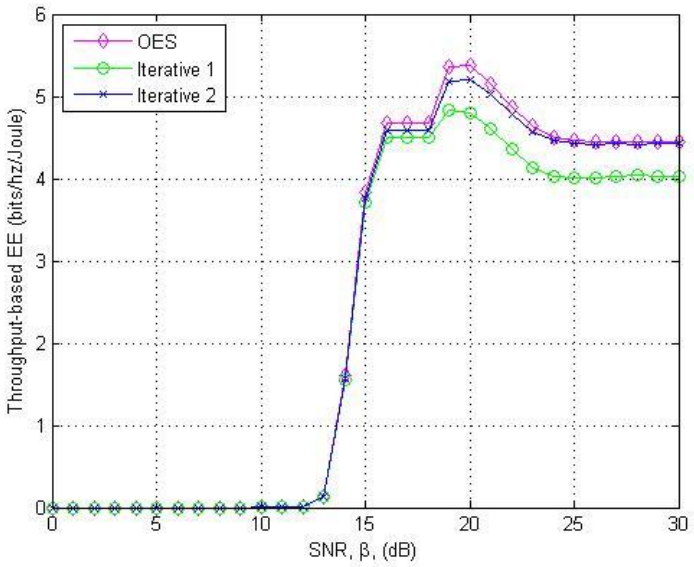

Figure 5.4 Plot of normalized TB-EE against SNR (16-QAM) for OES, Iterative I and II

EE_{TB} less times than Iterative I because it uses both $\lambda_{min}(\boldsymbol{H}_{cr})$ and $\|\boldsymbol{H}_{int}\|_F^2$. Iterative II is not necessarily less complex than Iterative I; this is because Iterative II additionally computes $\lambda_{min}(\boldsymbol{H}_{cr})$, for each transmit antenna subset. But Iterative II is less complex than OES, since computing the singular values of $\boldsymbol{H}_{cr}$ is less complex than computing $[\boldsymbol{H}_{cr}^H \boldsymbol{H}_{cr}]^{-1}$[25] [127], and EE_{TB} is computed less times. A detailed complexity analysis for the algorithms is found in Appendix F. The computational complexities, expressed in terms of floating point operations (flops), for OES, Iterative I and Iterative II, are given below:

$$\sum_{M_{cr}=1}^{M} \binom{M}{N_{cr}} \{8N_{PU}M_{cr} + 72(M_{cr})^3 + 4(M_{cr})^2(8N_{cr}+1)\} \tag{5.22}$$

$$\frac{A_{m1}}{M}\left\{\sum_{M_{cr}=1}^{M} \{72(M_{cr})^3 + 4(M_{cr})^2(8N_{cr}+1)\}\right\} + \sum_{M_{cr}=1}^{M} \binom{M}{M_{cr}} \{8N_{PU}M_{cr}\} \tag{5.23}$$

$$\frac{A_{m2}}{M}\left\{\sum_{M_{cr}=1}^{M}\{72(M_{cr})^3+4(M_{cr})^2(8N_{cr}+1)\}\right\} + \sum_{M_{cr}=1}^{M}\binom{M_T}{M_{cr}}\{8N_{PU}M_{cr}+32N_{cr}(M_{cr})^2-32(M_{cr})^3/3\} \quad (5.24)$$

A_{m1} in (5.23) and A_{m2} in (5.23) is the average number of times Iterative I and Iterative II compute EE_{TB} respectively. For 4×4 CR MIMO system and a PU RX with 4 antennas, the computational complexity for OES, Iterative I and Iterative II, in flops, is 27712, 19438 and 21430 (for 4-QAM). Therefore, Iterative II is less complex than OES, but more complex than Iterative I. The reduction in complexity for Iterative I and Iterative II, compared to OES, is 29.9% and 22.7% respectively.

5.4 Chapter Summary and Conclusions

In this chapter, energy-efficient transmit antenna selection for underlay MIMO systems, from a cross-layer perspective, was investigated. The results show that energy-efficient transmit antenna selection greatly enhances the system performance – in comparison with the system with no antenna selection - in terms of energy efficiency and throughput. Additionally, near-optimal and sub-optimal iterative algorithms were developed; their performance was far superior to that of the system without antenna selection.

Chapter 6 Conclusions and Future Work

This chapter presents the research results, and it highlights the overall contributions of the thesis, against the set objectives. A summary of each chapter, indicating the contributions in each, if any, is presented. After that, several recommendations and suggestions for future work are presented.

6.1 Summary and Key Contributions of the Thesis

This thesis has studied energy-efficient transmit antenna selection for spatial multiplexing multiple-antenna systems from a cross-layer perspective. In the thesis, multiple-antennas systems were identified as MIMO and underlay CR MIMO systems. The thesis focused on the proposal, development and analysis of optimal (exhaustive search) full complexity, near and sub-optimal reduced complexity, novel cross-layer energy-efficient transmit selection algorithms. The contributions and results of this thesis were presented in Chapters 3-5.

In summary, the thesis is organized into six chapters. Chapter 1 introduced the thesis by presenting the motivation, the problem statement and the objectives of the research; the publications arising from this research were also given. Chapter 2 presented fundamental background information on the techniques used in the thesis; a literature review on the related works was also presented. The review revealed the need for investigating energy-efficient antenna selection - from a cross-layer perspective.

Chapter 3 investigated the performance of throughput-based transmit antenna selection for spatial multiplexing multiple-antenna systems; with ZF linear receivers and N-SAW as the ARQ protocol. As cross-layer antenna selection schemes are framework (system model) dependent, the analytical expression for throughput for the system under consideration, was derived. The cross-layer schemes were then developed, and their performance evaluated. Moreover, several factors that affect throughput, including packet size and the number of SAW process, were considered. The research contributions of the chapter are as summarized below:

- The analytical throughput expression for spatial multiplexing multiple-antenna systems, equipped with ZF linear receivers and N-SAW as the ARQ protocol, was derived.
- A performance analysis of throughput-based transmit antenna selection for MIMO systems, which considered - the impact of packet size, the number of SAW processes and the stalling of packets inside the receiver reordering buffer due to N-SAW- was carried out.
- Throughput-based transmit antenna selection for underlay CR MIMO systems was proposed and its performance was analyzed.

The results of the chapter are as follows:

- Cross-layer transmit antenna selection results in overall improved system performance - in terms of throughput, transmission latency, packet error rate, receiver buffer requirements and dropped packets (when stall avoidance is implemented) – as compared with capacity-based transmit antenna selection.
- The throughput and number of dropped packets (buffer requirements) decrease with increasing packet size and increase with increasing number of SAW processes, while the transmission latency increases with increasing packet size.

Chapter 4 presented a performance evaluation of energy-efficient transmit antenna selection for spatial multiplexing MIMO systems, from a cross-layer perspective. The approach is cross-layer in the sense that a cross-layer energy efficiency criterion, based on throughput, is optimized. The proposed cross-layer scheme maximizes the energy efficiency by jointly optimizing the transmit antenna subset and transmit power, subject to transmit power and spectral efficiency constraints. The effect of the modulation scheme, spatial correlation among transmit antennas, packet size and the number of equipped transmit antennas, on energy efficiency was considered. The research contributions of the chapter are as follows:

- A cross-layer energy efficiency metric is proposed and derived; for spatial multiplexing MIMO systems with ZF linear receivers and N-SAW as the ARQ protocol.

- The proposal of cross-layer energy-efficient transmit antenna selection, and the analysis of its performance as a function of SNR, transmission distance and packet size.
- The proposal and analysis of cross-layer energy-efficient transmit antenna selection with adaptive modulation.
- The development of near-optimal reduced complexity cross-layer energy-efficient transmit antenna selection algorithms.

The following are some insights gained from this chapter:

- The proposed cross-layer energy efficiency metric is superior to the capacity-based energy efficiency metric. Cross-layer energy-efficient transmit antenna selection outperforms the physical-layer approach in terms of throughput, for the entire SNR regime and at all distances. Consequently, the physical-layer approach requires more retransmissions to send a given number of information bits successfully. Therefore, maximizing the capacity-based energy efficiency metric does not necessarily result in an energy efficient system. Additionally, because the cross-layer approach exhibits superior throughput, the performance enhancements attributed to throughput-based transmit antenna selection in Chapter 3, also apply.
- The spectral efficiency constraint ensures that there is a trade-off between the energy efficiency and throughput, for multiple-antenna systems with cross-layer energy-efficient transmit antenna selection.
- For a given number of antennas, packet size, ratio of information symbols per packet and modulation scheme, there exists an optimal value of SNR that maximizes the energy efficiency.
- For a given number of antennas, number of parity bits, modulation scheme and SNR value, there exists an optimal value of packet size that maximizes the energy efficiency.
- Increasing the number of transmit antennas increases the energy efficiency.
- Modulation schemes with larger constellation sizes perform better with increasing SNR and decreasing distance.

Chapter 5 investigated energy-efficient transmit antenna selection for spatial multiplexing underlay CR MIMO systems, from a cross-layer perspective. The cross-layer scheme maximizes the energy efficiency by jointly optimizing the transmit antenna subset and transmit power, subject to interference power and spectral efficiency constraints. The research contributions of the chapter are as follows:

- The proposal and analysis of cross-layer energy efficient transmit antenna selection, for underlay CR MIMO systems.
- The development of reduced complexity near-optimal and sub-optimal iterative algorithms.

The results of this chapter are as follows:

- Cross-layer energy-efficient transmit antenna selection greatly improves the performance of the underlay CR MIMO systems in terms of energy efficiency and throughput, with enhancements of up to 5.35 $bits/Hz/Joule$ and 7.04 $bits/Hz/s$ respectively.
- The reduced complexity algorithms achieve a reduction in complexity of up to 95% with a maximum performance degradation of 10.6% , in comparison with the optimal exhaustive search algorithm, for a practical number of antennas (between 3 and 10) - see Appendix F. It should be noted that even though there is a reduction in performance, this still represents enhancements in energy efficiency of up to 4.78 $bits/Hz/Joule$ in comparison with the system without antenna selection.

6.2 Suggestion for Future work

Some of the open research problems resulting from the work presented in this thesis are as given below:

- In this thesis, an un-coded spatial multiplexing system was considered. Therefore, it would be interesting to consider coded systems. Additionally, more sophisticated ARQ techniques and receiver structures can be included.
- In practical scenarios, the channel deviates from the spatially white channel, i.e. a channel modeled to experience Rayleigh fading and to consist of ZMCSCG elements with unit variance. In this thesis, a Rayleigh fading model was assumed, and the effect of spatial correlation on energy efficiency was also considered. The work can be extended to include more realistic channels, e.g. Ricean channels (the presence of a line-of-sight component) with correlated fading.
- A perfect channel estimation process and feedback channel were assumed in this thesis. In reality, it is hard to obtain perfect CSI. Additionally, it is difficult to provide a feedback channel devoid of delay and errors. These factors should be taken into consideration in order to derive more robust transmit antenna selection procedures.
- Massive MIMO, with base stations and devices equipped with a large number of antennas, is an emerging area of research. Massive MIMO promises significant improvements in spectral efficiency [135]. Energy-efficient transmit antenna selection for massive MIMO, from a physical-layer perspective, has been studied in [122]. The suggested focus would be on the analysis of the characteristics of a system with a large number of antennas, from a cross-layer perspective, and then using the results of the analysis to design cross-layer energy-efficient antenna selection algorithms.

Appendix A

In-Sequence Receiver Algorithm

Among the basic ARQ schemes, SAW is the simplest to implement; it has minimal signaling and buffer requirements. This is because the transmitter sends a packet and then waits for an ACK to be sent for the transmitted packet, before sending the next packet. The disadvantage of SAW is that the idle time spent waiting for ACKs negatively impacts the throughput of SAW. N-SAW runs multiple SAW processes so as to improve the throughput; this results in packets arriving out of sequence at the receiver. Therefore, N-SAW requires a reordering buffer at the receiver, where the received packets are stored temporarily, reordered and then delivered in-sequence to the higher layer. The flow chart of the in-sequence receiver algorithm, used to deliver the packets in sequence to the higher layer, is given in Figure A-A1. The algorithm was developed for the system described in Chapter 3. Table A-A1 gives the meaning of the symbols used in the algorithm.

Table A-A 1 The meaning of symbols used in the in-sequence receiver algorithm

Symbol	Meaning
$SeqNum$	The sequence number of the next packet to be passed to the higher layer
$Max\ ReTx$	The maximum number of times a packet can be retransmitted

The algorithm forms part of the work presented in [136].

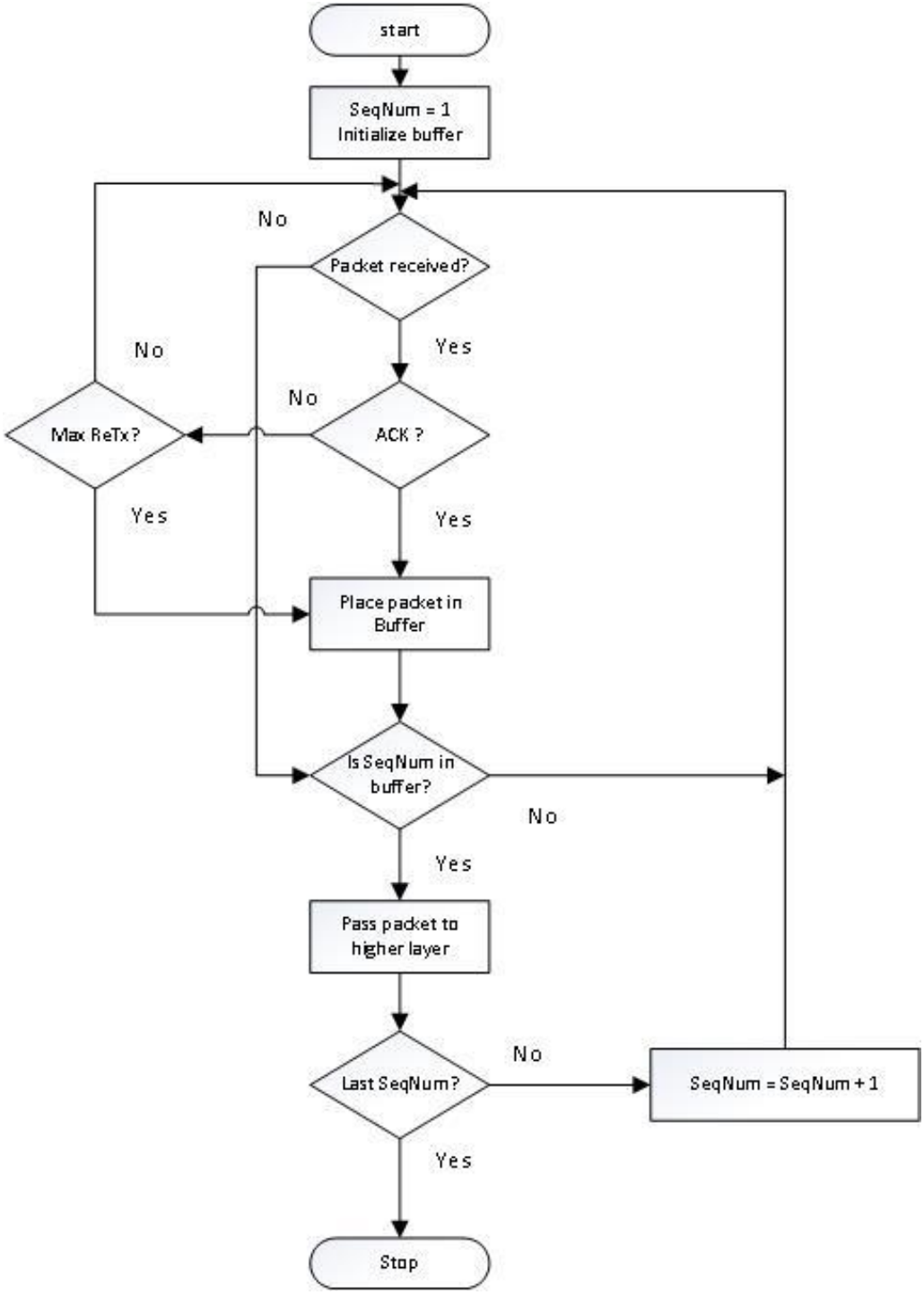

Figure A-A 1 Flowchart of In-sequence receiver algorithm

Appendix B

Symbol Error Rate Expressions

The symbol probability of error, i.e. the symbol error rate (SER), for QPSK is given by [137]:

$$2Q\left(\sqrt{\gamma}\right) - Q^2\left(\sqrt{\gamma}\right) \tag{A.B.1}$$

where γ is the signal to noise ratio (SNR) per symbol.

The symbol error rate for rectangular M-QAM, where $M = 2^n$, and n is even, is given by [137]:

$$1 - (1 - P_{sc})^2 \tag{A.B.2}$$

where P_{sc} is the per carrier SER, and is given by:

$$P_{sc} = 2\left(1 - \frac{1}{\sqrt{M}}\right) Q\left(\frac{3}{M-1}\gamma\right) \tag{A.B.3}$$

Therefore, the SER for 4-QAM is given by:

$$2Q(\gamma) - Q^2\left(\sqrt{\gamma}\right) \tag{A.B.4}$$

And that for 16-QAM is given by:

$$3Q\left(\frac{1}{5}\gamma\right) - \frac{9}{4}Q^2\left(\frac{1}{5}\gamma\right) \tag{A.B.5}$$

Appendix C

Validation of the Throughput Expression

Simulation is used to validate the analytical throughput expression for spatial multiplexing MIMO systems, equipped with ZF linear receivers, with N-SAW implemented at the data link layer, derived in Chapter 3. The MIMO system model is as described in Section 3.1.1. The simulation parameters used are as follows. The number of transmit and receive antennas is $M_t = N_r = 3$, $N = 3$ SAW processes are run in parallel and the round-trip delay is $W = 3$ slots. A packet length of $L = 528$ symbols is used with $l = 32/33$. The maximum number of packet retransmissions is set at 10. CRC-32 is used for QPSK while CRC-64 is used for 16-QAM, this ensures that l is the same for both modulation schemes. The number of bits per symbol, b, are 2 and 4 for QPSK and 16-QAM respectively.

The performance results, corresponding to a system without antenna selection, are presented in Figures A-C 1 and A-C 2, for QPSK and 16-QAM respectively. The practical normalized throughput is calculated by transmitting a total of 300 packets per session, and then averaging the results over 1000 sessions. The practical throughput is calculated using (3.13) as given in Section 3.1.3.1. The theoretical normalized throughput is calculated from the derived analytical throughput expression, given below:

$$\eta = b \times N \times M_t \frac{l \times (1 - PER)}{(1 + W)} \ \ bits/Hz/s \qquad \text{(A-C.1)}$$

From Figures A-C 1 and A-C 2, it is observed that there is a close matching between the practical and theoretical throughput curves at high SNR values, i.e. $\geq 15dB$ and $\geq 19dB$ for QPSK and 16-QAM respectively. The practical throughput at low SNR values is affected by the limit imposed on the number of times a packet can be retransmitted; this results in a higher throughput value.

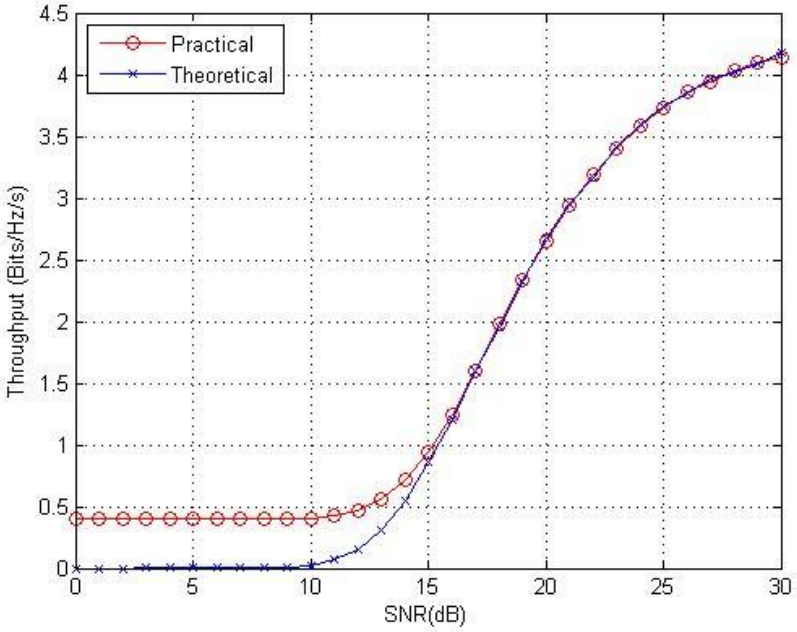

Figure A-C 1 Validation of analytical throughput expression for QPSK

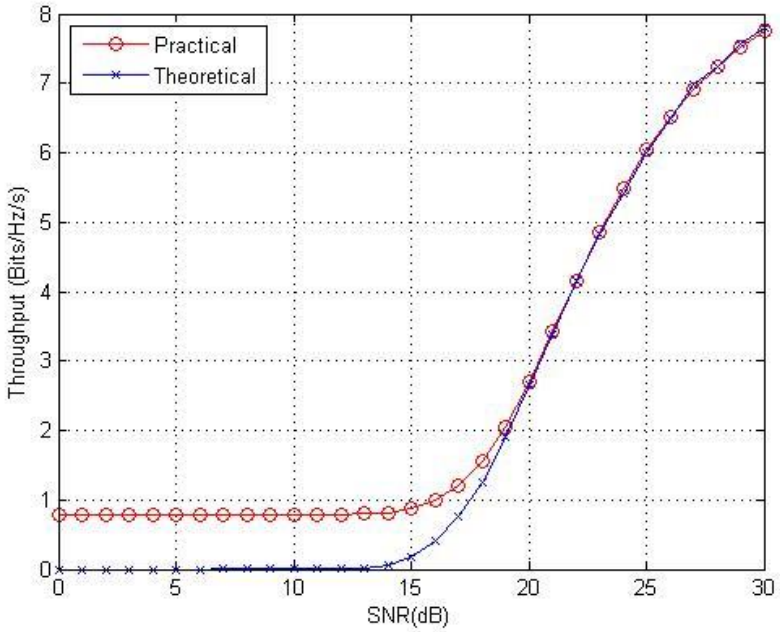

Figure A-C 2 Validation of analytical throughput expression for 16-QAM

Appendix D

Buffer storage requirements for MIMO systems with N-SAW

Simulation is used to analyze the buffer storage requirements for MIMO systems with N-SAW as the ARQ protocol. The system model described in Section 3.1.1 is used, with the simulation parameters as follows: the number of transmit and receive antennas is $M_t = N_r = 3$. A packet length of $L = 528$ symbols is used with $l = 32/33$. The maximum number of packet retransmissions is set at 10. CRC-32 is used, with QPSK as the modulation scheme, therefore, the number of bits per symbol is 2.

In Figure A-D 1, the average number of packets in the receiver reordering buffer, i.e. the size of the buffer storage in packets, is plotted against the SNR, for $N = 3$ and $N = 6$ (i.e. the number of SAW processes run in parallel), with $W = 3$ and $W = 6$ (i.e. the round-trip delay in slots) respectively. The plot is for a system without antenna selection. Packets are passed on, in-sequence, to the higher layer from the reordering buffer, using the in-sequence receiver algorithm described in Appendix A. From Figure A-D 1, it is observed that the number of packets in the buffer increases with N. Increasing the number of SAW processes increases the number of packets received per second, which increases the probability of stalling occurring.

At low SNR values, the packet error rate (PER) is high, therefore the probability of packets being retransmitted the maximum number of times is very high. Consequently, the probability of packets arriving in sequence is also high, resulting in reduced stalling. For SNR values of $\leq 7dB$, the buffer storage requirements are low for both $N = 3$ and $N = 6$. As the SNR increases, the PER decreases resulting in decreased packet retransmissions; this leads to a decrease in the probability of packets being retransmitted the maximum number of times, this results in increased stalling. But as the SNR, the packet retransmissions continue decreasing, which contributes positively to the probability of packets arriving in sequence at the receiver. Consequently, the buffer storage size increases, peaks, and then reduces as the SNR increases. At high SNR values, packet

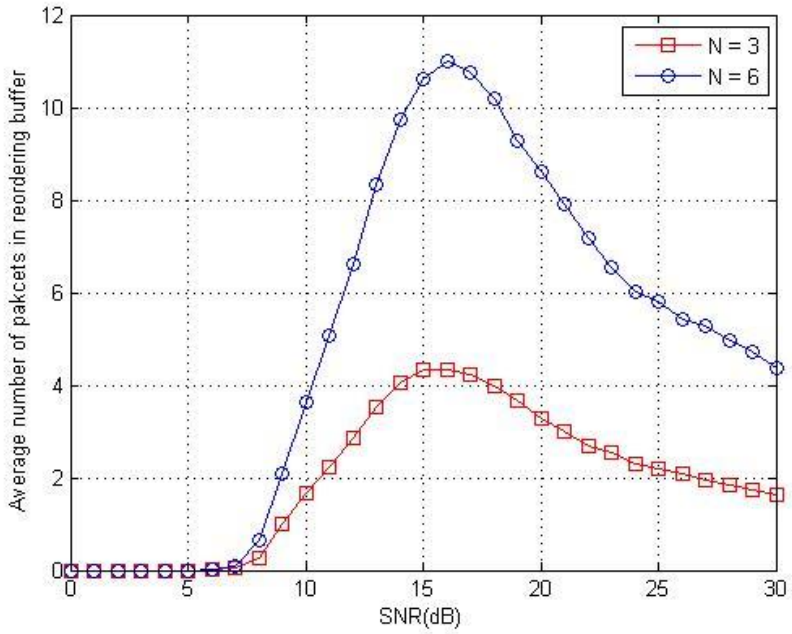

Figure A-D 1 Plot of average number of packets in the reordering buffer against SNR

retransmissions are very low, and this increases the probability of in-sequence packet arrival, which reduces stalling.

Appendix E

Detailed Complexity Analysis for Cross-Layer Energy-Efficient Transmit Antenna Section for MIMO System

A detailed analysis of the computational complexity of the optimal exhaustive search (OES), full complexity algorithm, and the reduced complexity algorithms, i.e. Algorithm I and Algorithm II, developed in Chapter 4, is presented. The analysis is limited to matrix operations, which are complex, and bear the most computational burden. The system under consideration is a $N_r \times M_T$ MIMO system; the channel matrix $\boldsymbol{H} \in \mathbb{C}^{N_r \times M_T}$ consists of ZMCSCG elements. Energy-efficient antenna selection selects M_t $(1 \leq M_t \leq M_T)$ transmit antennas, and the channel matrix after antenna selection is $\boldsymbol{H}_t \in \mathbb{C}^{N_r \times M_t}$.

First, the computational complexity of the OES algorithm will be determined. Before EE_{TB} can be calculated, the SNR, SER, PER, transmit power (P_T), total power consumption of the system (P_{total}) and the normalized system throughput (η), have to be determined. The only matrix operation required to compute EE_{TB} is the matrix inverse $[\boldsymbol{H}_t^H \boldsymbol{H}_t]^{-1}$. The matrix inverse will be computed via the singular value decomposition (SVD) of the channel matrix. The SVD of $\boldsymbol{H}_t$ is given by:

$$\boldsymbol{H}_t = \boldsymbol{U}\boldsymbol{S}\boldsymbol{V}^H \tag{A-E.1}$$

with $\boldsymbol{U} \in \mathbb{C}^{N_r \times M_t}$, $\boldsymbol{V} \in \mathbb{C}^{M_t \times M_t}$ and:

$$\boldsymbol{S} = diag\{\lambda_1, \lambda_2, \ldots \lambda_{M_t}\} \tag{A-E.2}$$

with $\lambda_i \geq 0$ and $\lambda_i \geq \lambda_{i+1}$, where λ_i is the ith singular value of $\boldsymbol{H}_t$. From [127], the matrix inverse, $[\boldsymbol{H}_t^H \boldsymbol{H}_t]^{-1}$, is then given by:

$$[\boldsymbol{H}_t^H \boldsymbol{H}_t]^{-1} = \boldsymbol{V}(\boldsymbol{S}^2)^{-1}\boldsymbol{V}^H \tag{A-E.3}$$

Using the Golub–Reinsch algorithm, performing an SVD of $\boldsymbol{H}_t$ to compute only $\boldsymbol{V}$ and $\boldsymbol{S}$ requires $4N_r(M_t)^2 + 8(M_t)^3$ number of multiplications and an equal number of additions [25]. After $\boldsymbol{V}$ and $\boldsymbol{S}$ are computed; forming $[\boldsymbol{H}_t^H \boldsymbol{H}_t]^{-1}$, according to (A-E.3) requires $(M_t)^3 + (M_t)^2$ multiplications and $(M_t)^3 - (M_t)^2$ additions. Therefore computing $[\boldsymbol{H}_t^H \boldsymbol{H}_t]^{-1}$, requires a total of $9(M_t)^3 + (4N_r + 1)(M_t)^2$ multiplications and $9(M_t)^3 + (4N_r - 1)(M_t)^2$ additions [127]. One complex multiplication/division requires six floating point operations (flops) while one complex addition/subtraction requires two flops. Given that $[\boldsymbol{H}_t^H \boldsymbol{H}_t]^{-1}$ is computed once for every transmit antenna subset, i.e. $\sum_{M_t=1}^{M_T} \binom{M_T}{M_t}$ times; therefore, the complexity of OES algorithm, in flops, is given by:

$$\sum_{M_t=1}^{M_T} \binom{M_T}{M_t} \{72(M_t)^3 + 4(M_t)^2(8N_r + 1)\} \tag{A-E.4}$$

Next, the computational complexity of Algorithm I is determined. Algorithm I performs antenna selection in two stages, intra-level and inter-level selection. Intra-level selection uses $\lambda_{min}(\boldsymbol{H}_t)$, i.e. the minimum singular value of $\boldsymbol{H}_t$, as the selection criterion. To compute $\lambda_{min}(\boldsymbol{H}_t)$, SVD needs to be performed to compute only $\boldsymbol{S}$. This requires $4N_r(M_t)^2 - 4(M_t)^3\ /3$ products and an equal number of additions [25]. $\lambda_{min}(\boldsymbol{H}_t)$ is computed once per transmit antenna subset. Inter-level selection uses EE_{TB} as the selection criterion, therefore, the matrix inverse $[\boldsymbol{H}_t^H \boldsymbol{H}_t]^{-1}$, is computed once at each level, i.e. M_T times. Therefore, the complexity of Algorithm I, in flops, is given by:

$$\sum_{M_t=1}^{M_T} \left\{ 72(M_t)^3 + 4(M_t)^2(8N_r + 1) + \binom{M_T}{M_t} \{32N_r(M_t)^2 - 32(M_t)^3\ /3\} \right\} \tag{A-E.5}$$

Finally, the computational complexity of Algorithm II is determined. Similar to Algorithm I, Algorithm II performs antenna selection by using intra-level and inter-level selection. The intra-level selection uses a combination of $\lambda_{min}(\boldsymbol{H}_t)$ and EE_{TB} as the selection criteria. At each level, $\lambda_{min}(\boldsymbol{H}_t)$ is required for each transmit antenna subset, while EE_{TB} needs to be calculated for a

fraction of the transmit antenna subsets. To compute $\lambda_{min}(\boldsymbol{H}_t)$, SVD needs to be performed to compute only $\boldsymbol{S}$, which requires $4N_r(M_t)^2 - 4(M_t)^3\ /3$ products. Therefore, the number of flops required to compute $\boldsymbol{S}$ are:

$$\sum_{M_t=1}^{M_T} \binom{M_T}{M_t} \{32N_r(M_t)^2 - 32(M_t)^3\ /3\} \tag{A-E.6}$$

The average number of times that EE_{TB} is computed by Algorithm II is determined through simulations. If the average number of times EE_{TB} is calculated is A_m; then $[\boldsymbol{H}_t^H \boldsymbol{H}_t]^{-1}$ is computed A_m times. Inter-level selection, performed after intra-level selection, uses EE_{TB} as the selection criterion, which has already been computed in intra-level selection. Let $A_{rem} = A_m - M_T$; from (A-E.4) and (A-E.6), the complexity of Algorithm II in flops is given by:

$$\begin{aligned} &\sum_{M_t=1}^{M_T} \{72(M_t)^3 + 4(M_t)^2(8N_r + 1)\} \\ &\qquad + \frac{A_{rem}}{M_T} \left\{ \sum_{M_t=1}^{M_T} \{72(M_t)^3 + 4(M_t)^2(8N_r + 1)\} \right\} \\ &\qquad + \sum_{M_t=1}^{M_T} \binom{M_T}{M_t} \{32N_r(M_t)^2 - 32(M_t)^3\ /3\} \end{aligned} \tag{A-E.7}$$

The first term in (A-E.7) arises from the fact that Algorithm II computes EE_{TB} at least once for each level; EE_{TB} is then computed an average of A_{rem} times per level, this is represented by the second term. (A-E.7) reduces to:

$$\begin{aligned} &\frac{A_m}{M_T} \left\{ \sum_{M_t=1}^{M_T} \{72(M_t)^3 + 4(M_t)^2(8N_r + 1)\} \right\} \\ &\qquad + \sum_{M_t=1}^{M_T} \binom{M_T}{M_t} \{32N_r(M_t)^2 - 32(M_t)^3\ /3\} \end{aligned} \tag{A-E.8}$$

Table A-E 1 Number of times EE_{TB} is computed by the algorithms for MIMO system

M_T	3	4	5	6	7	8	9	10
OES	7	15	31	63	127	255	511	1023
Algorithm I	3	4	5	6	7	8	9	10
Algorithm II	3.1	4.3	5.7	7.3	8.9	10.6	12.2	13.5

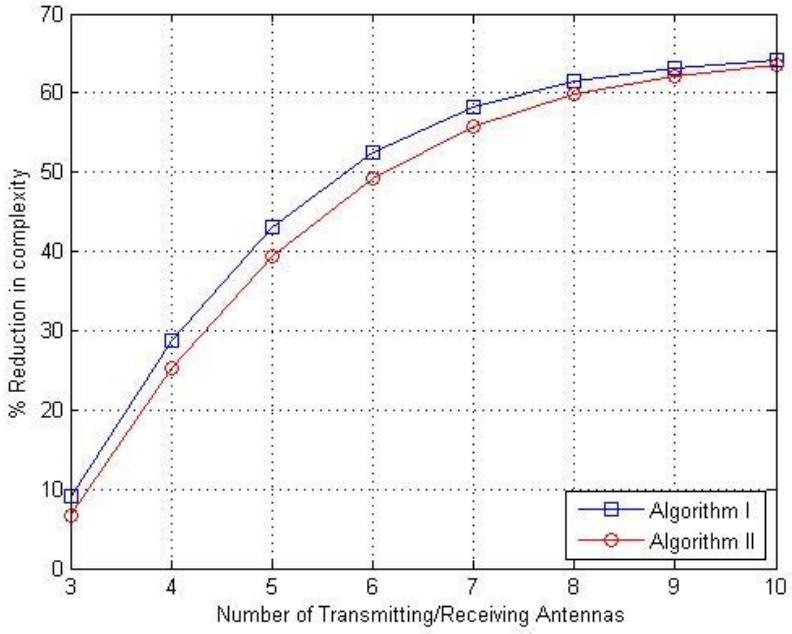

Figure A-E 1 Plot of percentage reduction in complexity against M_T/N_r for MIMO system

In Table A-E 1, the number of times EE_{TB} is calculated for OES, Algorithm I and Algorithm II is given for $3 \leq M_T \leq 10$, with $N_r = M_T$. The average number of times Algorithm II computes EE_{TB} is determined through simulations, for 4-QAM, at $d = 200m$ and a SNR value of $20dB$. In Figure A-E 1, the percentage reduction in complexity for Algorithm I and Algorithm II with respect to algorithm OES is plotted against the number of transmit/receive antennas with $N_r = M_T$. The reduced complexity algorithms are highly computationally efficient in comparison to OES, with Algorithm I being slightly less complex than Algorithm II.

Appendix F

Detailed Complexity Analysis for Cross-Layer Energy-Efficient Transmit Antenna Selection for Underlay CR MIMO System

A detailed analysis of the computational complexity of the optimal exhaustive search (OES), full complexity algorithm, and the reduced complexity algorithms, i.e. Iterative I and Iterative II, developed in Chapter 5, is presented. The analysis is limited to matrix operations, which are complex, and bear the most computational burden. The system under consideration consists of a CR user, equipped with, M and N_{cr}, transmit and receive antennas respectively. As for the PU, the PU RX is equipped with N_{PU} antennas. The cognitive ($\boldsymbol{H} \in \mathbb{C}^{N_{cr} \times M}$) and interference ($\boldsymbol{H}_{SP} \in \mathbb{C}^{N_{PU} \times M}$) channels are made up of ZMCSCG elements. Energy efficient antenna selection selects M_{cr} $(1 \leq M_{cr} \leq M)$ cognitive transmit antennas, and the cognitive and interference channel matrices after antenna selection are $\boldsymbol{H}_{cr} \in \mathbb{C}^{N_{cr} \times M_{cr}}$ and $\boldsymbol{H}_{int} \in \mathbb{C}^{N_{PU} \times M_{cr}}$ respectively.

First, the computational complexity of the OES algorithm will be determined. The matrix operations required when computing EE_{TB} are $\|\boldsymbol{H}_{int}\|_F^2$ and $[\boldsymbol{H}_{cr}^H \boldsymbol{H}_{cr}]^{-1}$; both are computed for each transmit antenna subset, i.e. a total of $\sum_{M_{cr}=1}^{M} \binom{M}{M_{cr}}$ times. $\|\boldsymbol{H}_{int}\|_F^2$ can be expressed as:

$$\|\boldsymbol{H}_{int}\|_F^2 = Tr(\boldsymbol{H}_{int} \boldsymbol{H}_{int}^H) \tag{A-F.1}$$

Therefore, computing $\|\boldsymbol{H}_{int}\|_F^2$ requires $\boldsymbol{H}_{int} \boldsymbol{H}_{int}^H$ to be computed first. Computing $\boldsymbol{H}_{int} \boldsymbol{H}_{int}^H$ requires $M_{cr} N_{PU}$ products and $N_{PU}(M_{cr} - 1)$ additions. The trace of $\boldsymbol{H}_{int} \boldsymbol{H}_{int}^H$ is then determined, this requires N_{PU} additions; therefore, the number of flops required to compute $\|\boldsymbol{H}_{int}\|_F^2$, for all transmit antenna subsets, is given by:

$$\sum_{M_{cr}=1}^{M} \binom{M}{N_{cr}} 8 N_{PU} M_{cr} \tag{A-F.2}$$

The matrix inversion $[\boldsymbol{H}_{cr}^{H}\boldsymbol{H}_{cr}]^{-1}$; will be computed via the SVD of $\boldsymbol{H}_{cr}$; as described in Appendix E. Computing $[\boldsymbol{H}_{cr}^{H}\boldsymbol{H}_{cr}]^{-1}$ requires $9(M_{cr})^3 + (4N_{cr}+1)(M_{cr})^2$ products and $9(M_{cr})^3 + (4N_{cr}-1)(M_{cr})^2$additions. Therefore, the number of flops required to compute $[\boldsymbol{H}_{cr}^{H}\boldsymbol{H}_{cr}]^{-1}$; for all transmit antenna subsets, is given by:

$$\sum_{M_{cr}=1}^{M} \binom{M}{M_{cr}} \{72(M_{cr})^3 + 4(M_{cr})^2(8N_{cr}+1)\} \tag{A-F.3}$$

Consequently, the computational complexity of the OES algorithm, in flops, is given by:

$$\sum_{M_{cr}=1}^{M} \binom{M}{N_{cr}} \{8N_{PU}M_{cr} + 72(M_{cr})^3 + 4(M_{cr})^2(8N_{cr}+1)\} \tag{A-F.4}$$

Next, the computational complexity of Iterative I is determined. Iterative I performs antenna selection in two stages, intra-level and inter-level selection. Intra-level selection uses an iterative technique that uses a combination of $\|\boldsymbol{H}_{int}\|_F^2$, EE_{TB} and the constraint given below:

$$\frac{\sum_{k=1}^{M_{cr}}[(\boldsymbol{H}_{cr}^{H}\boldsymbol{H}_{cr})^{-1}]_{k,k}}{\|\boldsymbol{H}_{int}\|_F^2} \geq \frac{N_o\beta}{I_{int}} \tag{A-F.5}$$

to perform transmit antenna selection. Iterative I first orders transmit antennas in each level by $\|\boldsymbol{H}_{int}\|_F^2$, before performing antenna selection using the iterative technique. Therefore, $\|\boldsymbol{H}_{int}\|_F^2$ needs to be computed for all transmit antenna subsets. EE_{TB} and the constraint in (A-F.5) are calculated the same number of times, and only for a faction of the number of transmit antenna subsets. Therefore, only $[\boldsymbol{H}_{cr}^{H}\boldsymbol{H}_{cr}]^{-1}$ needs to be computed, since $\|\boldsymbol{H}_{int}\|_F^2$ has already been computed for all transmit antenna subsets. The average number of times that $[\boldsymbol{H}_{cr}^{H}\boldsymbol{H}_{cr}]^{-1}$ needs to be computed by algorithm Iterative I, is equal to the number of iterations required to perform intra-level selection, and this is determined through simulations. After intra-level selection is complete, inter-level selection is performed, and it uses EE_{TB} as the selection criterion, which does not need to be calculated again, since it was already computed in the intra-level selection stage. Let A_{m1} be the average number of times $[\boldsymbol{H}_{cr}^{H}\boldsymbol{H}_{cr}]^{-1}$ is computed and $A_{rem1} = A_{m1} - M$. From

(A-F.2) and (A-F.3), the complexity of Iterative I in flops (similar to the definition in (A-E.7) is given by:

$$\frac{A_{rem1}}{M}\left\{\sum_{M_{cr}=1}^{M}\{72(M_{cr})^3+4(M_{cr})^2(8N_{cr}+1)\}\right\} + \sum_{M_{cr}=1}^{M}\{72(M_{cr})^3+4(M_{cr})^2(8N_{cr}+1)\} + \sum_{M_{cr}=1}^{M}\binom{M}{M_{cr}}\{8N_{PU}M_{cr}\} \quad \text{(A-F.6)}$$

which reduces to:

$$\frac{A_{m1}}{M}\left\{\sum_{M_{cr}=1}^{M}\{72(M_{cr})^3+4(M_{cr})^2(8N_{cr}+1)\}\right\}+\sum_{M_{cr}=1}^{M}\binom{M}{M_{cr}}\{8N_{PU}M_{cr}\} \quad \text{(A-F.7)}$$

Finally, the computational complexity of algorithm Iterative II is determined. Similar to Iterative I, Iterative II performs antenna selection by using intra-level and inter-level selection, with the same iterative technique used to perform intra-level selection; but the transmit antennas are ordered by $\lambda_{min}(\boldsymbol{H}_{cr})\|\boldsymbol{H}_{int}\|_F^2$ in each level. $\lambda_{min}(\boldsymbol{H}_{cr})$, is the minimum singular value of $\boldsymbol{H}_{cr}$; to compute $\lambda_{min}(\boldsymbol{H}_{cr})$, the SVD of $\boldsymbol{H}_{cr}$ needs to be performed to compute only the singular values. Therefore, the number of flops required to compute $\lambda_{min}(\boldsymbol{H}_{cr})$, is given by:

$$\sum_{M_{cr}=1}^{M}\binom{M_T}{M_{cr}}\{32N_{cr}(M_{cr})^2-32(M_{cr})^3/3\} \quad \text{(A-F.8)}$$

Similar to Iterative I, Iterative II uses an iterative technique, in intra-level selection, which combines EE_{TB} and the constraint given in (A-E.5). The average number of times that Iterative II computes $[\boldsymbol{H}_{cr}^H\boldsymbol{H}_{cr}]^{-1}$ is determined through simulations. Inter-level selection uses EE_{TB} as the selection criterion, which requires no additional matrix computations. If A_{m2} is the average

number of times Iterative II computes $[\boldsymbol{H}_{cr}^{H}\boldsymbol{H}_{cr}]^{-1}$ and $A_{rem2} = A_{m2} - M$; then from (A-E.2), (A-E.3) and (A-E.8), the complexity of Iterative II in flops is given by:

$$\frac{A_{rem2}}{M}\left\{\sum_{M_{cr}=1}^{M}\{72(M_{cr})^3 + 4(M_{cr})^2(8N_{cr}+1)\}\right\} + \sum_{M_{cr}=1}^{M}\{72(M_{cr})^3 + 4(M_{cr})^2(8N_{cr}+1)\} + \sum_{M_{cr}=1}^{M}\binom{M_T}{M_{cr}}\{8N_{PU}M_{cr} + 32N_{cr}(M_{cr})^2 - 32(M_{cr})^3/3\} \quad \text{(A-F.9)}$$

which reduces to:

$$\frac{A_{m2}}{M}\left\{\sum_{M_{cr}=1}^{M}\{72(M_{cr})^3 + 4(M_{cr})^2(8N_{cr}+1)\}\right\} + \sum_{M_{cr}=1}^{M}\binom{M_T}{M_{cr}}\{8N_{PU}M_{cr} + 32N_{cr}(M_{cr})^2 - 32(M_{cr})^3/3\} \quad \text{(A-F.10)}$$

In Table A-F1, the number of times EE_{TB} is calculated for OES, Iterative I and Iterative II is given for $3 \leq M \leq 10$, with $N_{cr} = M$ and $N_{PU} = 4$. The average number of times Iterative I and II compute EE_{TB} is determined through simulations, for 4-QAM, at a SNR value of $20dB$, using the simulation parameters given in Chapter 5. It is observed that using $\lambda_{min}(\boldsymbol{H}_{cr})\|\boldsymbol{H}_{int}\|_F^2$ instead of $\|\boldsymbol{H}_{int}\|_F^2$, in the intra-level selection reduces the number of times $[\boldsymbol{H}_{cr}^{H}\boldsymbol{H}_{cr}]^{-1}$has to be computed; Iterative II computes $[\boldsymbol{H}_{cr}^{H}\boldsymbol{H}_{cr}]^{-1}$ slightly less times than Iterative I.

In Figure A-F1, the percentage reduction in complexity for Iterative I and Iterative II with respect to algorithm OES is plotted against the number of transmit/receive antennas with $N_{cr} = M$. It is

Table A-F 1 Number of times EE_{TB} is computed by the algorithms in CR MIMO system

M_T	3	4	5	6	7	8	9	10
OES	7	15	31	63	127	255	511	1023
Iterative I	3.8	5.6	7.2	8.7	10.5	12.2	14.1	16.6
Iterative II	2.9	4.3	6.13	8.06	9.1	11.6	13.3	15.3

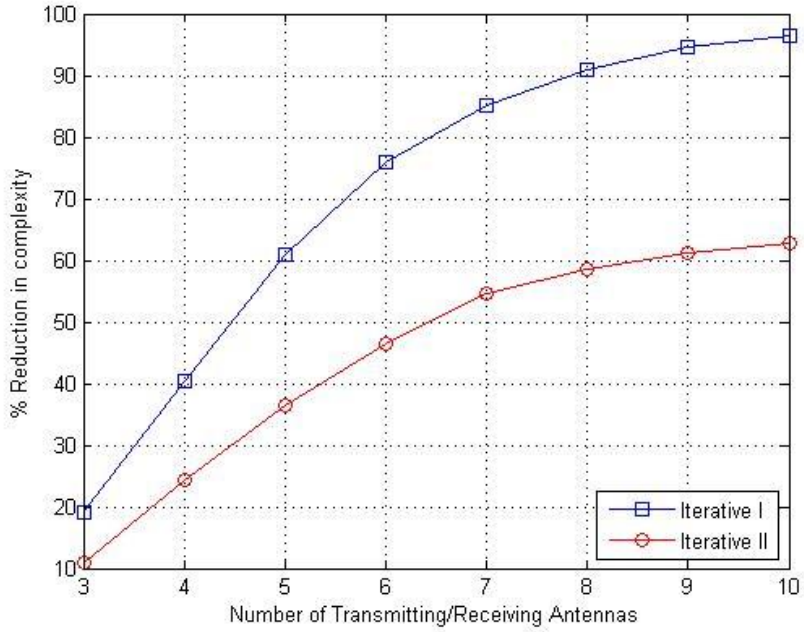

Figure A-F 1 Plot of % reduction in complexity against M/N_{cr} for CR MIMO system

observed that the percentage reduction in complexity increases as the number of transmit/receive antennas increases, for both reduced complexity algorithms. The reduced complexity algorithms are highly computationally efficient in comparison to OES, with Iterative I being less complex than Iterative II.

References

[1] G. J. Foschini and M. J. Gans, “On Limits of Wireless Communications in a Fading Environment when Using Multiple Antennas,” *Wirel. Pers. Commun.*, vol. 6, no. 3, pp. 311–335, 1998.

[2] S. M. Alamouti, “A simple transmit diversity technique for wireless communications,” *IEEE J. Sel. Areas Commun.*, vol. 16, no. 8, pp. 1451–1458, 1998.

[3] E. Perahia and Intel Corporation, “IEEE 802 . 11n Development : History , Process , and Technology,” *IEEE Stand. Commun. Netw.*, vol. 46, no. 7, p. 64, 2013.

[4] Q. Li *et al.*, “MIMO techniques in WiMAX and LTE: A feature overview,” *IEEE Commun. Mag.*, vol. 48, no. 5, pp. 86–92, 2010.

[5] K. J. R. Liu, “Advances in cognitive radio networks: A survey,” *IEEE J. Sel. Top. Signal Process.*, vol. 5, no. 1, pp. 5–23, 2011.

[6] M. Agiwal, A. Roy, and N. Saxena, “Next generation 5G wireless networks: A comprehensive survey,” *IEEE Communications Surveys and Tutorials*, vol. 18, no. 3. pp. 1617–1655, 2016.

[7] A. Fehske, G. Fettweis, J. Malmodin, and G. Biczok, “The global footprint of mobile communications: The ecological and economic perspective,” *IEEE Communications Magazine*, vol. 49, no. 8. pp. 55–62, 2011.

[8] I. F. Akyildiz, W. Su, Y. Sankarasubramaniam, and E. Cayirci, “Wireless sensor networks: a survey,” *Comput. Networks*, vol. 38, no. 4, pp. 393–422, 2002.

[9] A. Asadi, Q. Wang, and V. Mancuso, “A survey on device-to-device communication in cellular networks,” *IEEE Commun. Surv. Tutorials*, vol. 16, no. 4, pp. 1801–1819, 2014.

[10] A. F. Molisch and M. Z. Win, “MIMO systems with antenna selection,” *IEEE Microw. Mag.*, vol. 5, no. 1, pp. 46–56, 2004.

[11] A. Paulraj, R. U. Nabar, and D. Gore, *Introduction to Space-Time Wireless Communications*. 2003.

[12] F. Rashid-Farrokhi, K. J. R. Liu, and L. Tassiulas, “Transmit beamforming and power

control for cellular wireless systems," *IEEE J. Sel. Areas Commun.*, vol. 16, no. 8, pp. 1437–1450, 1998.

[13] S. A. Jafar and A. Goldsmith, "Transmitter optimization and optimality of beamforming for multiple antenna systems," *IEEE Trans. Wirel. Commun.*, vol. 3, no. 4, pp. 1165–1175, 2004.

[14] N. B. Mehta, S. Kashyap, and A. Molisch, "Antenna selection in LTE: From motivation to specification," *IEEE Commun. Mag.*, vol. 50, no. 10, pp. 144–150, 2012.

[15] C. Jiang and L. J. Cimini, "Antenna selection for energy-efficient MIMO transmission," *IEEE Wirel. Commun. Lett.*, vol. 1, no. 6, pp. 577–580, 2012.

[16] X. Zhou, B. Bai, and W. Chen, "An iterative algorithm for joint antenna selection and power adaptation in energy efficient MIMO," in *2014 IEEE International Conference on Communications, ICC 2014*, 2014, pp. 3812–3816.

[17] V. Srivastava and M. Motani, "Cross-layer design: A survey and the road ahead," *IEEE Commun. Mag.*, vol. 43, no. 12, pp. 112–119, 2005.

[18] H. Meyr, M. Moeneclaey, and S. A. Fechtel, *Digital Communication Receivers: Synchronization, Channel Estimation, and Signal Processing*. 1998.

[19] N. W. K. Lo, D. D. Falconer, and A. U. H. Sheikh, "Channel interpolation for digital mobile radio communications," pp. 773–777, 1991.

[20] C. Budianu and L. Tong, "Channel estimation for space-time orthogonal block codes," *IEEE Trans. Signal Process.*, vol. 50, no. 10, pp. 2515–2528, 2002.

[21] Z. Ding and Y. Li, "On Channel Identification Based on Second-Order Cyclic Spectra," *IEEE Trans. Signal Process.*, vol. 42, no. 5, pp. 1260–1264, 1994.

[22] G. J. Foschini, "Layered space-time architecture for wireless communications in a fading environment when using multi-element antennas," *Bell labs Tech. J.*, vol. 1, no. 2, pp. 41–59, 1996.

[23] E. Telatar, "Capacity of Multi-antenna Gaussian Channels," *Eur. Trans. Telecommun.*, vol. 10, no. 6, pp. 585–595, 1999.

[24] A. Lozano and C. Papadias, “Layered space-time receivers for frequency-selective wireless channels,” *IEEE Trans. Commun.*, vol. 50, no. 1, pp. 65–73, 2002.

[25] G. H. Golub and C. F. Van Loan, “Matrix Computations, third edition,” *John Hopkins Univ. Press*, pp. 508–554, 1996.

[26] T. M. Cover and J. A. Thomas, *Elements of Information Theory*. 2005.

[27] C.-N. Chuah, J. M. Kahn, and D. Tse, “Capacity of Multi-Antenna Array Systems in Indoor Wireless Environment,” in *Global Telecommunications Conference, IEEE GLOBECOM, The Bridge to Global Integration*, 1998, vol. 4, pp. 1894–1899.

[28] T. K. Y. Lo, “Maximum Rat io Transmission,” in *Communications, 1999. ICC ’99. 1999 IEEE International Conference on*, 1999, pp. 1310–1314.

[29] V. Tarokh, H. Jafarkhani, and A. R. Calderbank, “Space – Time Block Codes from Orthogonal Designs,” *IEEE Trans. Inf. Theory*, vol. 45, no. 5, pp. 1456–1467, 1999.

[30] V. Tarokh, N. Seshadri, S. Member, and A. R. Calderbank, “Space – Time Codes for High Data Rate Wireless Communication : Performance Criterion and Code Construction,” *IEEE Trans. Inf. Theory*, vol. 44, no. 2, pp. 744–765, 1998.

[31] J. Radon, “Lineare scharen orthogonaler matrizen,” *Math. Semin.*, pp. 1–14, 1922.

[32] J. G. Biglieri, Ezio, Dariush Divsalar, Marvin K. Simon, Peter J. McLane, *Introduction to trellis-coded modulation with applications*. Prentice-Hall, Inc.., 1991.

[33] C. L. Feng, Xiaoyan, “A new optimal transmit and receive diverstiy scheme,” in *Communications, Computers and signal Processing, 2001. PACRIM IEEE*, 2001, pp. 538–541.

[34] L. Xiaodong, H. Huang, G. J. Foschini, and R. A. Valenzuela, “Effects of iterative detection and decoding on the performance of BLAST,” in *Global Telecommunications Conference, 2000. GLOBECOM ’00. IEEE*, 2000, vol. 2, pp. 1061–1066 vol.2.

[35] G. D. Golden, C. J. Foschini, R. A. Valenzuela, and P. W. Wolniansky, “Detection algorithm and initial laboratory results using V-BLAST space-time communication architecture,” *Electron. Lett.*, vol. 35, no. 1, p. 14, 1999.

[36] B. Hassibi and B. M. Hochwald, "High-rate codes that are linear in space and time," *IEEE Trans. Inf. Theory*, vol. 48, no. 7, pp. 1804–1824, 2002.

[37] U. Fincke and M. Pohst, "Improved methods for calculating vectors of short length in a lattice, including a complexity analysis," *Math. Comput.*, vol. 44, no. 170, pp. 463–463, 1985.

[38] E. Viterbo and J. Boutros, "A universal lattice code decoder for fading channels," *IEEE Trans. Inf. Theory*, vol. 45, no. 5, pp. 1639–1642, 1999.

[39] O. Damen, A. Chkeif, and J. C. Belfiore, "Lattice code decoder for space-time codes," *IEEE Commun. Lett.*, vol. 4, no. 5, pp. 161–163, 2000.

[40] R. W. Heath, S. Sandhu, and A. Paulraj, "Antenna selection for spatial multiplexing systems with linear receivers," *IEEE Commun. Lett.*, vol. 5, no. 4, pp. 142–144, 2001.

[41] R. A. V. Wolniansky, Peter W., Gerard J. Foschini, G. D. Golden, "V-BLAST: An architecture for realizing very high data rates over the rich-scattering wireless channel," in *Signals, Systems, and Electronics, ISSSE 98. URSI International Symposium on, IEEE*, 1998, pp. 295–300.

[42] L. C. Godara, "Application of antenna arrays to mobile communications, part II: Beam-forming and direction-of-arrival considerations," *Proc. IEEE*, vol. 85, no. 8, pp. 1195–1245, 1997.

[43] M. H. Islam *et al.*, "Spectrum survey in Singapore: Occupancy measurements and analyses," in *Proceedings of the 3rd International Conference on Cognitive Radio Oriented Wireless Networks and Communications, CrownCom 2008*, 2008.

[44] D. Datla, A. M.Wyglinski, and G. J. Minden, "A Spectrum Surveying Framework for Dynamic Spectrum Access Networks," *IEEE Trans. Veh. Technol.*, vol. 58, no. 8, pp. 4158–4168, 2009.

[45] Federal Communications Commission, "Spectrum Policy Task Force Report," *Rep. Docket no. 02-135.*, 2002.

[46] J. Mitola and G. Q. Maguire, "Cognitive radio: making software radios more personal," *IEEE Pers. Commun.*, vol. 6, no. 4, pp. 13–18, 1999.

[47] S. Haykin, “Cognitive radio: Brain-empowered wireless communications,” *IEEE J. Sel. Areas Commun.*, vol. 23, no. 2, pp. 201–220, 2005.

[48] C. P. Kim, Chang-Joo, Sang-won Kim, Jinup Kim, “Dynamic Spectrum Access/Cognitive Radio Activities in Korea,” *IEEE Symp. New Front. Dyn. Spectr.*, 2010.

[49] E. F. Karimi, Hamid Reza, Martin Fenton, Gerard Lapierre, “European Harmonized Technical Conditions and Band Plans for Broadband Wireless Access in the 790-862 MHz Digital Dividend Spectrum,” *IEEE Symp. New Front. Dyn. Spectr. (DySPAN*, 2010.

[50] K. G. Shin, H. Kim, a. W. Min, and a. Kumar, “Cognitive Radios for Dynamic Spectrum Access: From Concept to Reality,” *IEEE Wirel. Commun.*, vol. 17, no. 6, pp. 64–74, 2010.

[51] Y. C. Liang, K. C. Chen, G. Y. Li, and P. Mähönen, “Cognitive radio networking and communications: An overview,” *IEEE Trans. Veh. Technol.*, vol. 60, no. 7, pp. 3386–3407, 2011.

[52] R. Zhang and Y.-C. Liang, “Exploiting Multi-Antennas for Opportunistic Spectrum Sharing in Cognitive Radio Networks,” *IEEE J. Sel. Top. Signal Process.*, vol. 2, no. 1, pp. 88–102, 2008.

[53] Y. J. Zhang and A. M. C. So, “Optimal spectrum sharing in MIMO cognitive radio networks via semidefinite programming,” *IEEE J. Sel. Areas Commun.*, vol. 29, no. 2, pp. 362–373, 2011.

[54] C. Shen and M. P. Fitz, “Dynamic spatial spectrum access with opportunistic orthogonalization,” in *Proceedings - 43rd Annual Conference on Information Sciences and Systems, CISS 2009*, 2009, pp. 600–605.

[55] C. Han *et al.*, “Green radio: Radio techniques to enable energy-efficient wireless networks,” *IEEE Commun. Mag.*, vol. 49, no. 6, pp. 46–54, 2011.

[56] “EARTH, “Energy aware radio and network technologies project.” [Online]. Available: https://www.ict-earth.eu/default.html.

[57] M. A. Imran and P. Partners, “Most promising tracks of green network technologies,” 2010.

[58] “OPERA-Net, “Optimising power efficiency in mobile radio networks project.” [Online].

Available: http://opera-net.org/default.aspx.

[59] R. Esnault, “Optimising Power Efficiency in Mobile Radio Networks (OPERA-Net), Project Presentation,” 2008.

[60] E. C. Strinati and L. Hérault, “Holistic Approach for Future Energy Efficient Cellular Networks,” *e i Elektrotechnik und Informationstechnik*, vol. 127, no. 11, pp. 314–320, 2010.

[61] D. Feng, C. Jiang, G. Lim, L. J. Cimini, G. Feng, and G. Y. Li, “A survey of energy-efficient wireless communications,” *IEEE Commun. Surv. Tutorials*, vol. 15, no. 1, pp. 167–178, 2013.

[62] M. Meinshausen *et al.*, “Greenhouse-gas emission targets for limiting global warming to 2 °C,” *Nature*, vol. 458, no. 7242, pp. 1158–1162, 2009.

[63] “Policy Basics: Policies to Reduce Greenhouse Gas Emissions.” [Online]. Available: http://www.cbpp.org/research/policy-basics-policies-to-reduce-greenhouse-gas-emissions.

[64] G. Y. Li *et al.*, “Energy-efficient wireless communications: Tutorial, survey, and open issues,” *IEEE Wirel. Commun.*, vol. 18, no. 6, pp. 28–35, 2011.

[65] S. Cui, A. J. Goldsmith, and A. Bahai, “Energy-efficiency of MIMO and cooperative MIMO techniques in sensor networks,” *IEEE J. Sel. Areas Commun.*, vol. 22, no. 6, pp. 1089–1098, 2004.

[66] H. Kim, C. B. Chae, G. De Veciana, and R. W. Heath, “A cross-layer approach to energy efficiency for adaptive MIMO systems exploiting spare capacity,” *IEEE Trans. Wirel. Commun.*, vol. 8, no. 8, pp. 4264–4275, 2009.

[67] G. Miao, N. Himayat, Y. Li, and A. Swami, “Cross-layer optimization for energy-efficient wireless communications: A survey,” *Wirel. Commun. Mob. Comput.*, vol. 9, no. 4, pp. 529–542, 2009.

[68] S. C. Cripps, *RF Power Amplifiers for Wireless Communications*. 2006.

[69] T. Birdsall, “Channel capacity in bits per joule,” *IEEE J. Ocean. Eng.*, vol. 11, no. 1, pp. 97–99, 1986.

[70] F. Heliot, M. Imran, and R. Tafazolli, “On the Energy Efficiency-Spectral Efficiency Trade-

Off over the MIMO Rayleigh Fading Channel," *IEEE Trans. Commun.*, vol. 61, no. 9, pp. 3741–3753, 2012.

[71] V. Kawadia and P. R. Kumar, "A cautionary perspective on cross-layer design," *IEEE Wireless Communications*, vol. 12, no. 1. pp. 3–11, 2005.

[72] "The Evolved Packet Core." [Online]. Available: http://www.3gpp.org/technologies/keywords-acronyms/100-the-evolved-packet-core.

[73] S. Shakkottai, T. S. Rappaport, and P. C. Karlsson, "Cross-layer design for wireless networks," *IEEE Commun. Mag.*, vol. 41, no. 10, pp. 74–80, 2003.

[74] G. Carneiro, J. Ruela, and M. Ricardo, "Cross-layer design in 4G wireless terminals," *IEEE Wirel. Commun.*, vol. 11, no. 2, pp. 7–13, 2004.

[75] B. Fu, Y. Xiao, H. J. Deng, and H. Zeng, "A survey of cross-layer designs in wireless networks," *IEEE Commun. Surv. Tutorials*, vol. 16, no. 1, pp. 110–126, 2014.

[76] R. Knopp and P. a. Humblet, "Information capacity and power control in single-cell multiuser\ncommunications," in *Proceedings IEEE International Conference on Communications ICC '95*, 1995, vol. 1, pp. 331–335.

[77] F. Foukalas, V. Gazis, and N. Alonistioti, "Cross-layer design proposals for wireless mobile networks: a survey and taxonomy," *IEEE Commun. Surv. Tutorials*, vol. 10, no. 1, pp. 70–85, 2008.

[78] S. Khan, K. K. Loo, and Z. U. Din, "Cross Layer Design for Routing and Security in Multi-hop Wireless Networks," *Communication*, vol. 4, pp. 170–173, 2009.

[79] J. M. C. Huang, Chin-Tser, Manton Matthews, Matthew Ginley, Xinliang Zheng, Chuming Chen, "Efficient and Secure Multicast in WirelessMAN: A Cross-Layer Design," *J. Commun. Softw. Syst.*, vol. 3, no. 3, pp. 199–206, 2007.

[80] I-Hsun Chuang, Chou-Ting Hsieh, and Yau-Hwang Kuo, "An adaptive cross-layer design approach for network security management," in *Advanced Communication Technology (ICACT), 2011 13th International Conference on*, 2011, pp. 1085–1089.

[81] S. Kunniyur and R. Srikant, "End-to-End Congestion Control Schemes: Utility Functions,

Random Losses and ECN Marks," *IEEE/ACM Trans. Netw.*, vol. 11, no. 5, pp. 689–702, 2003.

[82] R. H. K. Balakrishnan, Hari, "Explicit loss notification and wireless web performance," in *Proceedings of the IEEE Globecom Internet Mini-Conference.*, 1998, pp. 1–5.

[83] A. J. Goldsmith and S. G. Chua, "Adaptive coded modulation for fading channels," *IEEE Trans. Commun.*, vol. 46, no. 5, pp. 595–602, 1998.

[84] B.-J. Kim, "A network service providing wireless channel information for adaptive mobile applications. I. Proposal," in *Communications, 2001. ICC 2001. IEEE International Conference on*, 2001, pp. 1345–1351.

[85] J. Camp and E. Knightly, "Modulation rate adaptation in urban and vehicular environments: Cross-layer implementation and experimental evaluation," *IEEE/ACM Trans. Netw.*, vol. 18, no. 6, pp. 1949–1962, 2010.

[86] M. Miyoshi, M. Sugano, and M. Murata, "Performance improvement of TCP on wireless cellular networks by adaptive FEC combined with explicit loss notification," *IEEE Veh. Technol. Conf.*, vol. 2, pp. 982–986, 2002.

[87] L. Taylor, R. Titmuss, and C. Lebre, "Challenges of seamless handover in future mobile multimedia networks," *IEEE Pers. Commun.*, vol. 6, no. 2, pp. 32–37, 1999.

[88] M. Adrian, H. Zen, and A. K. Othman, "A survey of vertical handover decision algorithms in fourth generation heterogeneous wireless networks," *Asian J. Inf. Technol.*, vol. 13, no. 4, pp. 247–251, 2014.

[89] D. J. Costello and M. J. Miller, "Automatic-repeat-request error-control schemes," *IEEE Commun. Mag.*, vol. 22, no. 12, pp. 5–17, 1984.

[90] D. J. C. Lin, Shu, *Error control coding*, Vol. 2. Englewood Cliffs: Prentice Hall., 2004.

[91] A. E. M. Taha, H. S. Hassanein, and N. A. Ali, *LTE, LTE-Advanced and WiMAX: Towards IMT-Advanced Networks*. 2011.

[92] Q. Liu, S. Zhou, and G. B. Giannakis, "Cross-layer combining of adaptive modulation and Coding with truncated ARQ over wireless links," *IEEE Trans. Wirel. Commun.*, vol. 3, no.

5, pp. 1746–1755, 2004.

[93] a. Maaref and S. Aissa, “Combined adaptive modulation and truncated ARQ for packet data transmission in MIMO systems,” in *IEEE Global Telecommunications Conference, 2004. GLOBECOM ’04.*, 2004, vol. 6, pp. 3818–3822.

[94] S. Sanayei and A. Nosratinia, “Antenna selection in MIMO systems,” *IEEE Commun. Mag.*, vol. 42, no. 10, pp. 68–73, 2004.

[95] W. Jakes, *Microwave Mobile Communications*. 1974.

[96] J. H. Winters, “Switched Diversity with Feedback for DPSK Mobile Radio Systems,” *IEEE Trans. Veh. Technol.*, vol. 32, no. 1, pp. 134–150, 1983.

[97] M. Z. Win and J. H. Winters, “Virtual branch analysis of symbol error probability for hybrid selection/maximal-ratio combining in rayleigh fading,” *IEEE Trans. Commun.*, vol. 49, no. 11, pp. 1926–1934, 2001.

[98] A. F. Molisch, M. Z. Win, and J. H. Winters, “Performance of reduced-complexity transmit/receive-diversity systems,” *Int. Symp. Wirel. Pers. Multimed. Commun. WPMC*, vol. 2, no. 11, pp. 738–742, 2002.

[99] D. A. Gore and A. J. Paulraj, “MIMO antenna subset selection with space-time coding,” *IEEE Trans. Signal Process.*, vol. 50, no. 10, pp. 2580–2588, 2002.

[100] R. W. Heath and A. Paulraj, “Antenna Selection for Spatial Multiplexing Systems Based on Minimum Error Rate,” in *ICC 2001. IEEE International Conference on Communications. Conference Record (Cat. No.01CH37240)*, 2001, vol. 7, pp. 2276–2280.

[101] a. F. Molisch, M. Z. Win, and J. H. Winters, “Capacity of MIMO systems with antenna selection,” *IEEE Trans. Wirel. Commun.*, vol. 4, no. 4, pp. 1759–1772, 2005.

[102] J. Zhou and J. Thompson, “Single-antenna selection for MISO cognitive cadio,” *2008 IET Semin. Cogn. Radio Softw. Defin. Radios Technol. Tech.*, pp. 1–5, 2008.

[103] J. P. C. Wang, Yue, “Difference Antenna Selection and Power Allocation for Wireless Cognitive Systems,” *IEEE Trans. Commun.*, vol. 59, no. 12, pp. 3494–3503, 2011.

[104] J. Zhou, J. Thompson, and I. Krikidis, “Multiple antennas selection for linear precoding

MISO cognitive radio," *IEEE Wirel. Commun. Netw. Conf. WCNC*, pp. 0–5, 2009.

[105] Z. Nan, X. Yemao, and G. Xiao, "A New Antenna Selection Algorithm in Cognitive MIMO Systems," *Journals Sci. Technol. J. Sel. Areas Telecommun.*, pp. 1–6, 2011.

[106] M. Hanif, H. C. Yang, and M. S. Alouini, "Receive antenna selection for underlay cognitive radio with instantaneous interference constraint," *IEEE Signal Process. Lett.*, vol. 22, no. 6, pp. 738–742, 2015.

[107] M. F. Hanif, P. J. Smith, D. P. Taylor, and P. A. Martin, "MIMO cognitive radios with antenna selection," *IEEE Trans. Wirel. Commun.*, vol. 10, no. 11, pp. 3688–3699, 2011.

[108] M. Gharavi-Alkhansari and A. B. Gershman, "Fast antenna subset selection in MIMO systems," *IEEE Trans. Signal Process.*, vol. 52, no. 2, pp. 339–347, 2004.

[109] R. S. Blum, Z. Xu, and S. Sfar, "A near-optimal joint transmit and receive antenna selection algorithm for mimo systems," *RWS 2009 IEEE Radio Wirel. Symp. Proc.*, pp. 554–557, 2009.

[110] H. Yongqiang, L. Wentao, and L. Xiaohui, "Particle swarm optimization for antenna selection in MIMO system," *Wirel. Pers. Commun.*, vol. 68, no. 3, pp. 1013–1029, 2013.

[111] a. Dua, K. Medepalli, and A. J. Paulraj, "Receive antenna selection in MIMO systems using convex optimization," *IEEE Trans. Wirel. Commun.*, vol. 5, no. 9, pp. 2353–2357, 2006.

[112] M. Z. Milani, Alessio, Velio Tralli, "Improving protocol performance in BLAST-based wireless systems using channel adaptive antenna selection," in *IEEE Vehicular Technology Conference*, 2002, pp. 409–413.

[113] J. L. Vicario, M. a. Lagunas, and C. Anton-Haro, "A cross-layer approach to transmit antenna selection," *IEEE Trans. Wirel. Commun.*, vol. 5, no. 8, pp. 1993–1997, 2006.

[114] H. A. Abou Saleh and W. Hamouda, "Cross-layer based transmit antenna selection for decision-feedback detection in correlated Ricean MIMO channels," *IEEE Trans. Wirel. Commun.*, vol. 8, no. 4, pp. 1677–1682, 2009.

[115] M. Lari, A. Mohammadi, and A. Abdipour, "Cross layer transmit antenna selection in MQAM modulation MIMO systems," in *2010 5th International Symposium on*

Telecommunications, IST 2010, 2010, pp. 308–312.

[116] A. A. Lari, Mohammad, Abbas Mohammadi, “New throughput-based antenna selection scheme,” *Turkish J. Electr. Eng. Comput. Sci.*, vol. 22, no. 4, pp. 1017–1031, 2014.

[117] J. López-Vicario, C. F. Mecklenbräuker, and C. Antón-Haro, “Reduced-complexity methods for throughput maximization in {MIMO} Channels,” *Proc. IEEE ICC-2004*, vol. 5, no. c, pp. 2678–2682, 2004.

[118] P. A. Tohidi, Masumeh Sadat, “Low-complexity throughput-based antenna selection method,” *Wirel. Pers. Commun.*, vol. 75, no. 1, pp. 385–395, 2014.

[119] A. Ghosh and W. Hamouda, “Combined Antenna Selection and Beamforming in Cross-Layer Design for Cognitive Networks,” in *IEEE Communications Conference (ICC)*, 2012, pp. 4949–4953.

[120] X. Zhou, B. Bai, and W. Chen, “Iterative antenna selection for multi-stream MIMO under a holistic power model,” *IEEE Wirel. Commun. Lett.*, vol. 3, no. 1, pp. 82–85, 2014.

[121] O. K. Rayel, G. Brante, J. L. Rebelatto, R. D. Souza, and M. A. Imran, “Energy efficiency-spectral efficiency trade-off of transmit antenna selection,” *IEEE Trans. Commun.*, vol. 62, no. 12, pp. 4293–4303, 2014.

[122] H. Li, L. Song, D. Zhu, and M. Lei, “Energy efficiency of large scale MIMO systems with transmit antenna selection,” *2013 IEEE Int. Conf. Commun.*, vol. 10, no. 6, pp. 4641–4645, 2013.

[123] M. T. Kakitani, G. Brante, R. D. Souza, and M. A. Imran, “Energy efficiency of transmit diversity systems under a realistic power consumption model,” *IEEE Commun. Lett.*, vol. 17, no. 1, pp. 119–122, 2013.

[124] S. Jin and X. Zhang, “Optimal Energy Efficient Scheme for MIMO-Based Cognitive Radio Networks With Antenna Selection,” in *Information Sciences and Systems (CISS), IEEE*, 2015, pp. 1–6.

[125] G. Y. Hu, Teck, David Afshartous, “Parallel Stop and Wait ARQ in UMTS - Performance and Modeling,” in *In Proceedings of the 2004 World Wireless Congress*, 2004.

[126] S. Cui, A. J. Goldsmith, and A. Bahai, “Energy-constrained modulation optimization,” *IEEE Trans. Wirel. Commun.*, vol. 4, no. 5, pp. 2349–2360, 2005.

[127] J. Benesty, Y. Huang, and J. Chen, “A fast recursive algorithm for optimum sequential signal detection in a BLAST system,” *IEEE Trans. Signal Process.*, vol. 51, no. 7, pp. 1722–1730, 2003.

[128] A. J. Goldsmith, “Variable-rate variable-power MQAM for fading channels,” *IEEE Trans. Commun.*, vol. 45, no. 10, pp. 1218–1230, 1997.

[129] S. Catreux, P. F. Driessen, and L. J. Greenstein, “Data throughputs using Multiple-Input Multiple-Output (MIMO) techniques in a noise-limited cellular environment,” *IEEE Trans. Wirel. Commun.*, vol. 1, no. 2, pp. 226–234, 2002.

[130] P. Sebastian, H. Sampath, and A. Paulraj, “Adaptive Modulation for Multiple Antenna Systems,” *Conf. Rec. Thirty-Fourth Asilomar Conf. Signals, Syst. Comput. (Cat. No.00CH37154)*, vol. 1, no. 1, pp. 506–510, 2000.

[131] H. Zhuang, L. Dai, S. Zhou, and Y. Yao, “Low Complexity Per-Antenna Rate and Power Control Approach for Closed-Loop V-BLAST,” *IEEE Trans. Commun.*, vol. 51, no. 11, pp. 1783–1787, 2003.

[132] S. L. Loyka, “Channel capacity of MIMO architecture using the exponential\ncorrelation matrix,” *IEEE Commun. Lett.*, vol. 5, no. 9, pp. 369–371, 2001.

[133] UCLA, “The Central Limit Theorem.” [Online]. Available: http://www.stat.ucla.edu/~nchristo/introeconometrics/introecon_central_limit_theorem.pdf.

[134] E. W. Weisstein, “Central Limit Theorem,” *MathWorld--A Wolfram Web Resource*. [Online]. Available: Central Limit Theorem.

[135] F. Rusek *et al.*, “Scaling up MIMO : Opportunities and challenges with very large arrays,” *IEEE Signal Process. Mag.*, vol. 30, no. 1, pp. 40–60, 2013.

[136] E. M. Okumu and M. E. Dlodlo, “N-Process Stop and Wait for MIMO Systems with Transmit Antenna Assignment,” in *Electrical and Computer Engineering (CCECE) IEEE*, 2016, pp. 1–5.

[137] V. Meghdad, “BER Caculations,” 2008. [Online]. Available: http://www.unilim.fr/pages_perso/vahid/notes/ber_awgn.pdf.